الجمهورية الجزائرية الديموقراطية الشعبية

PEOPLE's DEMOCRATIC REPUBLIC OF ALGERIA

وزارة التعليم العالي والبحث العلمي

MINISTRY OF HIGHER EDUCATION AND SCIENTIFIC RESEARCH

جامعة سعيدة – د. مولاي الطاهر

UNIVERSITY OF SAIDA - DR. MOULAY TAHAR

Faculty of Technology

A Dissertation Submitted to the Department of Telecommunication in Partial Fulfilment of the Requirements for Degree of Master of Systems of Telecommunications

Presented by:

Miss. ZINI Manel

Miss. SLIMANI Meriem Abir

Terahertz channel models of 6G wireless communication system

Defended on June\12\2024 in front of the jury composed of:

Miss. OUASSEI. A	**MCB**	President
Mr. TAMI Abdelkader	**MCA**	Supervisor
Mr. OUARDI. A	**MCA**	Examiner

2023/2024

ACKNOWLEDGMENTS

*First and foremost, all thanks and praise to our God "**Allah**" for giving us the strength and patience to finish this task.*

*We would like to express our gratitude to our project supervisor, **Dr. TAMI Abdelkader**, for their valuable guidance, helpful feedback, and ongoing support. Your expertise and encouragement have been instrumental in shaping the direction and quality of this project.*

A heartfelt thank you to our families, whose unwavering support and understanding have been a source of strength for us. Your belief in our abilities has always been a great motivator.

We express our sincere gratitude to our families for their support, both moral and material, during the preparation phase.

Finally, we would like to express our sincere gratitude to the jury members, the president, and the examiner for dedicating their valuable time to review and evaluate our work.

DEDICATION

To my beloved family: my mother and father, my sister Ikram, and my brother Houssem. Your unwavering support, endless love, and constant encouragement have been the cornerstones of my life. Mother and Father, you have always believed in me, even when I doubted myself. Your sacrifices and teachings have shaped me into the person I am today. Ikram and Houssem, you have been my companions through thick and thin, sharing in my joys and comforting me in my sorrows.

To my best friend Wafaa, your friendship is a precious gift that I cherish every day. Your loyalty, kindness, and understanding have made our bond unbreakable. You have been my confidante, my cheerleader, and my rock. I am forever grateful for your presence in my life.

And to the incredible Israa, your support and belief in me have been extraordinary. You have helped me in countless ways, inspiring me to strive for greatness and never give up. Has added immense value to my life.

To my supervisor, Dr.TAMI Abdelkader, your guidance and wisdom have been invaluable throughout this journey. Your encouragement and insights have pushed me to grow and achieve more than I ever thought possible. Thank you for believing in me and for your unwavering support.

To the jury, thank you for your time, your attention, and your valuable feedback. Your insights have been crucial in shaping this work, and I am deeply grateful for your contributions.

And to my partner, Meriem, your partnership and collaboration have been essential to this journey. Your dedication, hard work, and friendship have made this experience both successful and enjoyable. Thank you for being an exceptional partner.

Thank you all for being an integral part of my journey. Your love and support have been my guiding light, and I am eternally grateful for each of you.

ZINI Manel

DEDICATION

I would like to dedicate this project with esteem, and gratitude:

To my devoted family, whose consistent backing and motivation have served as my primary sources of resilience and motivation.

To my parents, for their unwavering love, selfless sacrifices, and unwavering confidence in my capabilities. Their mentorship has proven to be indispensable in my personal and academic development.

To my siblings, for always being there to cheer me on and for your constant support.

To my project supervisor, ***Dr. TAMI Abdelkader****, for their enduring patience, comprehension, and stead fast backing during times of difficulty and success.*

To my friends and colleagues, for their moral support, encouragement, and for making this journey enjoyable and fulfilling.

Finally, to my professors and the faculty members of the Department of Telecommunications, whose teachings and advice have provided a solid foundation for my academic career.

This project would not have been possible without the contributions and encouragement of each of you. Thank you.

SLIMANI Meriem Abir

ABSTRACT

The emergence of 6G wireless communication systems is anticipated to transform connectivity by offering unparalleled data speeds, extremely low latency, and extensive device connectivity. A critical component in the development and deployment of 6G technology is the understanding and modeling of terahertz (THz) communication channels, which operate in the 0.1-10 THz frequency range. This dissertation explores the use of the NYUSIM simulator, a state-of-the-art tool for channel modeling, to characterize THz channels in 6G systems.

The NYUSIM simulator, developed by New York University, provides a comprehensive platform for simulating realistic wireless communication environments, incorporating parameters such as pathloss, delay spread. By leveraging NYUSIM, this study investigates the propagation characteristics, channel modeling of THz waves in various scenarios, including urban and rural environments.

Keywords: 6G wireless communication, terahertz (THz) frequency, NYUSIM simulator, channel modeling, pathloss, delay spread, urban environments (UMi), rural environments (RMa), line of sight (LOS).

RÉSUMÉ

L'émergence des systèmes de communication sans fil 6G est prévue de transformer la connectivité en offrant des vitesses de données inégalées, une latence extrêmement faible et une connectivité étendue des appareils. Un composant critique dans le développement et le déploiement de la technologie 6G est la compréhension et la modélisation des canaux de communication térahertz (THz), qui opèrent dans la plage de fréquences de 0,1 à 10 THz. Ce projet fin d’étude explore l'utilisation du simulateur NYUSIM, un outil de pointe pour la modélisation des canaux, pour caractériser les canaux THz dans les systèmes 6G.

Le simulateur NYUSIM, développé par l'Université de New York, fournit une plateforme complète pour simuler des environnements de communication sans fil réalistes, en intégrant des paramètres tels que la perte de chemin, la dispersion temporelle. En exploitant NYUSIM, cette étude examine les caractéristiques de propagation, la modélisation des canaux des ondes THz dans divers scénarios, y compris les environnements urbains et ruraux.

Mots-clés: communication sans fil 6G, fréquence térahertz (THz), simulateur NYUSIM, modélisation de canal, affaiblissement du trajet, dispersion temporelle, environnements urbains (UMi), environnements ruraux (RMa), ligne de visée (LOS).

LIST OF ABBREVIATIONS

1G	First Generation
5G	Fifth Generation
6G	Sixth Generation
AI	Artificial Intelligence
APs	Access Points
AR	Augmented Reality
AoD	Angle of Departure
AoA	Angle of Arrival
BDMA	Beam Division Multiple Access
BS	Base Stations
BCI	Brain Computer Interface
B5G	Beyond Fifth-Generation
Co-Pol/	Co polarization
Co/X-Pol/	Co and cross-polarization
CIR	Channel Impulse response
DL	Deep Learning
DoA	Direction of Arrival
DoD	Direction of Departure
DNN	Deep Neural Network
EM	Electromagnetic
FSPL	Free Space Path Loss
FDTD	Finite-Domain Time-Domain
GSCMs	Geometry Stochastic Channel Models
GTD	Geometric Theory of Diffraction
GO	Geometric Optic
HD	Ultra High
HFSS	High Frequency Structure Simulator
IoNT	Internet of Nano-Things
IAB	Integrated Access Backhaul
ISAC	Integrated Sensing And Communication
InF	Indoor Factory
InH	Indoor Hotspot
IoST	Internet of Smart Things
IOT	Internet Of Things
KPI	Key Performance Indicators
LOS	line-of-Sight
LTE	Long Term Evolution
LEO	Low Earth Orbit
MIMO	Multiple Input Multiple Output
MR	Mixed Reality
mmWave	Millimeter wave
MPCs	Multipath Components
NYUSIM	New York University Simulator
NGSMs	Nongeometrical Stochastic Channel Models
NLOS	Non-line-of-sight
O2I	Outdoor To Indoor
PSMs	Parametric Stochastic Models
PL	Path loss
PDP	Power Delay Profile
QoE	Quality of Experience
QoS	Quality of Service
RT	Ray-Tracing
RX	Receiver
RMS	Root Mean Square
RF	Radio Frequency
RMa	Rural Macrocell
SF	Shadow Fading
THz	Terahertz
Tbps	Terabit-per-second
Tx	Transmitter
UT	User Terminal
UE	User Equipment
UM-MIMO	Ultra Massive Multiple Input Multiple Output
UHF	Ultra High Frequency
URA	Uniform Rectangular Array
UMi	Urban Microcell
UTD	Uniform Theory of Diffraction
ULA	Uniform Linear Array
UAVs	Unmanned Aerial Vehicals
UMa	Urban Macrocell
VR	Virtual Reality
WPT	Wireless Power Transmission
WiNoC	Wireless Networks-on-Chip Communications
WLAN	Wireless Area Local Network
XR	Extended Reality
X-Pol/	cross-polarization

LIST OF CONTENT

CHAPTER III DESCRIPTION OF OPEN SOURCE NYUSIM SUMILATOR

CHAPTER IV SIMULATION AND RESULTS

LIST OF FIGURES

LIST OF TABELS

GENERAL INTRODUCTION

With the rapid development of 5G, not only humans will be better connected, but also more and more intelligent things such as industrial equipment, cars, sensors, and home devices will all be connected. This trend will continue beyond the next years, leading to intelligent connection of everything, anywhere, all-time. Accompanying the exponential boost of the number of interconnected devices, 6G in 2030 and beyond foresees the Key Performance Indicators (KPI) including:

1) Hundreds of Giga-bit-per-second and even Terabit-per second (Tbps) rates.

2) Lower latency of around one-tenth of millisecond, and close to zero jitter performance.

3) Higher positioning and sensing resolution and accuracy at millimeter level.

4) Reduced energy consumption and 100× improved energy efficiency.

5) 99.99999% improved reliability, security.

In forth coming wireless communication systems, it will be essential to utilize frequencies beyond 6 GHz and extending up to the terahertz (THz) range, in conjunction with current technologies, in order to fulfill anticipated performance requirements. The utilization of the terahertz band (0.1-10 THz) is regarded as a viable solution to address the requirements of 6G networks envisioned for the next future year and beyond.

The use of the THz frequency band will open up new applications for future ultra-high data rate communication and high resolution sensing scenarios, including Tbps indoor wireless links, and wireless backhaul and access in small cell networks, and also the interconnection among micro/nanoscale machines or nanomachines. In addition to the communication applications, the THz band will also enable high resolution and accuracy sensing scenarios, including the millimeter-resolution wireless positioning and tracking, gesture and motion recognition high-accuracy imaging and mapping, augmented human sense, among others.

This written document is organized into four chapters:

The initial chapter will introduce an overview about 6G wireless communication system which represents a revolutionary leap beyond 5G, promising to transform connectivity with data rates up to 1 Tbps, ultra-low latency, and extensive device inter connectivity. Leveraging cutting-edge technologies like terahertz frequencies, massive MIMO, and AI-driven network management, 6G aims to deliver unprecedented performance, energy efficiency, and security.

Second chapter represents models of wireless Terahertz channel in a frequency range (0.1-10 THz) is considered a crucial technology for the advancement of sixth-generation (6G) wireless networks.

The third chapter will focus on description of open source Nyusim simulator which is a powerful tool developed by NYU WIRELESS for modeling and simulating millimeter-wave (mmWave) and terahertz (THz) wireless communication channels. Designed to aid in the development of 5G and 6G technologies, NYUSIM provides users with accurate and customizable simulations of channel characteristics based on real-world measurements and advanced statistical models.

The final chapter will be devoted to show of different simulations of a comparative examination of Urban Micro (UMi) and Rural Macro (RMa) settings within the framework of terahertz communication channels, investigating the distinct challenges and prospects present in each environment.

CHAPTER I

OVERVIEW ABOUT 6G WIRELESS COMMUNICATION SYSTEMS

I.1. INTRODUCTION:

Fifth generation (5G) mobile communication systems have entered the stage of commercial development for several years, providing users with fast network services as well as a host of novel opportunities to various industries [1]. Since the requirement for higher rates was the main driver of wireless network evolution, 5G is insufficient, International industrial, academic, and standards groups have started researching sixth generation (6G) wireless communication systems in preparation for the creation of a quicker generation of telecommunications in the future. It has been attempted to define 6G in terms of needs, application scenarios, important technologies, etc. by the publication of a number of white papers and survey studies. The International Telecommunication Union's Radiocommunication Sector has been working on the 6G vision and is anticipated to come to an agreement on what 6G will be by the middle of 2023, although there are still many unresolved concerns in the relevant worldwide debates, according to the literature now in circulation. In previous studies, they mainly concentrated on the technologies and interactions with other subjects to assure that 6G can be widely and successfully used. In Terahertz Propagation Characteristics for 6G Mobile Communication Systems, it is shown that using terahertz bands beyond 100 GHz can satisfy the need for extremely high-speed communication because a noticeably wider frequency spectrum can be used than in 5G [2]. In Sensing Based Contention Access for 6G Low Latency Networks, in order to avoid contention within limited radio resources, it examines a useful sensing design broadcasting without a grant to provide a shared resource allocation framework for potential sixth generation networks [3].

The sixth generation mobile communication system (6G) connection will surpass personalized communication and fully realize the Internet of things (IoT) mode. It will not only connect persons, but also connect computing resources, vehicles, devices, wearable devices, sensors, and even robots. We can realize the intelligent network adaptation and management, and provide advanced services only by using 6G network [4].

I.2. SIXTH-GENERATION WIRELESS COMMUNICATION SYSTEM:

Sixth-generation wireless (6G) is the successor to 5G cellular technology. In comparison to 5G networks, 6G networks will be able to use higher frequencies while offering significantly more capacity and significantly lower latency. Supporting communications with a latency of one microsecond is one of the objectives of the 6G internet. This is 1,000 times faster than a millisecond throughput, or 1/1000th of the delay.

However, thanks to the immersion of the Internet of Things (IoT) paradigm, ubiquitous wireless connectivity that connects with more than11 billion devices is foreseen by 2020. Following this trend, Terabit-per-second (Tbps) links are expected to become a reality within the next decade. As summarized in Figure I.1, moving forward from 5G, the performance of 6G includes the following six aspects of disruptive improvement [5]:

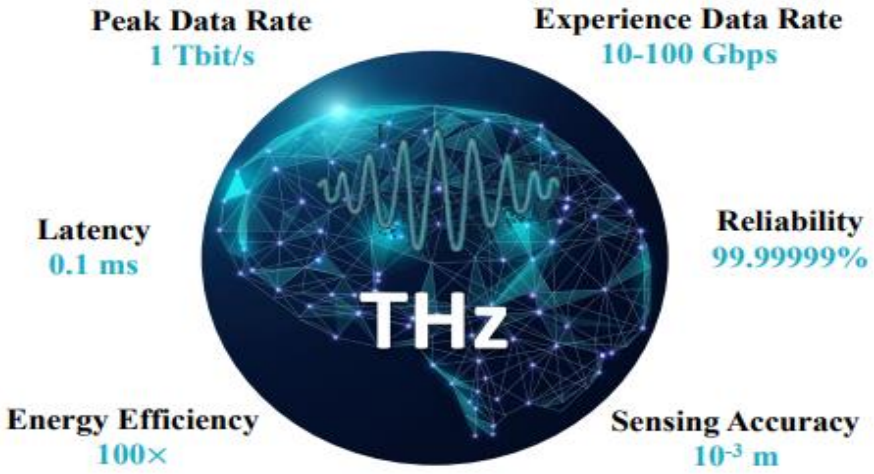

Figure I.1: Features of 6G technology.

Expected 6G network Supports ultra-low latency wireless communication and ultra-high reliability. The future 6G network also aims at this Supports ultra-fast mobility. In order to support ultra-high-speed wireless data transmission, MIMO is used on a large scale System and UHF are expected to be used through 6G network. Additionally, 6G networks aim to provide Ultra-high broadband connection and support for Ultra-High HD video streaming [6] [7]. Figure I.2 shows a schematic diagram of moving toward an ultra era in the future 6G networks:

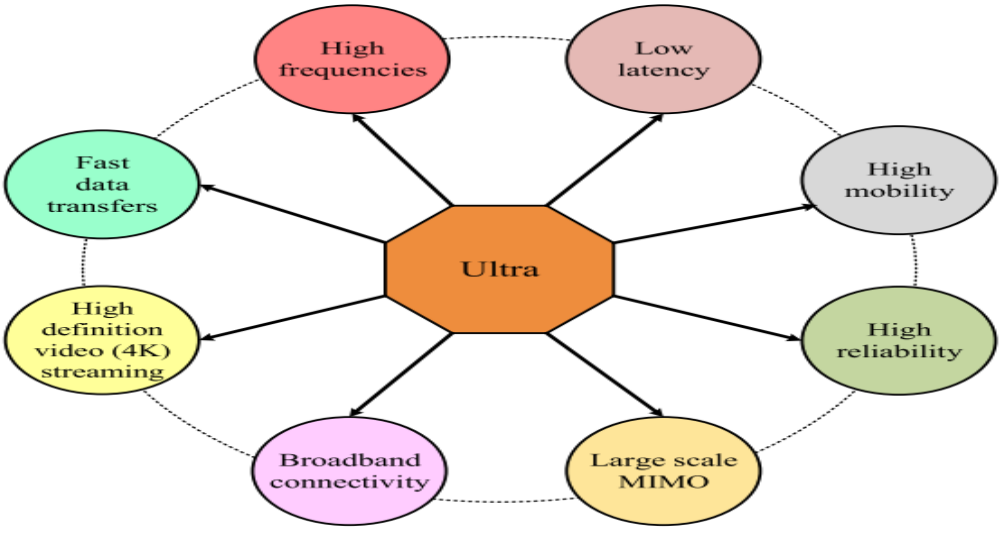

Figure I.2: Illustration of the ultra era in 6G networks.

Unlike previous networks, 6G wireless communications networks are expected to support many delay-sensitive applications such as Tactile Internet, holographic

teleportation (telepresence), Internet of Smart Things (IoST) and multi-sensory Extended Reality (XR), which involves Augmented Reality (AR), Mixed Reality (MR), and Virtual Reality (VR). IoST applications can be divided into smart city, smart radio environments, smart healthcare, smart grid, smart transportation, smart factories, smart farming and, smart home [8]. All these smart applications are expected to be fully supported by 6G wireless communications networks.

In terms of time delay, the development of mobile communication network is centered on service for people from 2G to 5G. Therefore, the time delay depends on the human response time, such as auditory response time (about 100ms), visual response time (about 10ms), and perceptual response time (about 1ms). For the application of tactile Internet, 5G technology will allow 1 millisecond delay time. However, this is "too long" for the Industrial Internet of Things (IIoT) and other delay sensitive applications. For example, minimum delay time is essential to reduce the collision rate and improve the safety of autonomous vehicles. Thus 6G aims to achieve a delay less than 1 millisecond .Table I.1,summarizes the key characteristics 6G in terms of various network aspects ,because it can enhance the application of autopilot, augmented reality and medical imaging. The demand in 6G network may change, and the frequency width adopted by 6G will be greatly increased. The data rate of 6G uplink and downlink can reach 1Tbps, and the reliability will reach 10-9. The supported mobile rate ranges from 500 kilometer per hour for 5G to 1000 kilometer per hour for 6G [4].

Delay	Data rate	Reliability	Mobile rate	Integration
<1ms	1Tbps	10^{-9}	1000km/h	Fully integrated with satellite , XR , AI , tactile , automation ,ect.

Table I.1: Properties of 6G standard.

I.2.1. Evolution of cellular networks from 1G to 6G:

In order to provide a clear vision of what 6G networks could offer, it is essential to give a brief background of the evolution of mobile communications networks from the first generation (1G) to the fifth-generation (5G). To date, there are five different generations of mobile communications systems, which belong to different standards and have different techniques and capabilities, as shown in Figure I.3 [9]:

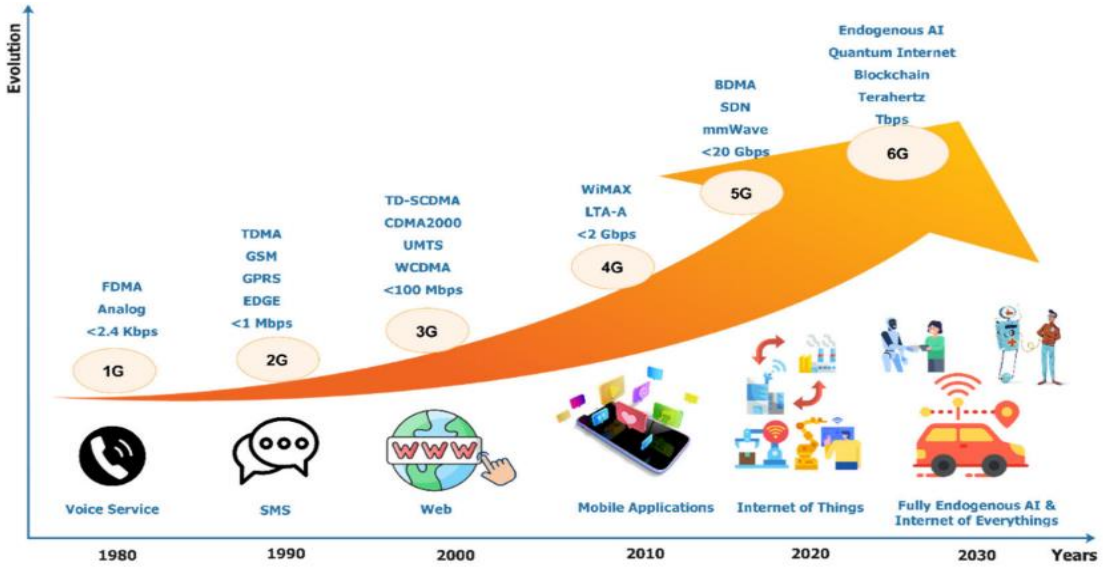

Figure I.3: Evolution of mobile wireless generations.

Notably, each generation of mobile communications networks has been developed roughly every ten years. The evolution from 1G to 6G mobile wireless communications networks is shown in Figure I.4 [10][6]:

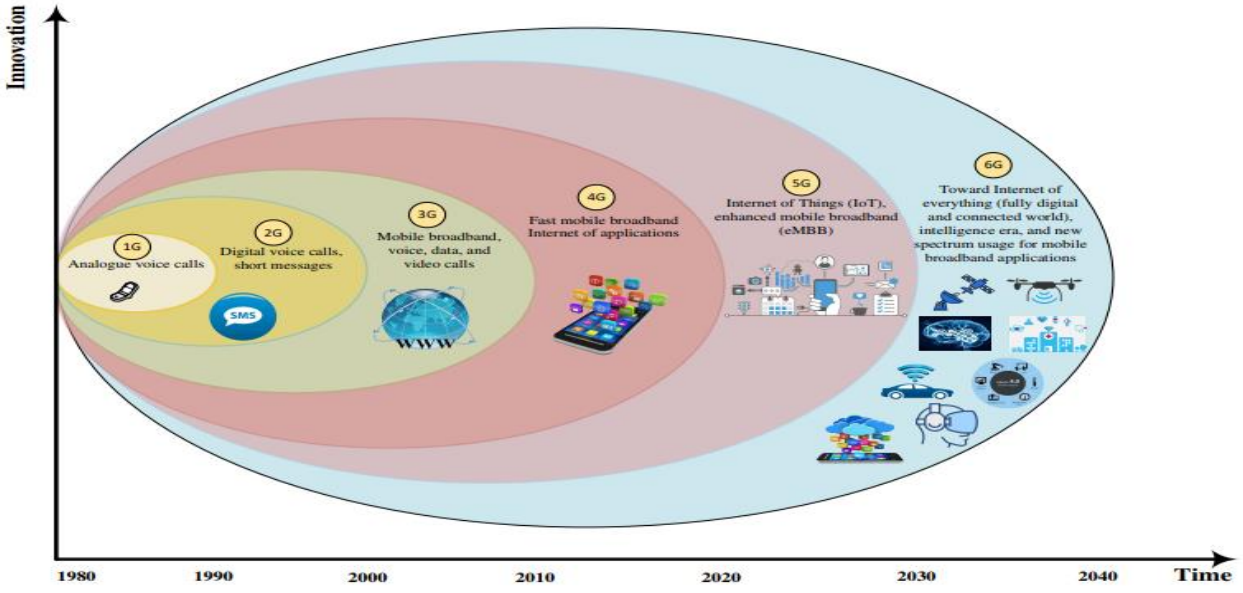

Figure I.4: Evolution of technologies of mobile generation from 1G to 6G.

These technologies have been developed to enable a wider transmission bandwidth, to achieve a high data rate, and to allow wider mobile broadband connections. LTE mobile communication system was extended to LTE-Advanced network in 2011, which allows the operation in unlicensed spectrum. 4G LTE network with a 2 × 2 MIMO provides a maximum data rate up to 150 Mb/s while LTE-Advanced networks are able to achieve a maximum data rate of up to 1Gb/s using a 4 × 4 MIMO system over a 100 MHz aggregated bandwidth [11].

Furthermore, an advanced multiple access technology termed as beam division multiple access (BDMA) can be exploited in 5G network to increase the system capacity. In this multiplexing technique, an orthogonal beam can be allocated to the users according to their locations [12].

I.3. 6G NETWORK ARCHITECTURE:

6G will be "**digital twin, intelligent ubiquitous**". If the 5G era can realize the ubiquitous acquirement of information, then 6G should fully support the digitization of the world on the basis of 5G, and combine with the development of AI and other technologies to realize the ubiquitous acquirement of information and comprehensively enable everything [4].

In the future, it will move towards a "**digital twin**" world that combines virtual and reality. The world will generate a digital twin virtual world based on the physical world. Information and intelligence can be transmitted among persons, persons and things, and things and things in the physical world through the 6G. The twin virtual world is the simulation and prediction of the physical world, which will accurately reflect and predict the real state of the physical world, help human beings further emancipate themselves, improve the quality of life, and improve the efficiency of social production and governance, so as to achieve the goal of "**creating a new world through digital innovation, and making all things intelligent**"[4].

I.3.1. 6G Time-Space-Frequency Characteristics:

According to the evolution and innovation direction of mobile network in the past, 6G will have super flexibility in the utilization of time, frequency and space resources, so as to provide faster rate, larger capacity and ultra-low delay than 5G application in the future.

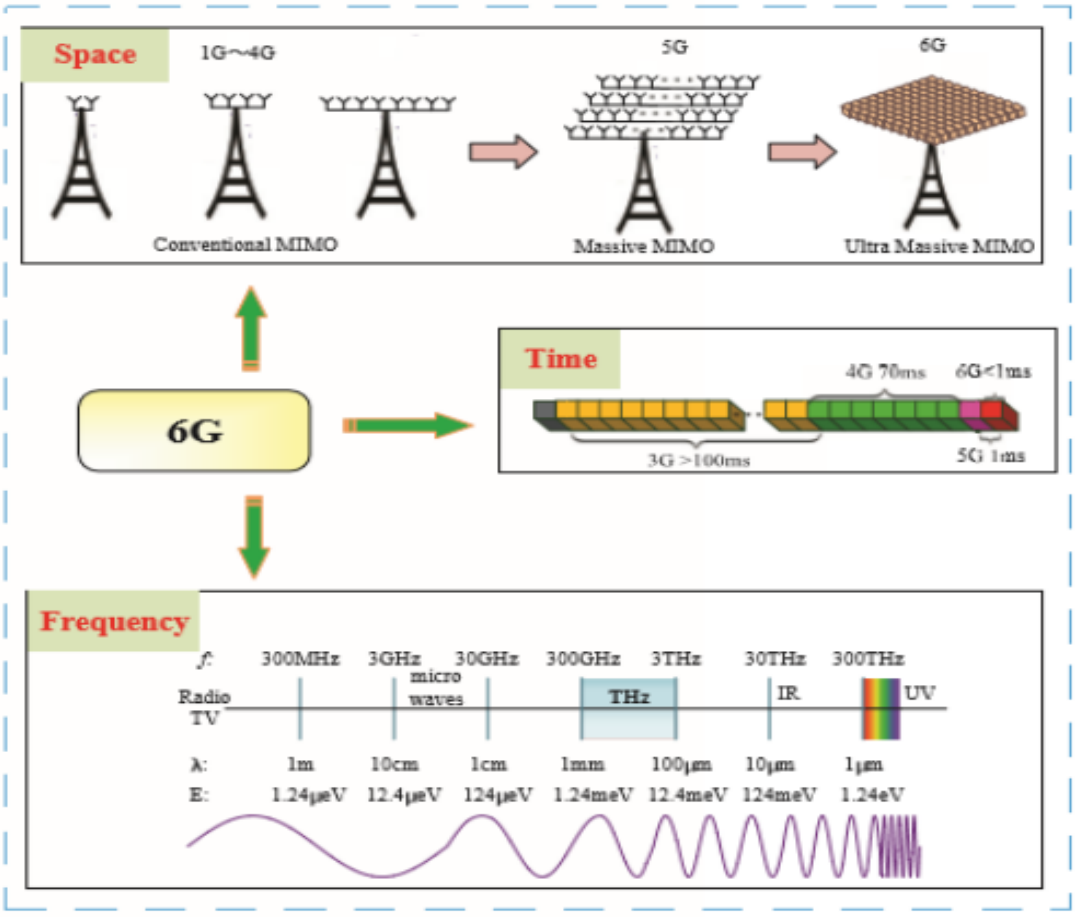

Figure I.5: Framework of 6G founded on the space resources use, frequency, time.

The specific characteristics are as follows [13] [14]:

(a) In the time dimension, the basic time slot in 6G can be compressed to use the high frequency band more effectively and meet the demand of delay sensitive service. The flexibility and versatility of the network will be improved as the time slot becomes shorter.

(b) In the spatial dimension, ultra massive multiple input multiple output (UM-MIMO) for THz communication can support hundreds to thousands of transmit and receive antennas, and further utilize the "multipath" technology.

(c) In the frequency dimension, on the one hand, THz band and even visible light band will be used for 6G transmissions; on the other hand, in the future, mobile network can be integrated with satellite system and Internet to build space-ground integrated network. From the perspective of personal mobile communication, this will indeed increase the frequency range for services. As a result, 6G will use higher frequencies than previous generations of mobile communication systems to increase data rates.

I.3.2.Architecture of 6G network:

A primary purpose of a 6G network is to provide global coverage. The current network architecture is based on the evolution and inheritance of terrestrial cell networks. This architecture, however, has the following two drawbacks:

- An inability to respond to communication scenarios that take place in the air or underwater, which is an unavoidable requirement for future services;
- The requirement of an excessively high cost to set up dense cell networks to provide worldwide communications. In order to solve the aforementioned drawbacks, the 6G design will be a completely integrated communication system that will include space, air, ground, and sea [15].

As described in Figure I.5the vision on aspects of 6G architecture that includes the following:

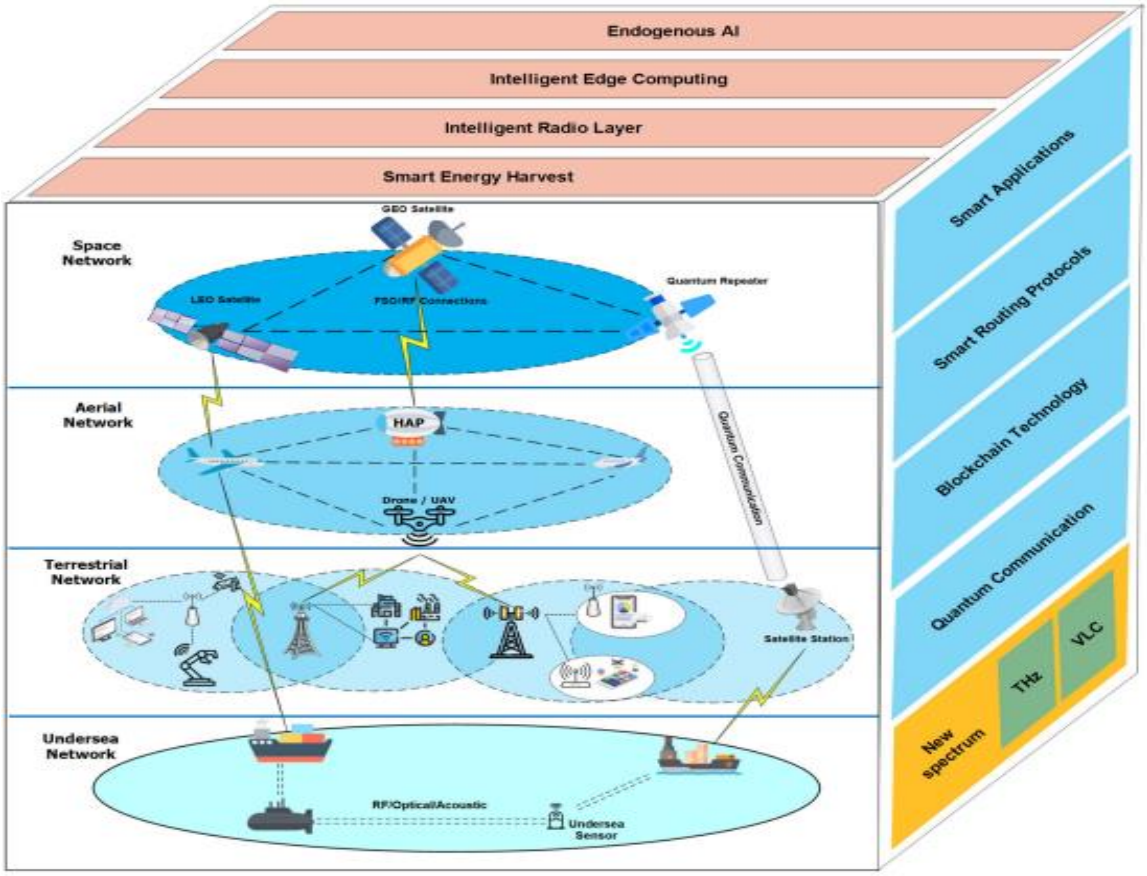

Figure I.6: The vision on aspects of 6G architecture.

I.3.3. New Network Topology:

When pursuing ultra-high rate, high capacity (especially uplink) and improving the reliability of wireless communication, it is ideal to communicate in the shortest possible distance and occlusion free environment (low path loss), and generate as many communication paths as possible to increase candidate paths (increase redundancy).

Therefore, 6G needs a distributed network topology in the spatial domain. In order to increase the path selection, 6G will pursue the topology of spatial non-orthogonal distribution network by abandoning the concept of "cell".

At the same time, with the rise of smart home, building, city and society, especially with the development of robot and automatic UAV system, 6G will meet the growing demand of human to machine communication and machine to machine (M2M) communication. In order to realize the future IOT, 6G will be a super flexible and super dense network, which can skillfully integrate different technologies to meet different service requirements at the same time. To provide a global mobile complex, 6G is expected to integrate ground, satellite and sky networks into a single wireless system. Through UAV and LEO earth satellite access networks, 3D connectivity will be ubiquitous. Big buildings, flying cars, airplanes and even space are the natural activity areas of persons and objects. Not only the ground, but also the sky and space are indispensable communication areas. In addition, the demand for maritime and submarine communication areas is increasing. Due to the needs of various sensor networks, communication areas such as unattended factories and unattended construction sites which without human beings, must also be constructed network. To sum up, the ground, sky and other places will become communication areas. Because the traditional cellular network can not completely cover many important service areas (such as sky, ocean and space), in order to provide services to UAVs, flying cars, ships and space stations, coverage expansion and topology technology are needed. Therefore, The new 6G network topology should be three-dimensional covered horizontally and vertically [4].

I.3.4. Integration of network and intelligence:

We expect that the number of 6G users and the density of access point deployment will be much higher. The integration of different technologies and application characteristics makes the network more heterogeneous, and the performance requirements of 6G are more stringent [4].

(a) learning and feature extraction technology :

Large amounts of data generated by future networked devices, such as sensors on autopilot, and it cannot guarantee the quality of service required. Therefore, distinguishing the value of information is the basis of maximizing the utility of users. In this case, the machine learning strategy can evaluate the correlation of observations, or extract characteristics from the input vector, and predict the posterior probability of the sequence based on the whole history of the sequence. In 6G, unsupervised reinforcement learning does not need to be labeled and can operate the network autonomously.

(b) Artificial intelligence :

Artificial intelligence is partly realized in 5G system, and artificial intelligence will become the core component of 6G. 6G will fully support artificial intelligence. The progress of machine learning will create more intelligent networks for 6G real-time communication. The introduction of artificial intelligence will simplify and improve the transmission of real-time data. Through a lot of analysis, artificial intelligence can determine the execution mode of complex target tasks. Artificial intelligence will improve efficiency and reduce processing delay of communication. Time consuming tasks, such as handoff and network selection, can be quickly completed by artificial intelligence. Artificial intelligence will also play an important role in M2M, machine to person and human to machine communication. It will also communicate in time at the brain computer interface (BCI). Communication systems based on artificial intelligence need to be supported by metamaterials, intelligent structures, intelligent networks, intelligent devices, intelligent cognitive radio, autonomous wireless networks and machine learning. Unsupervised reinforcement learning in networks has a bright future in 6G networks. By combining reinforcement learning with unsupervised learning, it is possible for the network to operate in a truly autonomous way. At present, the most powerful artificial intelligence technology, such as deep learning (DL), is based on deep neural network (DNN) [16].

With the increasing popularity of AI technologies, 6G enables various applications in communications such as network planning, network optimization, network operation and maintenance, and autonomous vehicle as shown in Figure I.6:

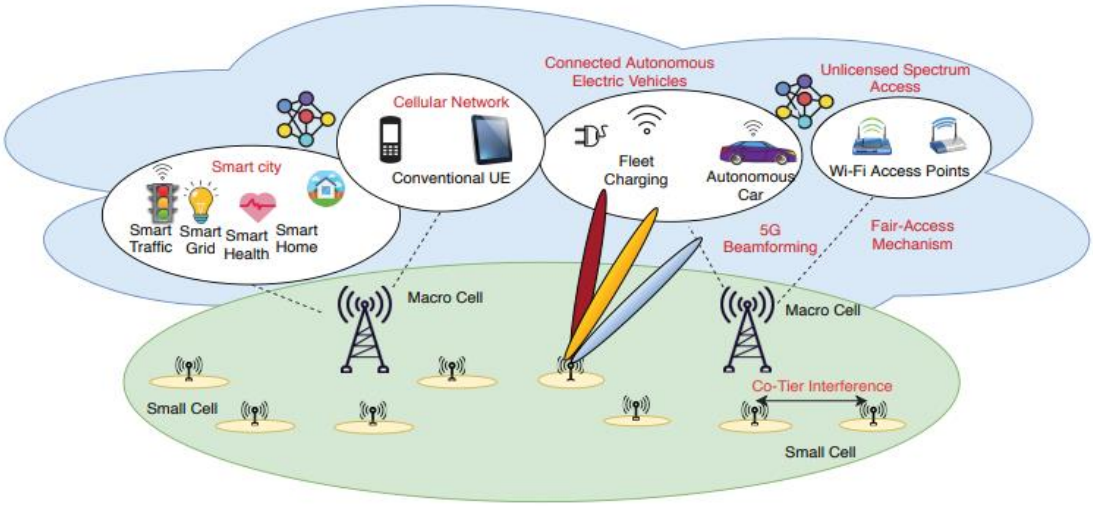

Figure I.7: An AI-Enabled 6G wireless network and related applications.

Empowered by 6G, a wide range of AI applications will evolve into “connected intelligence”, hence facilitating every aspect of our daily life. For example, advanced AI

approaches can be employed in network management or autonomy to save manpower. In addition, 6G revitalizes smart healthcare by providing real-time health monitoring, high-precision medical treatment, and reliable privacy protection. With the advent of 6G, Industry 4.0 will be fully realized as smart manufacturing will achieve high precision manufacturing. Intelligent robots connected by ubiquitous 6G network enable manufacturing systems to carry out complex and dangerous tasks without risking people's life. Moreover, the smart home that equips with intelligent IoT devices will provide a comfortable living environment to people, and 6G allows the smart home to ensure the residents' security. In terms of traffic and transportation, the sophisticated sensing and planning algorithms can be deployed for traffic optimization. Other applications such as smart grid and unmanned aerial vehicle will also be enhanced with the aid of 6G [17] [18].

I.4. 6G TECHNOLOGY CHARACTERISTICS:

New technologies will be introduced into the 6G mobile communication system as follows [4]:

1. Novel discontinuous communication technology:

When new frequency bands such as millimeter wave and terahertz wave are added to the applied frequency band, 6G will adopt a very wide frequency band compared with the past. Therefore, it seems that there are many related research fields, such as optimizing the selection of multi band according to the application, studying the method of frequency reuse between cells, upgrading the duplex mode in uplink and downlink, and studying the utilization mode of low frequency band.

2. Ultra high rate, high reliability communication:

Wireless communication highly reliable control information is an important requirement of many industrial use cases (such as remote control and factory automation), and 6G is expected to achieve higher reliability and security than 5G. With the popularity of robots, unmanned aerial vehicles, and the expansion of radio coverage to the sky, highly reliable communication is required not only in limited areas such as factories, but also in wider areas, and it is possible to achieve highly reliable communication in various scenarios.

3. Network based positioning and sensing:

The 6G network will use a unified positioning and communication interface to improve control operations, which can rely on context information to form beam forming patterns, reduce interference and predict switching, and provide innovative user services, such as vehicle and electronic health services.

4. Terahertz communication:

Spectrum efficiency can be achieved by using THz communication (0.1-10THz) and using advanced UM-MIMO technology [19] [20]. RF frequency band has been almost exhausted, and it is not enough to meet the requirement of 6G. THz band will play an important role in 6G communication. THz band will become the next frontier of high data rate communication. The small wavelength of THz signal allows more antenna elements to be integrated into the equipment and base stations operating in frequency band.

The THz spectrum can resolve the spectrum scarcity problem and tremendously enhance current wireless system capacity. Various promising applications are envisaged, such as Tbps WLAN system (Tera-WiFi), Tbps Internet-of-Things (Tera-IoT) in wireless data center, Tbps integrated access backhaul (Tera-IAB) wireless networks, and ultra-broadband THz space communications (Tera-SpaceCom), as illustrated in Figure I.7. Besides these macro/micro-scale applications, the THz band can be utilized for wireless connections in nanomachine networks, to enable wireless networks-on-chip communications (WiNoC) and the Internet of Nano-Things (IoNT), motivated by the state-of-the-art nanoscale transceivers and antennas that oscillate in the THz band [21].

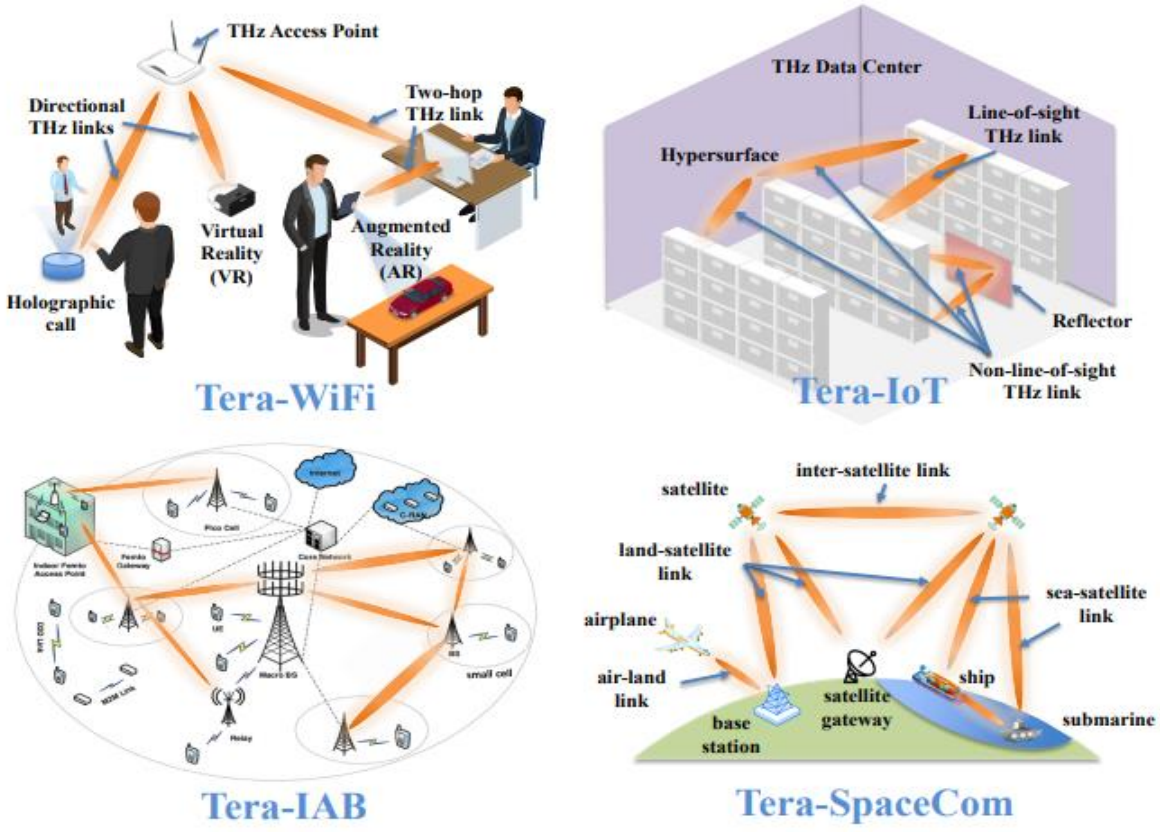

Figure I.8: 6G applications operating in the THz band.

Terahertz wave has many characteristics:

- Terahertz wave is easily absorbed by moisture in the air, which is more suitable for high-rate and short-range wireless communication;
- The wave beam is narrower and has better directionality, and has stronger anti interference ability;
- Terahertz wave has wide bandwidth, which can meet the demand of spectrum bandwidth in wireless broadband transmission.
- Terahertz wave can be widely used in space communication, especially for the communication between satellites or between satellite and ground;
- The propagation characteristics of electromagnetic wave show that the free space fading is proportional to the square of frequency, so terahertz has larger decline of free space compared with low frequency band.
- Terahertz signal is very sensitive to shadow and has great influence on coverage.
- At the moving rate, the channel coherence time is linearly related to the carrier frequency, which means that the coherent time of terahertz band is very small and the doppler spread is large, which is much faster than the frequency band used in the current cellular system.

Terahertz system is a highly spatially oriented signal transmission, which means that the path fading, service beam and cell correlation will change rapidly, and a fast adaptation mechanism is needed to overcome this fast changing intermittent connection problem [22] [23].

5. Unmanned Aerial Vehicals (UAVs):

UAV will be an important part of 6G wireless communication. In many cases, UAV technology will be used to provide high data rate wireless connections. The base station entity will be installed on the UAV to provide cellular connectivity. UAVs have some characteristics that are not available in a fixed base station infrastructure, such as ease of deployment, strong LoS links, and degree of freedom with controllable mobility. In emergency situations such as natural disasters, it is not economically feasible to deploy ground communication infrastructure, and sometimes it is impossible to provide any services in unstable environments. UAVs can easily handle these situations. UAV will become a new mode in the field of wireless communication [4].

6. Integration Of Sensing And Communication:

The key driver of autonomous wireless network is to be able to continuously sense the dynamic changes of the environment and exchange information among different nodes. In 6G, sensors will be tightly integrated with communications to support autonomous systems [4].

7. Big data analysis:

Big data analysis is a complex process of analyzing various big data sets. This process discovers information, such as hidden patterns, unknown correlations, and customer preferences, to ensure perfect data management. Big data is collected from a variety of sources, such as videos, social networks, images and sensors. This technology will be widely used in the processing of massive data in 6G system.

8. WPT and energy harvesting:

Any IOT device in 6G will consume more power due to the huge computing demands of AI processing. WPT doesn't play a key role in 5G, but in 6G, it will eventually shine. First of all, because the density of wireless network continues to increase, the communication distance will be greatly shortened. In addition, the use of UAV as base station further shortens the distance, which makes WPT more meaningful. UAVs will benefit a lot from wireless power transmission (WPT), which enables UAVs to move all the time. In addition, with the continuous progress of energy harvesting technology, energy harvesting from RF signals may become a feasible power supply for low-power applications.

I.5. CONCLUSION:

Based on the discussions presented above, the conclusions are obtained as follows:

The main development trends of 6G communication system has high bit rate, high reliability, high energy efficiency, high frequency spectrum efficiency, low delay and operate at new spectrum, etc. 6G will be a fully digital and interconnected system. Through the implementation of 6G, everything around us will be very intelligent, which will produce the concept of Internet of things (IOE), with a lot of data and information. Due to the availability of a large number of operational data and the improvement of computing power, artificial intelligence will become an important part of 6G. In 6G, we expect to see that AI runs with distributed training at the edge of the network, including microcellular base stations and UEs. It is expected that the world in the 6G era will become a prospect in which all people, information and goods can be accessed in a surreal experience anywhere, and the restrictions on work place and time are completely eliminated. This will greatly eliminate social and cultural differences among urban and rural areas, avoid urban population concentration, and promote local development. It can also make people's lives more convenient.

CHAPTER II

WIRELESS THz CHANNEL MODELS

II.1 INTRODUCTION:

Wireless data traffic has drastically increased accompanied by a growing demand for higher data rate transmissions. In particular and according to the Edholm's law of bandwidth, wireless data rates have been doubled every eighteen months over the last three decades and are quickly approaching the capacity of wired communication systems. In order to address this tremendous capacity demand, the mobile world has moved towards the fifth generation (5G) era, by introducing several novel wireless approaches, such as massive multiple-input multiple-output (MIMO) systems, full-duplexing, and millimeter wave (mmWave) communications. However, there is a lack of efficiency and flexibility in handling the huge amount of quality of service (QoS) and experience (QoE) oriented data services .Spectrum use will undoubtedly move to the terahertz (THz) frequencies in the beyond fifth-generation (B5G) mobile system era. With enormous bandwidth far greater than the amount available in the microwave and millimeter-wave bands combined, THz communication will open up new frontiers for exciting services and applications requiring ultra-broadband connectivity [24].

Neighboring to the mm-wave spectrum, the Terahertz (THz) band (0.1-10 THz) is revealing its potential as a key wireless technology to fulfill the future demands for 6G wireless systems, thanks to its four strengths: 1) tens up to hundred GHz bandwidth resource, 2) pico-second level symbol duration, 3) integration of thousands of sub millimeter-long antennas, 4) weak interference without full legacy regulation. Being known as the THz gap for many years, the THz band has been one of the least explored frequency bands in the electromagnetic (EM) spectrum, for lack of efficient THz transceivers and antennas. Nevertheless, practical THz communication systems are enabled by the major progress in the last ten years [25].

For 6G in 2030 and beyond, key performance metrics long for Terabit-per-second, one-tenth of millisecond latency with zero jitter, millimeter-precision sensing and positioning, and seamless connectivity, among others. To meet these demands, the Terahertz (0.1-10 THz) band comes into the horizon, with ultra-broad bandwidth and sub-millimeter wavelength, which however suffers from distance limitation and power consumption concern.

II.2 DEFINITION OF WIRELESS THz CHANNEL:

Terahertz (THz) communications, operating within the frequency range of 0.1-10 THz, are considered a crucial technology for the advancement of sixth generation (6G) wireless systems. The study of underlying THz wireless propagation channels provides the foundations for the development of reliable THz communication systems and their application. The wireless propagation channel serves as the conduit through which signals

are transmitted from the transmitter (Tx) to the receiver (Rx), with channel properties playing a crucial role in determining the overall performance capabilities of wireless communications, as well as the effectiveness of specific transmission strategies and transceiver configurations. Given that wireless channels form the fundamental basis for constructing wireless communication systems in novel frequency spectrums and diverse environments, it is essential to investigate the propagation channels for Terahertz (THz) radio frequencies in anticipation of future 6G wireless communication technologies. The examination of wireless channel characteristics hinges on conducting physical channel measurements using channel sounders. Subsequent analysis of these measurements aids in the development of channel models, which aim to encapsulate the behavior of wave propagation with a suitable level of complexity, facilitating equitable comparisons of various algorithms, designs, and performance metrics within wireless networks [26].

Following the trend of sensing and connecting all things in 6G communications, THz wireless systems are expected to simultaneously transmit billions of data streams and sense the environment or human activity, namely, THz Integrated Sensing And Communication (ISAC). On one hand, by sharing the frequency bands, hardware, and signal processing modules, the integration of THz communication and sensing can enhance spectrum efficiency, and reduce the hardware cost and computational complexity. On the other hand, by extracting features and information from THz signals, THz ISAC is able to prompt communication and sensing to assist each other and further realize Tbps links and millimeter-level sensing accuracy [27].

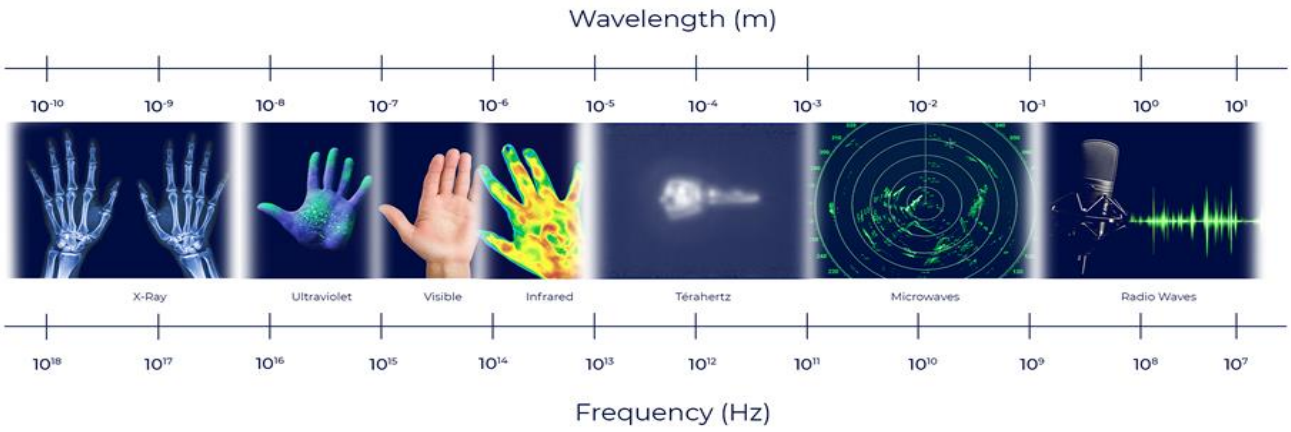

Figure II.1: THz range of the electromagnetic spectrum.

II.3 .SYSTEM MODEL FOR THE THz MASSIVE MIMO NETWORK:

As shown in Figure II.2. For the walkway scenario, we focus on the downlink where the evenly-spaced APs provide connectivity to the pedestrian users. We assume the APs are connected by Tbps wireless backhaul links and that each user is connected a single AP at each time instant. In the following subsections, we describe the channel model, the antenna array structure and the pre coding techniques employed.

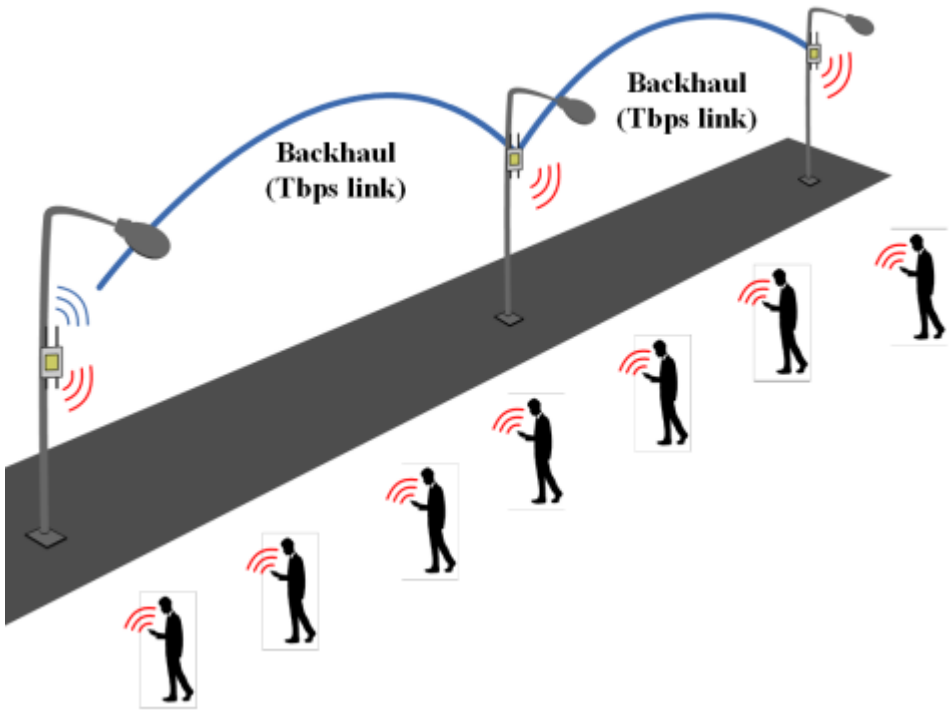

Figure II.2: Backhaul system deployment model.

II.3.1.THz Channel Model:

We consider a three dimensional (3D) statistical spatial channel model following the implementation in for the considered scenario. The large-scale fading is given by the effective omnidirectional path loss $\boldsymbol{PL_{eff}}$ which combines the path loss (PL) and the shadow fading (SF).

$$\boldsymbol{PL_{eff} = 20log_{10}\left(\frac{4\pi f_c}{c}\right) + 10\bar{n}log_{10}(d) + X(0,\sigma)} \quad \textbf{(1)}$$

Where $\boldsymbol{f_c}$ is the carrier frequency, $\boldsymbol{C = 3 * 10^8}$ m/sis the speed of light, $\boldsymbol{\bar{n}}$ is the path loss exponent, $\boldsymbol{d}$ is the 3D distance between the AP and UE, and $\boldsymbol{X}$ is the log-normal random SF variable with zero mean and $\boldsymbol{\sigma}$ standard deviation. For the small-scale fading,

the double-directional channel impulse response (CIR) $\boldsymbol{h_{dir}}$ with L multipath components (MPCs) for each transmission link is given as:

$$\boldsymbol{h_{dir}(t,\Phi) = \sum_{l=1}^{L} P_{RX,l}.e^{j\varphi l}.\ \delta(t-\tau_l).G_{TX}\left(\Phi-\Phi_l^{TX}\right).G_{RX}(\Phi-\Phi_l^{RX})} \quad \textbf{(2)}$$

Where $\boldsymbol{P_{RX,l}}$,$\boldsymbol{\varphi_l}$ and $\boldsymbol{\tau_l}$ denote the received power magnitude, phase and propagation time delay of the MPCs, respectively; $\boldsymbol{t}$ is time and $\boldsymbol{\Phi}$ is the azimuth angle offset from the bore sight direction. For each MPC, $\boldsymbol{\Phi_l^{TX}}$ is the angle of departure (AoD) at the AP and $\boldsymbol{\Phi_l^{RX}}$is the angle of arrival (AoA) for each UE. $\mathbf{G_{TX}}$ and $\mathbf{G_{RX}}$ are the transmit and receive antenna gains, respectively. Given that $\boldsymbol{G_{AE}}$ is the gain of an antenna element, $\boldsymbol{G_{TX}}$ and $\boldsymbol{G_{RX}}$ can be given by (3), where X represents the TX or RX as appropriate [28].

$$\boldsymbol{G_X(dB) = G_{AE}(dB) + 10log_{10}(N_X)} \quad \textbf{(3)}$$

II.3.2.Massive MIMO Antenna Model:

The AP and UEs are equipped with massive MIMO arrays with $\boldsymbol{N_{TX}}$ and $\boldsymbol{N_{RX}}$ antenna elements, respectively. We consider the uniform linear array (ULA) at both the AP and the UEs, with inter-element spacing $\boldsymbol{d_{TX} = d_{RX} = \lambda/2}$. The $\boldsymbol{h_{dir}}$ $\boldsymbol{(t+\Phi)}$in (2) is thus extended to the MIMO channel matrix H given by (4).

$$\mathbf{H} = \sqrt{\frac{N_{TX}N_{RX}}{L}}\sum_{l=1}^{L}\sqrt{PL_l(d)}.e^{j2\pi}\left(f_{c\tau l}+\frac{v_{RX}cos(\varphi_l)}{\lambda}\Delta t\right).a_{RX}\left(\Phi_l^{RX}\right).a_{TX}^{H}\left(\Phi_l^{TX}\right) \quad \textbf{(4)}$$

Where $\boldsymbol{v_{RX}}$ is the UE speed, $\boldsymbol{\lambda = C/f_c}$ is the wavelength, and $\boldsymbol{\varphi_l}$ is the phase, where $\boldsymbol{\varphi_l}$is composed of the distance dependent phase change and the velocity-induced Doppler shift. The array response vectors $\boldsymbol{a_{TX}}$ and $\boldsymbol{a_{RX}}$ are given by (5) and (6), for the ULA TX and RX [39].

$$\boldsymbol{a_{TX}(\Phi_l^{TX}) = \frac{1}{\sqrt{N_{TX}}}(e^{j\frac{2\pi}{\lambda}d_{TX}(n-1)sin(\Phi_l^{TX})}} \quad \textbf{(5)}$$

$$\forall_n = 1, 2, \dots \dots N_{TX}$$

$$\boldsymbol{a_{RX}(\Phi_l^{RX}) = \frac{1}{\sqrt{N_{RX}}}(e^{j\frac{2\pi}{\lambda}d_{RX}(m-1)sin(\Phi_l^{RX})}} \quad \textbf{(6)}$$

$$\forall_m = 1, 2, \dots \dots N_{RX}$$

II.3.3.Path-Loss:

The total path-loss,A, for a traveling wave in the terahertz band is defined as the additionof the spreading loss, A_{spread}, and the molecular absorption loss, A_{abs}.

$$A(f, d) = A_{spread}(f, d) + A_{abs}(f, d) \quad (7)$$

Where f stands for the wave frequency and d is the total path length. The spreading loss accounts for the attenuation due to the expansion of the wave as it propagates through the medium, and it is defined as:

$$A_{spread}(f, d) = \left(\frac{4\pi f d}{c}\right)^2 \quad (8)$$

Where f is the wave frequency, d is the total path length, and c stands for the speed of light in vacuum. The absorption loss accounts for the attenuation that a propagating wave will suffer because of molecular absorption, i.e., the process by which part of the wave energy is converted into internal kinetic energy of the excited molecules in the medium. Indeed, several molecules present in a standard medium are excited by electromagnetic radiation at certain frequencies within the terahertz band, converting part of the radiation into internal vibrations. The absorption loss A_{abs} reflects this reduction in the wave energy, and it is defined as:

$$A_{abs}(f, d) = \frac{1}{\tau(f,d)} \quad (9)$$

Where f stands for the wave frequency, d is the total path length, and τ is the transmittance of the medium. This parameter measures the fraction of incident radiation that is able to pass through the medium and can be calculated using the Beer-Lambert Law as [30]:

$$\tau = (f, d) = e^{-k(f)d} \quad (10)$$

Where f is the frequency of the EM wave, d stands for the total path length, and k is the mediumabsorption coefficient. This last parameter depends on the composition of the medium, the particular mixture of molecules found along the path, and it is defined as:

$$k(f) = \sum_{i,g} k^{i,g} \quad (11)$$

Where $k^{i,g}$ is the individual absorption coefficient for the isotopologue i of gas g. The absorption coefficient of an isotopologue i of gas g, $k^{i,g}$ in m^{-1}, for a molecular volumetric density, $Q^{i,g}$, in $molecules/m^3$ at pressure p and temperature T can be written as:

$$k^{i,g}(f) = \frac{p}{p_0}\frac{T_{STP}}{T} Q^{i,g}\sigma^{i,g} \quad (12)$$

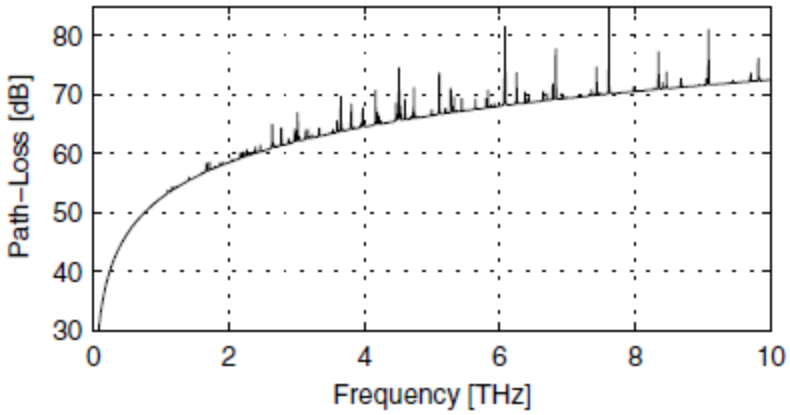

Figure II.3: Total path-loss as a function of frequency for a transmission distance equal to 10mm, in a standard medium with 1% of water vapor molecules.

Where p_0 and T_{STP} are the Standard-Pressure-Temperature values and $\sigma^{i,g}$ is the absorption cross section for the isotopologue i of gas g in $m^2/molucule$ Simply stated, the total absorption will depend on the number of molecules of a given gas that are found along the path. For a given gas mixture, the total number of molecules of the isotopologue i of gas g per volume unit, $Q^{i,g}$, at pressure p and temperature T, can be obtained from the Ideal Gas Law [31] as:

$$Q^{i,g} = \frac{n}{v} q^{i,g} N_A = \frac{P}{RT} q^{i,g} N_A \quad (13)$$

Where n is the total number of moles of the gas mixture that is being considered, V stands for the volume, $q^{i,g}$ is the mixing ratio for the isotopologue i of gas g,N_A stands for the Avogadro constant and R is the gas constant. The absorption cross section $\sigma^{i,g}$ in (18) can be further decomposed in terms of the line intensity and $S^{i,g}$ for the absorption of the isotopologue$i$of gas g and the spectral line shape $G^{i,g}$ as:

$$\sigma^{i,g}(f) = S^{i,g} G^{i,g}(f) \quad (14)$$

The line intensity $S^{i,g}$ is a parameter directly obtained from the HITRAN database. To obtain the line shape, $G^{i,g}$, we first need to determine the position of the resonant frequency $f_c^{i,g}$ For an isotopologue i of gas g. This increases linearly with the pressure from its zero-pressure position as:

$$f_c^{i,g} = f_{c0}^{i,g} + \delta^{i,g} P/_{P_0} \quad (15)$$

Where is $f_{c0}^{i,g}$ the zero-pressure position of the resonance, P_0 is the reference pressure and $\delta^{i,g}$ is the linear pressure shift. All these parameters are directly read from the HITRAN database [32]. The absorption from a particular molecule is not confined to a single frequency, but it is spread over a range of frequencies. For a system in which the pressure is above 0.1 atm, the spreading will be mainly governed by the collisions between molecules of the same gas. The amount of broadening depends on the molecules involved in the collisions and it is usually referred as the Lorentz half-width $\alpha_L^{i,g}$ [33]. This can be obtained as a function of the air and self broadened half widths, $\alpha_0^{i,g}$ and $\alpha_0^{i,g}$respectively, as:

$$\alpha_L^{i,g} = \left[(1 - q^g)\alpha_0^{air} + q_g \alpha_0^{i,g}\right]\left(\frac{p}{p0}\right)\left(\frac{T_0}{T}\right)^{\gamma} \quad (16)$$

In which the temperature broadening coefficient γ as well as α_0^{air} and are $\alpha_0^{i,g}$ obtained directlyfrom the HITRAN database [34]. For the terahertz frequency band, an appropriate line shape to represent the molecular absorption is the Van Vleck-Weisskopf asymmetric line shape [35]:

$$F^{i,g}(f) = \frac{\alpha_L^{i,g}}{\pi}\frac{f}{f_c^{i,g}}\left[\frac{1}{\left(f - f_c^{i,g}\right)^2 + \left(\alpha_0^{i,g}\right)^2} + \frac{1}{\left(f + f_c^{i,g}\right)^2 + \left(\alpha_0^{i,g}\right)^2}\right] \quad (17)$$

An additional adjustment to the far ends of the line shape can be done in order to account for the continuum absorption [36]:

$$G^{i,g}(f) = \frac{f}{f_c^{i,g}}\frac{\tanh\left(\frac{hcf}{2k_B T}\right)}{\tanh\left(\frac{hcf_c^{i,g}}{2k_B T}\right)} . F^{i,g}(f) \quad (18)$$

Where $\boldsymbol{h}$ is the Planck Constant, $\boldsymbol{c}$ is the speed of light in vacuum, $\boldsymbol{K_B}$ stands for the Boltzmann Constant and $\boldsymbol{T}$ is the system temperature. With this, we are able to compute the contributions to the total molecular absorption from each isotopologue $\boldsymbol{i}$ of each gas $\boldsymbol{g}$ present in the medium, and consequently, the total molecular absorption loss (15) can be obtained. Molecular absorption makes the terahertz channel highly frequency selective. As an example, the total path-loss that a wave will suffer when traveling 10mm in a standard medium with 1% of water vapor molecules.

II.4.INTEGRATION OF DELAY SPREAD IN TERAHERTZ (THz) CHANNEL MODELS:

The Terahertz (THz) frequency band, typically defined as frequencies between 0.1 THz and 10 THz, offers significant potential for high-capacity wireless communication systems. However, the unique propagation characteristics at these frequencies necessarily accurate channel modeling to ensure reliable system performance. One critical parameter in THz channel modeling is the delay spread, which characterizes the temporal dispersion of multipath components and impacts the system's data rates and signal quality [36].

II.4.1. Channel Impulse Response (CIR) :

The Channel Impulse Response (CIR) is fundamental in characterizing the behavior of a communication channel. For THz frequencies, the CIR can be expressed as:

$$\mathbf{h(t)} = \sum_{i=1}^{N} \boldsymbol{\alpha_i}(\boldsymbol{t} - \boldsymbol{\tau_i}) \quad \textbf{(19)}$$

Where $\boldsymbol{\alpha_i}$ and $\boldsymbol{\tau_i}$ are the amplitude and delay of $\boldsymbol{i}$ the multipath component, respectively. This representation captures the effects of multipath propagation, including reflections, diffractions, and scatterings, which are prominent at THz frequencies.

II.4.2.Power Delay Profile (PDP):

The Power Delay Profile (PDP) is a critical parameter in characterizing the temporal dispersion of multipath components in a communication channel. It provides a statistical representation of the power distribution of received signal components as a function of their propagation delays and it is defined as [37]:

$$\mathbf{P(\tau)} = \mathbf{E}\left[\left|\boldsymbol{h}(\boldsymbol{\tau})^{\mathbf{2}}\right|\right] \quad \textbf{(20)}$$

Where $\boldsymbol{h(\tau)}$ is the CIR and $\boldsymbol{E}$ denotes the expectation operator. The PDP thus provides a measure of how the signal power is distributed over various delays, reflecting the multipath propagation characteristics of the channel.

II.4.3. Mean Excess Delay and RMS Delay Spread:

The mean excess delay and Root Mean Square (RMS) delay spread are two key statistical measures used to characterize the temporal dispersion of multipath components in a communication channel [38]. The mean excess delay $\boldsymbol{\tau_{mean}}$ is the first moment of the PDP and is calculated as:

$$\boldsymbol{\tau_{mean}} = \frac{\sum_{i=1}^{N} \tau_i P(\tau_i)}{\sum_{i=1}^{N} P(\tau_i)} \quad \textbf{(21)}$$

Where $\boldsymbol{\tau_i}$ signifies the delay associated with the $\boldsymbol{i}$ the multipath component, and represents $\boldsymbol{P(\tau_i)}$ the power of the $\boldsymbol{i}$ the multipath component at delay $\boldsymbol{\tau_i}$. The RMS delay spread $\boldsymbol{\tau_{rms}}$ is the square root of the second central moment of the PDP [39]:

$$\boldsymbol{\tau_{rms}} = \sqrt{\frac{\sum_{i=1}^{N} (\tau_i - \tau_{mean})^2 P(\tau_i)}{\sum_{i=1}^{N} P(\tau_i)}} \quad \textbf{(22)}$$

II.5.MODELS OF WIRELESS THz CHANNEL:

As summarized in Figure II.4. , the methodologies for physical wireless channel modeling can be broadly categorized as **deterministic, stochastic** (or statistical), and **hybrid** approaches.

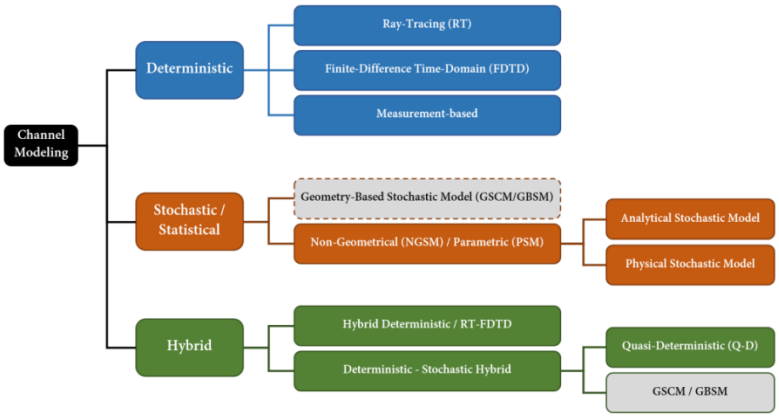

Figure II.4: Channel modeling methodologies.

II.5.1 Deterministic channel models:

Deterministic channel models accurately model the wave propagation based on the theory of electromagnetic (EM) wave propagation [40]. The approach is site-specific, and requires detailed geometric information of the propagation environment, dielectric properties of materials and spatial positions of the Tx and the Rx. Therefore, a deterministic approach provides a good agreement between the simulation results and the measurements in general, though the accuracy varies based on the specific method, the accuracy of the environmental information, and the analyzed frequency band [41].

Deterministic methods solve (approximately) Maxwell's equations in a given environment, and can achieve high accuracy, but require detailed information about the geometry and electromagnetic properties (dielectric constants, loss factors) of the environment and have high computational complexity [42].

a. **Ray-Tracing (RT):** RT has emerged as a popular technique for the analysis of site-specific scenarios, due to its ability to analyze very large structures with reasonable computational resources. The ray-tracing algorithm models the propagation of electromagnetic waves based on the high-frequency approximation of Maxwell's equations, geometrical optics. The locations of the Tx and the Rx are first specified, followed by determining all possible routes between the transceivers, based on high-frequency-approximation rules like geometric optic (GO), geometric theory of diffraction (GTD), uniform theory of diffraction (UTD), and Kirchhoff theory [43]. The technique is especially suitable for THz channels due to the fact that these approximations become more accurate due to the stronger corpuscular property in the THz band, which is associated with the wave-particle (wave corpuscle) duality of light [42].

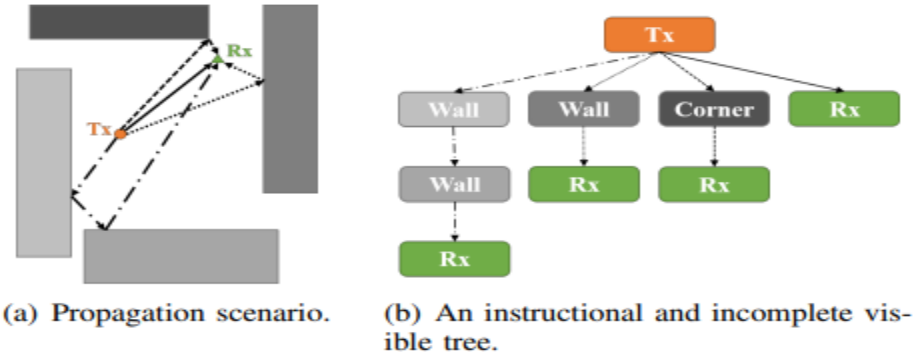

(a) Propagation scenario. (b) An instructional and incomplete visible tree.

Figure II.5: Illustration of the visible tree in a simple propagation scenario.

One strategy for efficiently capturing the individual propagation paths in the tracing process is the so-called visibility tree .The visibility tree is a layered structure used in tracing processes to efficiently capture individual propagation paths. It has nodes representing objects and branches representing LoS connections between nodes. The root node represents the antenna of the Tx. The tree's construction follows a recursive approach, connecting nodes in adjacent layers with branches representing LoS paths. The process is repeated until reaching the highest layer with a pre-set prediction order. After building the tree, a backtracking procedure determines the path of each ray by traversing the tree upwards and applying geometrical optics rules at each traversed node [44].

Deterministic channel models, such as ray tracing, provide detailed predictions of radio wave propagation by accounting for specific physical features of the environment. One fundamental equation used in these models is the Free Space PathLoss (FSPL), which quantifies the loss of signal strength over distance in a free-space environment and is given by:

$$\boldsymbol{FSPL(dB) = 20log_{10}(d) + 20log_{10}(f) - 147.55} \quad \textbf{(23)}$$

Where $\boldsymbol{d}$ is the distance between the transmitter and receiver in meters, and $\boldsymbol{f}$ is the signal frequency in Hz. Reflection loss, another crucial aspect, is calculated using the reflection coefficient and the angle of incidence. The power receives dafter a single reflection can be expressed as:

$$\boldsymbol{P_r = P_t \,.\, |\tau|^2 . \left(\frac{\lambda}{4\pi(d_1+d_2)}\right)^2} \quad \textbf{(24)}$$

Where $\boldsymbol{P_r}$ is the received power, $\boldsymbol{P_t}$ is the transmitted power, $\boldsymbol{\tau}$ is the reflection coefficient, $\boldsymbol{\lambda}$ is the signal wavelength, $\boldsymbol{d_1}$ is the distance from the transmitter to the reflection point, and $\boldsymbol{d_2}$ is the distance from the reflection point to the receiver.

b. Finite-Domain Time-Domain: FDTD is also known as Yee's method named after the Chinese American applied mathematician Kane S. Yee. It is a numerical analysis technique that directly solves Maxwell's equations. FDTD can resolve the impact of small and complex scatterers, and rough surfaces in the THz band, but suffers from very high computational complexity when applied to an environment that has large dimensions in units of wavelength, as often occurs for THz channels [45].

- To implement FDTD, the space is partitioned into grids called Yee cells in the first step. Then the magnetic and electric fields are sampled alternately in both temporal

domain and spatial domain so that each sampled point for magnetic field (H-field) is surrounded by six points for the electric field (Efield)and vice versa, as shown in Figure II.6. [46].

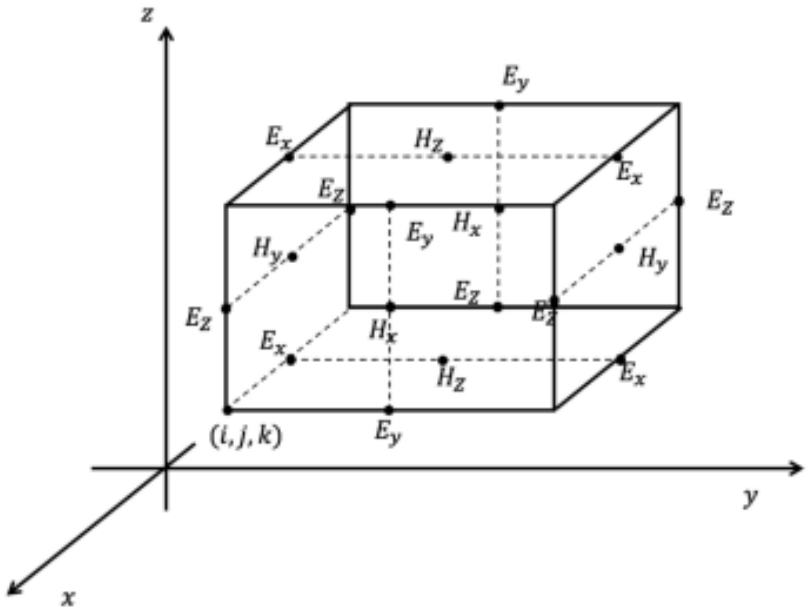

Figure II.6: FDTD implementation.

We assume the strength of electric field or magnetic field **F(x, y, z, t)** (which means, F can be replaced by E or H), is discretized in space and time domain as:

$$\boldsymbol{F^n(i,j,k) = F(i\Delta x, j\Delta y, k\Delta z, n\Delta t)} \quad \textbf{(25)}$$

Where $\Delta\boldsymbol{x}$, $\Delta\boldsymbol{y}$, $\Delta\boldsymbol{z}$ and $\Delta\boldsymbol{t}$ are the steps of three-dimensional space and time. By the central difference method, Maxwell's equations are discretized for further computation. Moreover, this method is especially adaptable for small and complex scattering scenarios in the THz band, where the surface material has a higher roughness level relative to the small wavelength. While RT generally requires a modified or calibrated scattering model, FDTD retains - in principle - accuracy under arbitrary conditions [47].

c. Measurement-based: The measurement-based approach relies on channel measurement along with data storage. The concept of "stored measurements" has been used at least since the 1990s, when channel sounder measurements started to be

stored digitally. Various projects, such as the Metamorp project, attempted to standardize formats for data storage both in the time domain (as impulse response) and frequency domain (transfer function). Major challenges revolve in particular around unified formats of metadata such as calibration data of the channel sounders, and descriptions of the measurement parameters and environments. More recently, the principle of "open source" data has motivated many researchers to place measurement results online for download. Various standardization groups, including the Next G Channel alliance aim to facilitate data exchange. The challenges in the context of THz channels revolve around the size of the measured data, both due to the large bandwidth, and large antenna arrays [48].

II.5.1 Statistical (Stochastic) channel models:

Although deterministic modeling methods provide accurate channel modeling results, they require detailed geometric knowledge of the propagation environment and suffer from high computational complexity. Alternatively, statistical modeling methods could be invoked to describe THz propagation characteristics. Statistical approaches capture statistical behaviors of wireless channels for different scenarios. They thus describe channels in a particular type of environment, not for a particular location. A main strength of statistical channel modeling is the low computational complexity which allows fast channel model construction based on key channel statistics, and thus fast system simulations. For this reason, they are popular for system design and testing, and have been used in the majority of standardized channel models.

Stochastic models are generally categorized into geometry based stochastic channel models (these have been originally abbreviated GSCMs, though the acronym GBSMs is also in use) and nongeometrical stochastic channel models (NGSMs). GSCMs have a geometrical component, while NGSMs follow a completely stochastic manner [49].

GSCM: It has some similarities to deterministic models, which are also based on geometry. The difference is that deterministic models prescribe scatterer locations based on an environmental database, while in GSCM, scatterer locations are chosen in a stochastic fashion according to a certain probability distribution. The similarity is that after the placement of scatterers, wave propagation is captured by applying the fundamental laws of specular reflection, diffraction, and scattering as in RT, though in practice the interaction processes are significantly simplified, with only a subset (such as first- and second-order specular or point scattering) taken into account [48].

NGSMs, also named parametric stochastic models (PSMs), are purely stochastic models. They describe and determine parameters such as direction of departure (DoD), direction of arrival (DoA), and delay, by prescribing underlying probability distribution functions, without taking into account the underlying propagation environment. NGSMs only define paths between transceivers, and aim to get the statistical properties of the parameters in a given channel response by using measurements or ray-tracing. NGSMs are popular in channel modeling due to their simple structure, and thus low computational complexity. However, they have difficulty describing complex relationships between parameters, in particular spatial consistency, and the relationship between the temporal changes of DoDs, DoAs, and delays as a device is moving over larger distances [50].

Stochastic modeling methods can also be divided into **physical and analytical** models. **Physical channel models** characterize the statistics of the double-directional channel characteristics, such as power delay profile, arrival time and angle distribution, which are all independent of the antenna characteristics. In contrast, **analytical models** directly characterize the impulse response of the channel and antenna characteristics in a mathematical way without explicitly accounting for wave propagation [51].

Statistical (stochastic) channel models are essential for representing the randomness and variability inherent in wireless communication environments. One fundamental model is the Rayleigh fading model, which applies to scenarios without a line-of-sight (LOS) component. The received signal amplitude follows a Rayleigh distribution, with the probability density function (PDF) given by:

$$\boldsymbol{P(r) = \frac{r}{\sigma^2} e^{-\frac{r^2}{2\sigma^2}}} \quad , \qquad \boldsymbol{r \geq 0} \qquad \textbf{(26)}$$

Where **r** is the signal amplitude and $\boldsymbol{\sigma}$ is the scale parameter of the distribution. For environments with a strong LOS component, the Rician fading model is more appropriate. The received signal amplitude follows a Rician distribution, described by:

$$\boldsymbol{P(r) = \frac{r}{\sigma^2} e^{-\frac{r^2+s^2}{2\sigma^2} I_0(\frac{TS}{\sigma^2})}} \quad , \qquad \boldsymbol{r \geq 0} \qquad \textbf{(27)}$$

Where $\boldsymbol{S}$ is the LOS component, $\boldsymbol{\sigma}$ is the scale parameter, and $\boldsymbol{I_0}$ is the modified Bessel function of the first kind with order zero.

II.5.2 Hybrid channel models:

As described above, deterministic channel modeling shows high accuracy with high time and resource consumption, while statistical channel modeling benefits from low computational complexity at the cost of accuracy. Therefore, an interesting and promising trend, is to develop hybrid methods by combining the benefits from two or more individual approaches as shown in Figure II.7. Following this path, several attempts on hybrid channel modeling methods have already been presented and channel models based on hybrid modeling methods are also proposed. Next, we introduce several hybrid channel modeling methods. Some of them combine two deterministic approaches (RT and FDTD) and are categorized by hybrid deterministic (RT-FDTD) approach, while others combine deterministic and stochastic approaches [52].

1) Hybrid deterministic / RT-FDTD Approach:

In the RT -FDTD hybrid modeling, FDTD is used to study regions close to complex discontinuities where ray-based solutions are not sufficiently accurate and RT is used to trace the rays outside of the FDTD regions. The RT-FDTD hybrid technique can retain accuracy while improving computation time by applying FDTD only in a small portion of the entire modeling environment, namely the near field of the scatterers, and leaving the rest for RT. This hybrid method is suitable for mmWave and THz channels, and is also implemented in some commercial EM solvers such as High Frequency Structure Simulator (HFSS) [53].

2) Deterministic-Stochastic Hybrid Approach:

While statistical channel models offer high efficiency, they cannot easily reproduce spatial consistency and the temporal evolution of cluster correlations. A variety of models thus exist that combine statistical and geometrical modeling approaches. This allows providing important features of the channel model that cannot be obtained from a purely stochastic model. First, statistical impulse response channel models fail to naturally capture the correlation between links in a multi-user communication system since the random generation for each link cannot guarantee all generated links in the same physical environment. Moreover, the rigid structure of the approach does not naturally support continuous channel descriptions over intervals larger than the stationarity distance, hence hampering the simulation of a large movement of the mobile station. Similarly, the inherent link between changes in angle and directions that follows from geometrical considerations is not easy to reproduce in statistical channel models. For all these reasons, hybrids between geometric and stochastic approaches are useful [54].

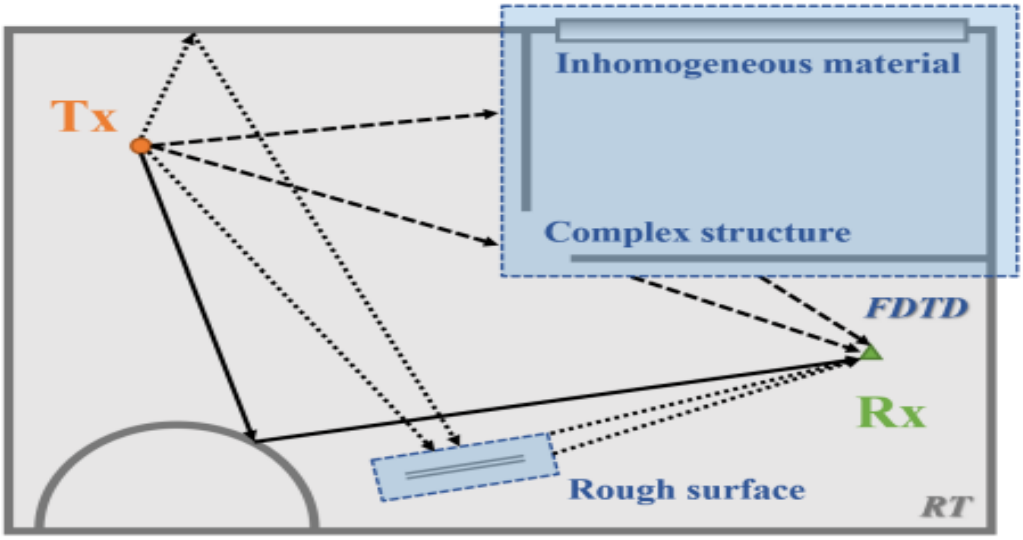

Figure II.7: Ray-tracing and FDTD hybrid approach.

II.6.CONCLUSION:

In this chapter, we have provided thorough and detailed overview about wireless THz channel models.

In conclusion, modeling wireless communication channels effectively requires a combination of deterministic and statistical approaches. Deterministic models provide detailed predictions based on the physical environment, while statistical models account for random variations in signal propagation. Hybrid models integrate both methods, offering a comprehensive frame work that captures the complexities of real-world environments. This blend of approaches ensures robust and accurate analysis and design of wireless communication systems.

CHAPTER III

DESCRIPTION OF OPEN SOURCE NYUSIM SUMILATOR

III.1. OVERVIEW ABOUT NYUSIM SOFTWAR SIMULATOR:

NYUSIM (New York University Simulator) is a sophisticated 5G and 6G wireless communications simulator developed by the NYU WIRELESS research center. It is designed to model and simulate the propagation of radio waves in various environments, providing crucial insights for the development and optimization of next-generation wireless communication systems.

NYU WIRELESS conducted extensive millimeter-wave (mmWave) and sub-Terahertz (THz) measurements spanning from 2012 to 2022, amassing a total of more than 2 TB of raw measurement data [55], [57], at frequencies ranging from 28 to 142 GHz across diverse outdoor and indoor settings including urban microcell (UMi), urban macrocell (UMa), rural macrocell (RMa), indoor hotspot for offices (InH), and indoor factory (InF) environments. The research and analysis detailed in previous works resulted in the creation of the NYUSIM channel simulator, with the latest iteration being NYUSIM version 4.0 released on February 27, 2023. This updated version now includes the capability to simulate wireless channels specifically in the indoor factory (InF) scenario, covering carrier frequencies from 500 MHz to 150 GHz and a RF bandwidth from 0 Hz to 1 GHz.

NYUSIM 4.0 extends the simulation scenario to factory environments by implementing a 3D spatial statistical channel model [73] derived from extensive propagation channel measurements. Furthermore, NYUSIM 4.0 extends the allowable carrier frequency to 500 MHz-150 GHz for all five simulation scenarios (UMi, UMa, RMa, InH, and InF). The maximum RF bandwidth are kept as 800 MHz for carrier frequencies below 100 GHz and extended to 1 GHz for carrier frequencies above 100 GHz, because the 142 GHz propagation measurements conducted in office [65]–[67], outdoor [69]–[70], [81], and factory [71]–[73] environments used wideband probing signals with 1 GHz RF bandwidth. In addition, NYUSIM 4.0 enables spatial consistency-based channel simulations running for all five simulation scenarios to generate realistic channel evolution over time and space. Overall, with this release, the listing of channel models in NYUSIM 4.0 includes the following:

- Indoor channel models for the InF scenario for carrier frequencies from 0.5 to 150 GHz with an RF bandwidth from 0 Hz (CW) to 1 GHz [71]–[73], [81].
- Outdoor channel models for the UMi scenario for carrier frequencies from 0.5 to 150 GHz with an RF bandwidth from 0 Hz (CW) to 1 GHz. [56], [58], [67]–[70], [74], [77], [81], [83]–[89].
- Outdoor channel models for the UMa scenario for carrier frequencies from 0.5 to 150 GHz with an RF bandwidth from 0 Hz (CW) to 1 GHz. [84]–[85], [90], [91].
- Outdoor channel models for the RMa scenario for carrier frequencies from 0.5 to 150z with an RF bandwidth from 0 Hz (CW) to 1 GHz. [60], [86], [92], [93].

- Indoor channel models for the InH scenario for carrier frequencies from 0.5 to 150 GHz with an RF bandwidth from 0 Hz (CW) to 1 GHz. [64]–[66], [78], [94]–[96].

III.2.CHARACTERISTICS OF NYUSIM SOFTWAR:

The software is specifically designed to simulate the characteristics of wireless communication channels, particularly for millimeter-wave (mmWave) and Terahertz (THz) frequencies. Here are the main characteristics of NYUSIM software:

- ✓ **Wide Frequency range:** NYUSIM supports a broad frequency range from 500 MHz to 150 GHz, covering both current and future communication bands, including millimeter-wave (mmWave) frequencies which are crucial for 5G and beyond.
- ✓ **3D Propagation Model:** The simulator employs a 3D statistical spatial channel model to effectively simulate the propagation characteristics of radio waves in various urban, suburban, and rural settings. This encompasses the representation of both line-of-sight (LOS) and non-line-of-sight (NLOS) scenarios.
- ✓ **Multiple Environments:** NYUSIM can simulate various environments such as urbanmicrocells (UMi), urbanmacrocells (UMa), and rural macrocells (RMa), allowing researchers to test and validate their systems in different real-world settings.
- ✓ **Empirical Data Integration:** The simulation model utilized in this study incorporates a comprehensive set of empirical measurements obtained from NYU WIRELESS, ensuring that the results are realistic and reliable. This empirical data covers different building materials, environmental layouts, and weather conditions.
- ✓ **Temporal and Spatial Consistency:** NYUSIM provides consistent modeling over time and space, which is essential for studying mobile user scenarios and hand off strategies in cellular networks.
- ✓ **Stochastic Channel Modeling:** The tool incorporates stochastic processes to model the small-scale fading and large-scale pathloss, including parameters like delay spread, angular spread, and Doppler shift, crucial for MIMO (Multiple Input Multiple Output) and beam forming technologies.
- ✓ **Open Source Availability:** NYUSIM is available as open-source software, which allows researchers and developers to freely use, modify, and enhance the simulator according to their needs. This promotes collaboration and accelerates advancements in wireless technology research.

NYUSIM provides an accurate rendering of actual channel impulse responses in both time and space, as well as realistic signal levels that were measured, and may be utilized to support realistic physical-level and link-level simulations such as those conducted in [70], [79], [98]–[99]. The models and simulation approach in NYUSIM.

III.3.DESCRIPTION OF NYUSIM:

III.3.1.Graphical User Interface and Simulator Basics:

The screenshot in Figure III.1 shows the GUI of NYUSIM 4.0. The simulator performs Monte Carlo simulations, generating samples of CIRs at specific T-R separation distances. Note that the range of T-R separation is provided by the user, and the actual T-R separation distance is uniformly selected from the user-specified distance range. Two running modes, drop-based mode and spatial consistency mode are made available from NYUSIM 2.0. When the spatial consistency button is “on”, NYUSIM runs spatial consistency procedure and generates successive and correlated CIRs along the UT trajectory. When the spatial consistency button is “off”, NYUSIM runs the drop-based model which is the same as previous versions of NYUSIM and generates independent CIRs for different distances. Note that human blockage module works for both drop based mode and spatial consistency mode. While earlier versions of NYUSIM provided outdoor channel models coupled with outdoor-to-indoor penetration and indoor office scenario NYUSIM 4.0 introduces the indoor factory scenario. The indoor factory scenario can be selected under the “Scenario” drop-down list. **The spatial consistency feature is now enabled for all scenarios including indoor office and indoor factory scenarios.** NYUSIM 4.0 can also simulate frequencies from 500 MHz - 150 GHz with RF bandwidths 0 - 800 MHz (for frequencies less than 100 GHz) and 0 - 1 GHz (for frequencies greater than or equal to 100 GHz).

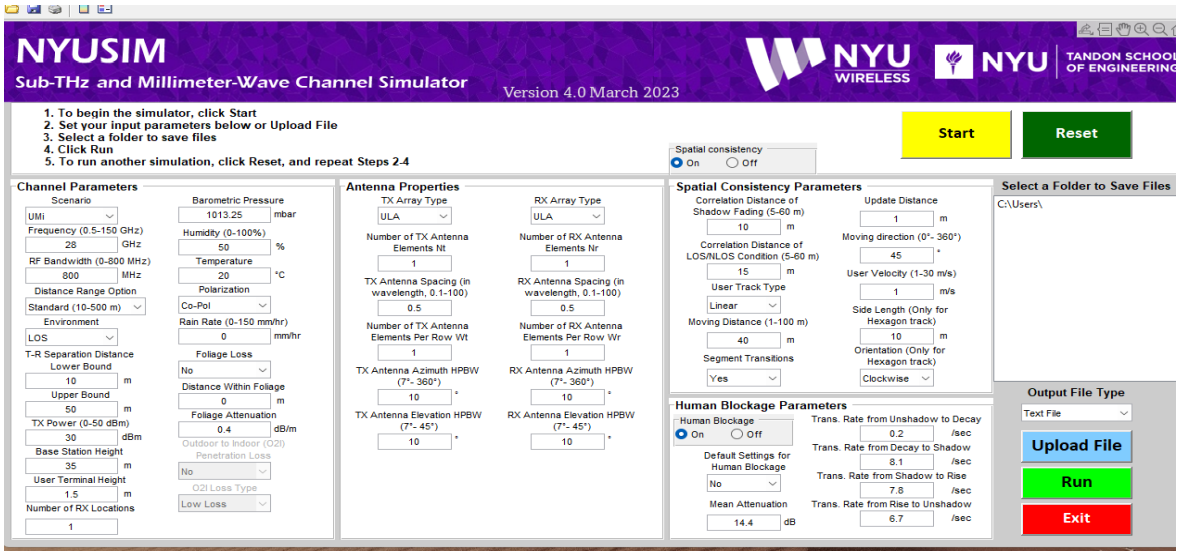

Figure III.1: Graphical User Interface (GUI) of NYUSIM 4.0 with four panels: channel parameters, antenna properties, spatial consistency parameters, human blockage parameters.

III.3.2.Input Parameters Of The Channel Simulator:

There are 49 input parameters to the channel simulator, which are grouped into four main categories: **Channel Parameters, Antenna Properties, Spatial Consistency Parameters,** and **Human Blockage Parameters**, as shown on the GUI in Figure III.1. Note that two input parameters for O2I penetration loss are put into the panel Channel Parameters.

The panel **Channel Parameters** contains 19 fundamental input parameters about the propagation channel, as listed and explained below:

1) Scenario: a selectable parameter denoting the scenario. Five channel scenario options, urban microcell (“UMi”), urban macrocell (“UMa”), rural macrocell (“RMa”), indoor hotspot (“InH”) and indoor factory (”InF”) are applicable. The default scenario option is “UMi”. All scenarios support carrier frequency range from 0.5 - 150 GHz. Selecting "InH" or "InF" will change the distance range option from “Standard (10-500m)” to “Indoor (5-100 m), the upper limit of base station height from 150 m (for outdoor scenarios) to 3 m. Selecting the “InH” or "InF" option will also disable following options: “Rain Rate”, “Foliage Loss”, “Distance Within Foliage”, “Foliage Attenuation”, “Outdoor to Indoor (O2I) Penetration Loss”, “O2I Loss Type”.

2) Frequency (GHz): an editable parameter denoting the carrier frequency in GHz. The default value is 28 (GHz), and it can be varied from 0.5 to 150 (GHz) with at most one decimal place for all the scenarios.

3) RF Bandwidth (MHz): an editable parameter denoting the RF bandwidth of the transmitted signal in MHz. The default value is 800 MHz, and it can be varied from 0 to 800 MHz for frequencies less than 100 GHz and 0 to 1000 MHz for frequencies greater than or equal to 100 GHz. As the simulator was developed from real-world measurements obtained with an RF bandwidth of 800 MHz for frequencies less than 100 GHz, it can only scale down from 800 MHz for the frequencies less than 100 GHz. For frequencies above 100 GHz the measurements were conducted at 142 GHz using probing signals with 1 GHz RF bandwidth, thus NYUSIM has been extended to support RF bandwidths of 0 - 1 GHz for frequencies above 100 GHz.

4) Distance Range Option: a selectable parameter denoting the distance range. Three options, “Standard (10-500 m)”, “Extended (10-10,000 m)", and “Indoor (5-100 m)” are applicable. The default setting is “Standard (10-100 m)”. For distances less than 500 m, the dynamic range (largest possible path loss) is set to 190 dB in NYUSIM based on field measurement results [58], [68], [76], while for the distance range beyond 500 m, the dynamic range is set to 220 dB. When “InH” or "InF" is selected, the “Distance Range Option” is fixed to be “Indoor (5-100 m)” option.

5) Environment: a selectable parameter denoting the environment, either line-of sight (LOS) or non-line-of-sight (NLOS). The default setting is LOS.

6) Lower Bound of T-R Separation Distance (m): an adjustable parameter indicating the minimum separation distance in meters between the transmitter (TX) and receiver (RX) with precision to one decimal place. The default setting is 10 meters, and it is adjustable within the range of 10 meters to 500 meters for standard distances (validated through comprehensive assessments by NYU), 10 meters to 10 kilometers for extended distances, and 5 meters to 50 meters for indoor distances, while not exceeding the maximum separation distance between the transmitter and receiver.

7) Upper Bound of T-R Separation Distance (m): an adjustable parameter represents the maximum distance between the transmitter (TX) and receiver (RX) in meters, with precision to one decimal place. The default setting is 50 meters, and it can be adjusted within the range of 10 to 500 meters for standard distances (validated through comprehensive assessments conducted by NYU), 10 meters to 10 kilometers for extended distances, and 5 meters to 50 meters for indoor distances, ensuring it does not fall below the minimum separation distance between the transmitter and receiver.

8) TX Power (dBm): an adjustable parameter representing the transmission power level in decibels relative to one milliwatt (dBm). The initial setting is 30 dBm, with the ability to be adjusted within a range of 0 to 50 dBm.

10) Base Station Height (m): an editable parameter denoting the base station height in meters. The default value is 35 (m) [101], and can be set to any value ranging from 10 to 150 (m) [60]. This base station height is only applicable to RMa modeling and is ignored for UMi and UMa scenarios. The maximum height of stations is 5 m for the InH and InF scenarios.

11) User Terminal Height (m): an editable parameter denoting the UT height in meters. The default value is 1.5 (m) [101], and can be set to any value ranging from 1 to 10 (m) above the ground [60].

12) Barometric Pressure: an editable parameter denoting the barometric pressure in mbar used in evaluating propagation path loss induced by dry air. The default and typical value is 1013.25 mbar (millibar) (nominal for sea level), and may range from 10−5to 1013.25 (mbar) [106].

13) Humidity: an editable parameter denoting the relative humidity in percentage used in evaluating propagation path loss induced by vapor. The default value is 50 (%), and can be set to any number between 0 and 100 (%).

14) Temperature: an editable parameter denoting the temperature in degrees Celsius used in evaluating propagation path loss induced by haze/fog. The default and typical value is 20 (◦C), and may range from -100 to 50 (◦C) [106].

15) Rain Rate: an editable parameter denoting the rain rate in mm/hr used in evaluating additional propagation path loss induced by rain. The default value is 0 (mm/hr), and the typical range is 0 to 150 (mm/hr) [58]. This option is disabled for the InH and InF scenarios.

16) Polarization: a selectable parameter denoting the polarization relation between the TX and RX antennas or antenna arrays. The default setting is Co-Pol (co polarization), and can be changed to X-Pol (cross-polarization), Co/X-Pol (co and cross-polarization), and all-Pol (V-V, H-H, V-H, and H-V polarization).

17) Foliage Loss: a selectable parameter indicating whether or not foliage loss will be considered in the simulation. The default setting is "No" (which implies foliage loss will not be considered), and can be changed to "Yes" (which means foliage loss will be considered). This option is disabled for the InH and InF scenarios.

18) Distance Within Foliage: an editable parameter representing the distance in meters that the transmitted signal travels within foliage. The default value is 0, and can be set to any non-negative number no larger than the lower bound of the T-R separation distance. This option is disabled for the InH and InF scenarios.

19) Foliage Attenuation: an editable parameter denoting the propagation loss induced by foliage in dB/m. The default value is 0.4 (dB/m) based on the measurement results in [108], and can be set to any value between 0 and 10 (dB/m). For more detailed background, please refer to [108]. This option is disabled for the InH and InF scenarios.

20) Number of RX Locations: an editable parameter denoting the number of RX locations. It can be any positive integer number. The default value is 1, and can be set to any integer from 1 to 10,000.

21) Outdoor to Indoor (O2I) Penetration Loss: a selectable parameter denoting that a UT is in an indoor or outdoor scenario. Two options, "Yes" and "No", are provided. The default value is "No". If "Yes" is selected, additional building penetration loss will be added to the total received power before small-scale parameters are generated [105], [109]. If "No" is selected, penetration loss is not considered. This option is disabled for the InH and InF scenarios.

22) O2I Loss Type: a selectable parameter denoting the O2I loss type. Two options, "Low Loss" and "High Loss", are provided. The "Low Loss" model corresponds to low loss building materials such as standard glass and wood [104], [105]. The "High Loss" corresponds to high loss building materials such as infrared reflecting (IRR) glass and concrete [104], [105]. This option is disabled for the InH and InF scenarios.

The panel **Antenna Properties** contains 12 input parameters related to the TX and RX antenna arrays, as listed and explained below:

1) **TX Array Type:** a selectable parameter denoting the TX antenna array type. The default setting is ULA (uniform linear array), and can be changed to URA (uniform rectangular array).
2) **RX Array Type:** a selectable parameter denoting the RX antenna array type. The default setting is ULA, and can be changed to URA.
3) **Number of TX Antenna Elements Nt:** an editable parameter denoting the total number of TX antenna elements in the array. The default value is 1, and can be set to any integer from 1 to 128.
4) **Number of RX Antenna Elements Nr:** an editable parameter denoting the total number of RX antenna elements in the array. The default value is 1, and can be set to any integer from 1 to 64.
5) **TX Antenna Spacing (in wavelength):** an editable parameter denoting the spacing between adjacent TX antennas in the array in terms of the carrier wavelength. The default value is 0.5, and can be set to any positive number with up to one decimal place from 0.1 to 100.
6) **RX Antenna Spacing (in wavelength):** an editable parameter denoting the spacing between adjacent RX antennas in the array in terms of the carrier wavelength. The default value is 0.5, and can be set to any positive number with up to one decimal place from 0.1 to 100.
7) **Number of TX Antenna Elements Per Row Wt:** an editable parameter denoting the number of TX antennas in one dimension when the TX Array Type is ULA or URA, which should divide the number of TX antenna elements. The default value is 1.
8) **Number of RX Antenna Elements Per Row Wr:** an editable parameter denoting the number of RX antennas in one dimension when the RX Array Type is ULA or URA, which should divide the number of RX antenna elements. The default value is 1.
9) **TX Antenna Azimuth HPBW (degrees):** an editable parameter denoting the azimuth half-power-beamwidth (HPBW) of the TX antenna (array) in degrees. The default value is 10◦, and can be set to any value from 7◦to 360◦ (since the smallest azimuth HPBW of the antennas used in the measurements for the simulator was 7◦).
10) **TX Antenna Elevation HPBW (degrees):** and can be set to any value from 7◦to 45◦ (since the smallest elevation HPBW of the antennas used in the measurements for the simulator was 7◦). An editable parameter denoting the elevation HPBW of the TX antenna (array) in degrees. The default value is 10◦.
11) **RX Antenna Azimuth HPBW (degrees):** an editable parameter denoting the azimuth HPBW of the RX antenna (array) in degrees. The default value is 10◦, and can be set to any value from 7◦to 360◦.
12) **RX Antenna Elevation HPBW (degrees):** an editable parameter denoting the elevation HPBW of the RX antenna (array) in degrees. The default value is 10◦, and can be set to any value from 7◦to 45◦.

The panel **Spatial Consistency** contains 10 input parameters related to the spatial consistency implementation, as listed and explained below:

1) Correlation Distance of Shadow Fading (5-60 m): an editable parameter denoting the correlation distance of shadow fading. The default value is 10 m. Correlation distance of shadow fading, also known as "local area" determines the length of a channel segment. Correlation distance is the distance beyond which the auto-correlation value of a large-scale parameter (LSP) falls below 0.5 [62].

2) Correlation Distance of LOS/NLOS Condition (5-60 m): an editable parameter denoting the correlation distance of LOS/NLOS condition.

3) UT Track Type: a selectable parameter denoting the UT track type. Two options, "Linear" and "Hexagon" are provided to the user. The default option is "Linear" [64].

4) Track Distance (1-100 m): an editable parameter denoting the track length of a UT trajectory. Note that the input track distance for the "Hexagon" track should not be larger than the perimeter of the hexagon. Realistic CIR generation cannot be guaranteed out of the limit. The track distance is divided into multiple channel segments based on the correlation distance of shadow fading.

5) Update Distance (<1 m): an editable parameter denoting the distance interval between two channel snapshots. The default value is 1 m.

6) Moving direction (0◦-360◦): an editable parameter denoting the initial UT moving direction. The default value is 45◦. Both "Linear" and "Hexagon" track require an initial moving direction.

7) UT Velocity (1 - 30 m/s): an editable parameter denoting the UT velocity. The default value is 1 m/s, close to the typical human walking speed. The UT velocity in concert with the update distance determine the update time which is the time interval between two consecutive CIRs.

8) Side Length: an editable parameter denoting the side length of the hexagon track. This parameter only works for the "Hexagon" track. The default value is 10.

9) Orientation: a selectable parameter denoting the orientation of the hexagon track. This parameter only works for the "Hexagon" track. Two options, "Clockwise" and "Counter", are provided.

10) Segment Transitions: a selectable parameter denoting whether the smooth transitions between two segments. Two options, "Yes" and "No" are provided. With "Yes" selected a post-processing is done to "connect" generated channel segments via cluster birth and death. "No" generates independent channel segments, with channel snapshots are spatially correlated in each channel segment [64].

The panel **Human Blockage** contains 6 input parameters related to the human blockage shadowing loss due to a person near the mobile phone (UT), as listed and explained below. Human blockage can be turned "on" or "off". As explained in Section 3, the length of a Markov trace is 20 s long, and the time resolution is 1ms.

1) **Default Settings for Human Blockage:** a selectable parameter. Two options, "Yes" and "No", are provided. If the user chooses "Yes", the transition rates and average mean attenuation are implemented based on a linear fit to the data given in [95], and changes to fit the work in [95] as the RX antenna azimuth HPBW changes. If the user chooses "No", the transition rates and mean attenuation are free to edit for user-specified preferences, in case other Markov model parameters are preferred or discovered in the future [95], [103].
2) **Mean Attenuation:** an editable parameter denoting the mean attenuation of blockage events (SEmean). The default value is 14.4 dB.
3) **Trans. Rate from Unshadow to Decay (1/s):** an editable parameter denoting the transition rate from unshadowed state to decay state. The default value is 0.20 when the RX antenna azimuth HPBW is 10◦.
4) **Trans. Rate from Decay to Shadow (1/s):** an editable parameter denoting the transition rate from decay state to shadowed state. The default value is 8.08 when the RX antenna azimuth HPBW is 10◦.
5) **Trans. Rate from Shadow to Rise (1/s):** an editable parameter denoting the transition rate from shadowed state to raise state. The default value is 7.85 when the RX antenna azimuth HPBW is 10◦.
6) **Trans. Rate from Rise to Unshadow (1/s):** an editable parameter denoting the transition rate from rise state to unshadowed state. The default value is 6.70 when the RX antenna azimuth HPBW is 10◦.

III.3.3.Output Files:

Since the last Versions, NYUSIM provides two running simulation modes, drop-based mode and spatial consistency mode, which depends on that the spatial consistency feature, is "on" or "off". In this chapter we are going to focus only on the spatial consistency mode.

III.3.4. Spatial Consistency Mode:

The spatial consistency mode in NYUSIM involves the assumption that a User Terminal (UT) follows a defined trajectory, resulting in the generation of correlated and consecutive channel impulse responses for each sampling point along the path. This mode allows for the creation of a sequence of spatially correlated and time-varying channel responses within the NYUSIM framework. Through simulation, numerous closely spaced channel impulse responses can be produced based on the movement and speed of the UT.

For each simulation run, four figures will be generated and stored that are based on the particular results of the simulation that is being run. These four figures will pop up on the screen for visual purposes. The contents of those figures are as follows:

- A spatially correlated shadow fading map depicting the locations of User Terminals (UT) and Base Stations (BS), along with the UT track, is presented in Figure III.2. The figure includes essential details such as frequency, environmental conditions, distance between transmitter and receiver (T-R separation), and standard deviation of shadow fading, track distance, and velocity.

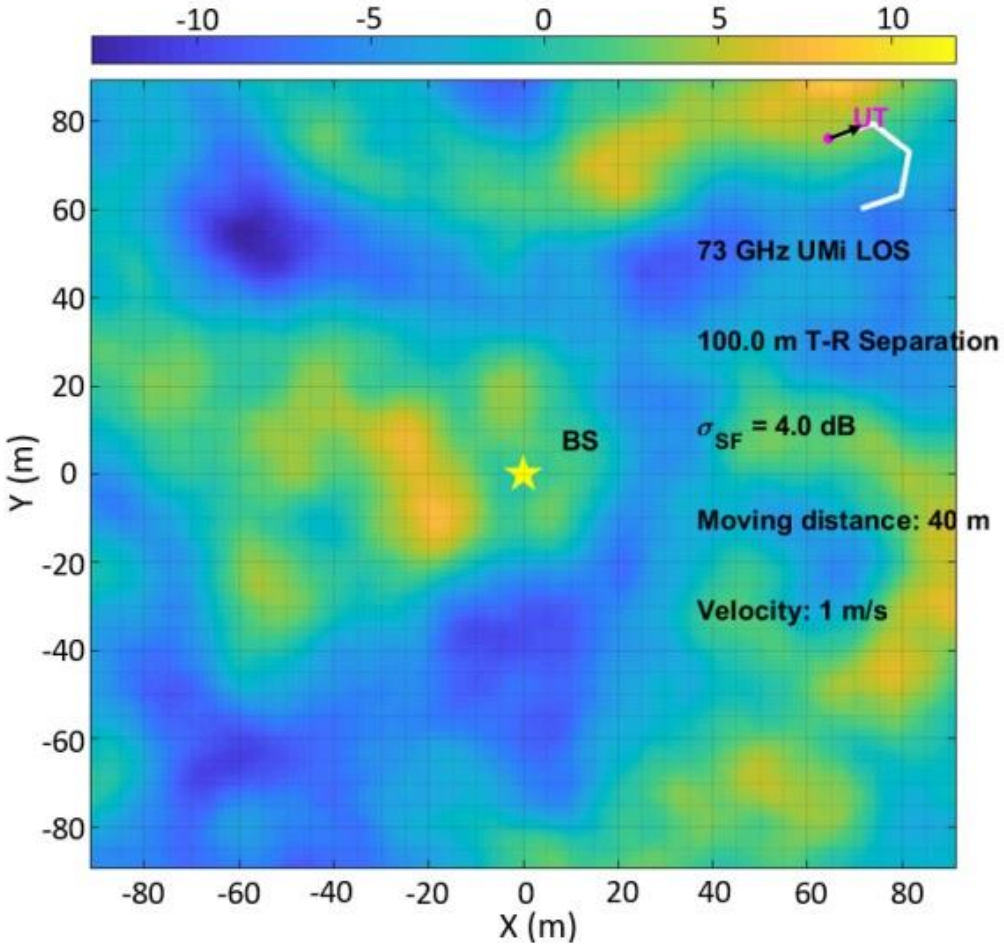

Figure III.2: Map of spatially correlated shadow fading with the BS and UT locations.

- A spatially correlated map depicting Line-of-Sight (LOS) and Non-Line-of-Sight (NLOS) conditions based on scenario-specific LOS probability is presented in Figure III.3. This map high lights that all sites within a given area encounter consistent propagation conditions. Essential details including frequency, environment characteristics, and transmitter-receiver separation distance, standard deviation of shadowing fading, track distance, and velocity are provided within the illustration.

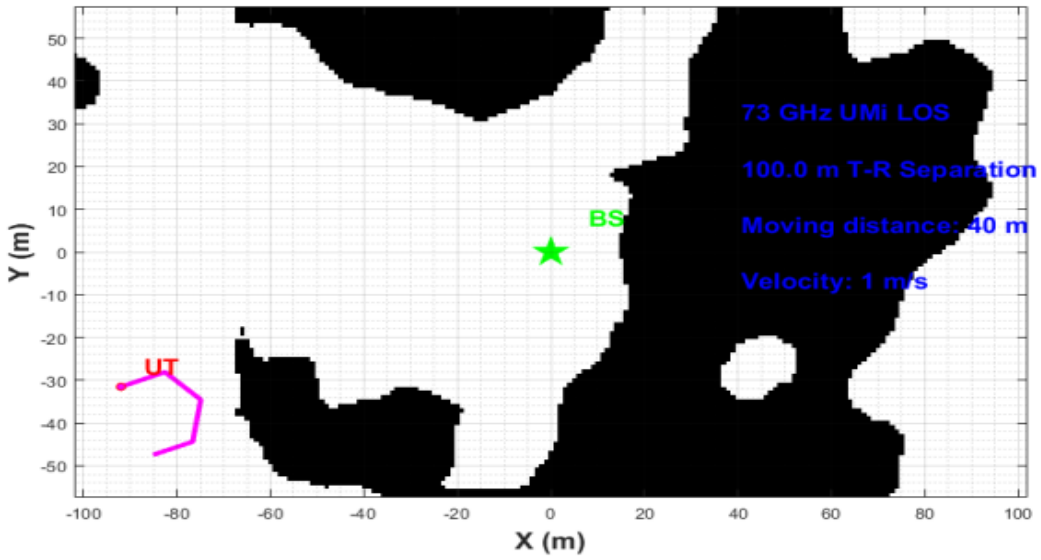

Figure III.3: Sample map of spatially correlated LOS/NLOS condition.

- User track: The part of the map for spatially correlated shadow fading along which the UT moves as illustrated in Figure III.4. The moving direction and track distance are shown in this figure:

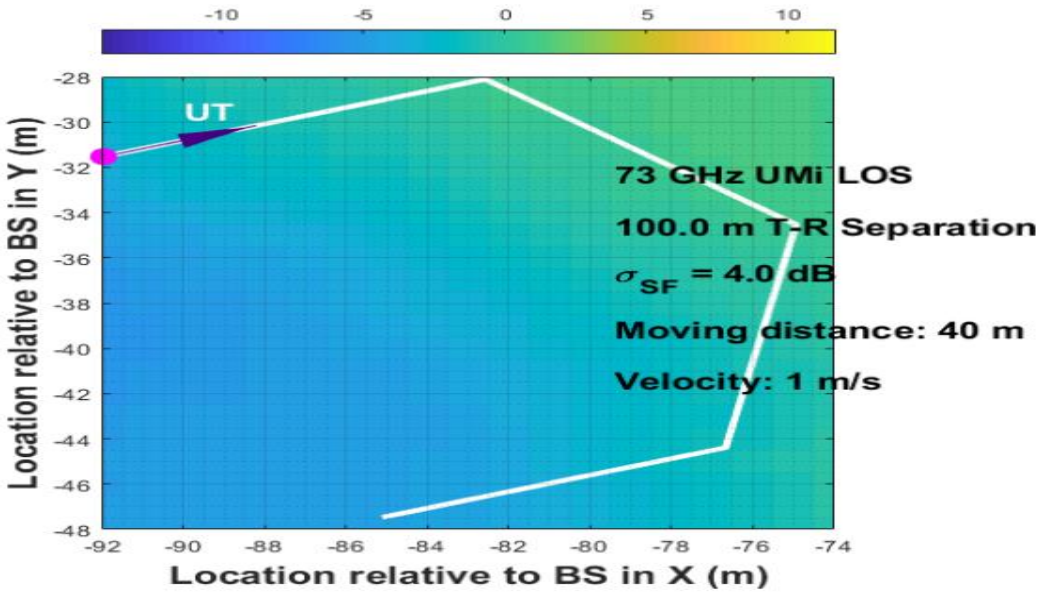

Figure III.4: Sample user track.

- Sequential omnidirectional Power Delay Profiles (PDPs) are illustrated in Figure III.5 to demonstrate the fluctuation in power levels and temporal displacement of Multipath Components (MPCs) as the user moves along a trajectory. These profiles incorporate directional antenna gain patterns at the transmitter (TX) and/or receiver (RX). The PDP plot includes essential details such as frequency, environmental conditions, distance between transmitter and receiver, trajectory length, and velocity.

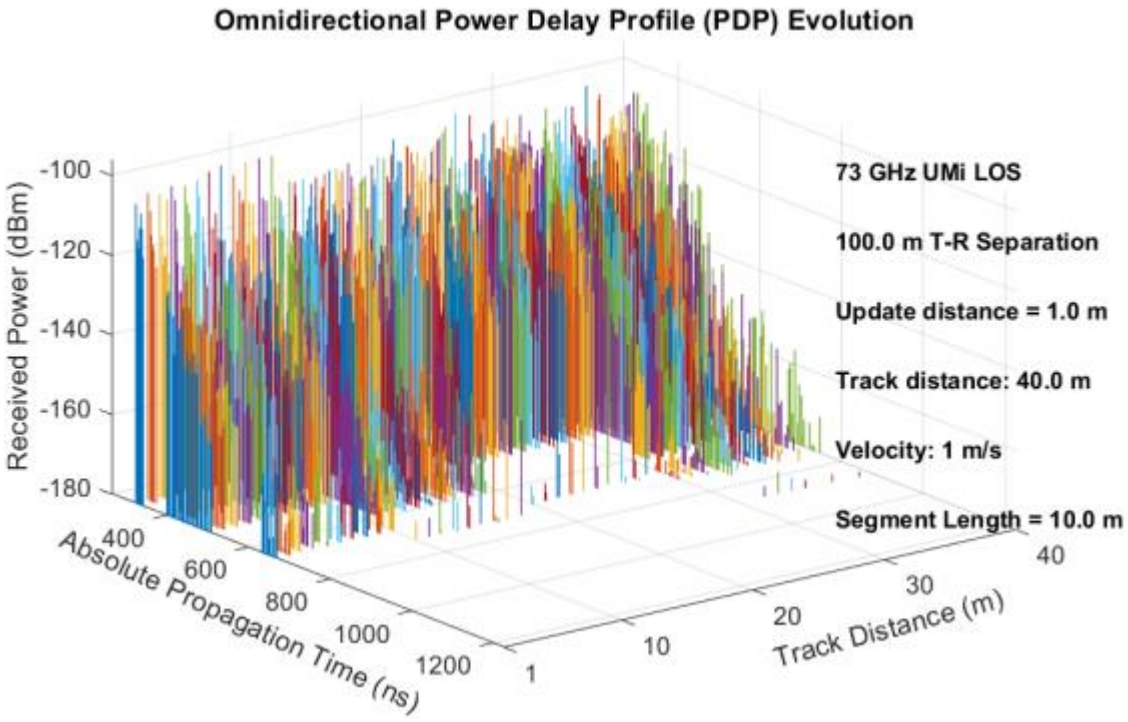

Figure III.5: Sample consecutive omnidirectional PDPs.

III.4.CONCLUSION:

NYUSIM, an innovative simulation tool created by NYU WIRELESS, has been developed to enhance the wireless communications domain by offering a precise and adaptable platform for simulating radio wave propagation within a broad frequency spectrum spanning from 500 MHz to 150 GHz. Through the incorporation of empirical data, three-dimensional propagation models, and compatibility with diverse environments, NYUSIM facilitates the generation of realistic and dependable simulations that are essential for advancing research in 5G and 6G technologies.

CHAPTER IV

SIMULATION AND RESULTS

IV.1. INTRODUCTION:

The evolution of wireless communication technologies has increasingly focused on higher frequency bands, particularly the terahertz (THz) spectrum, which promises unprecedented data rates and bandwidth. As the demand for faster and more reliable communication grows, understanding the distinct characteristics of different propagation environments is crucial.

This chapter delves into an examination of Urban Micro (UMi) and Rural Macro (RMa) environments in the context of terahertz communication channels, exploring their unique characteristics and factors.

In this final chapter we present the simulation results. We use NUYSIM software to simulate the THz Channel as a main program according with MATLAB to simulate the results.

IV.2.DEFINING UMi AND RMa ENVIRONMENTS:

Urban Micro (UMi): The UMi environment is characterized by densely packed buildings, a high density of users, and numerous obstacles such as vehicles and street furniture. This environment necessitates a robust understanding of non-line-of-sight (NLOS) conditions and multipath propagation, which significantly affect THz signal behavior.

Rural Macro (RMa): In contrast, the RMa environment features sparse settlements, open fields, and fewer obstacles. The propagation in RMa scenarios is primarily line-of-sight (LOS), but the challenges include extended distances and the presence of foliage and terrain variations, which can affect signal strength and reliability over longer ranges.

IV.3 KEY PARAMETERS IN THz COMMUNICATION:

To effectively analysis UMi and RMa environments, several key parameters must be considered:

- **Path Loss:** The rate at which the signal attenuates as it travels through the environment.
- **Shadowing Effects:** The impact of obstacles causing signal blockage and shadowing.
- **Multipath Propagation:** The behavior of reflected signals causing constructive and destructive interference.
- **Atmospheric Absorption:** The degree to which atmospheric constituents absorb THz signals.
- **Antenna Design and Placement**: Strategies for optimizing signal transmission and reception in diverse environments.

IV.4. SIMULATION RESULTS:

The use of multiple antennas, specifically two antennas at both the transmitter and receiver, significantly affects the channel response in both Urban Micro (UMi) and Rural Macro (RMa) environments in the context of terahertz (THz) communication channels. This setup typically leverages Multiple Input Multiple Output (MIMO) techniques to enhance signal quality and data rates.

- For UMi scenarios:

Parameter	Value	Parameter	Value
Frequency	150	RxAzHPBW	10
Bandwidth	800	RxElHPBW	10
TXPower	30	SCenable	On
Environment	LOS	CorrDistanceSF	16
Scenario	UMi	CorrDistanceLOS	13
TXHeight	35	TrackType	Linear
RXHeight	1.5	MovDistance	46
Pressure	1.0132e+03	MovDirection	45
Humidity	50	UpdateDist	1
Temperature	20	Velocity	3.2
RainRate	0	HBenable	On
Polarization	Co-Pol	HBdefault	No
Foliage	No	SEMean	15.8
DistFol	0	U2Drate	0.21
FoliageAttenuation	0.4	D2Srate	7.88
TxArrayType	ULA	S2Rrate	7.7
RxArrayType	ULA	R2Urate	7.67
NumberOfTxAntenna	1	distType	Standard (10-500 m)
NumberOfRxAntenna	1	dmin	10
NumberOfTxAntennaPerRow	1	dmax	50
NumberOfRxAntennaPerRow	1	Nsim	1
TxAntennaSpacing	0.5	o2iLoss	No
RxAntennaSpacing	0.5	o2iType	Low Loss
TxAzHPBW	10	side_length	12
TxElHPBW	10	orient	Clockwise
transExist	Yes		

Table IV.1: Parameters of channel (UMi scenario S1).

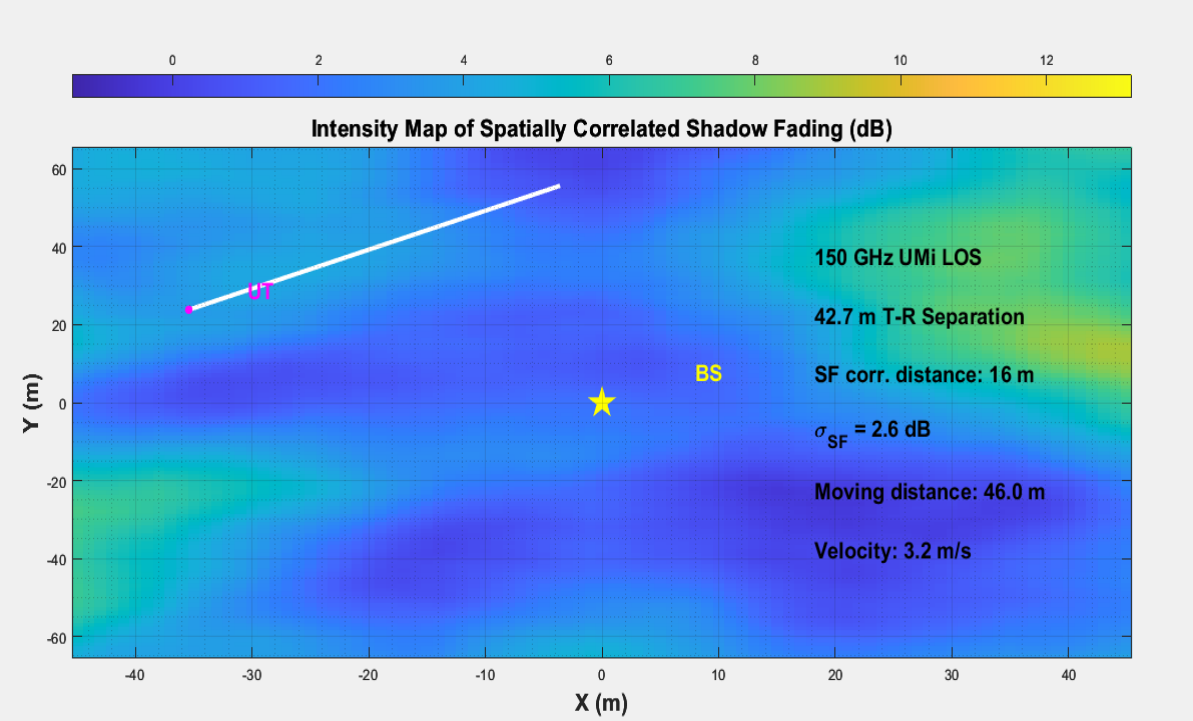

FigureIV.1: Map of spatially correlated shadow fading with the BS and UT locations (UMi scenario S1).

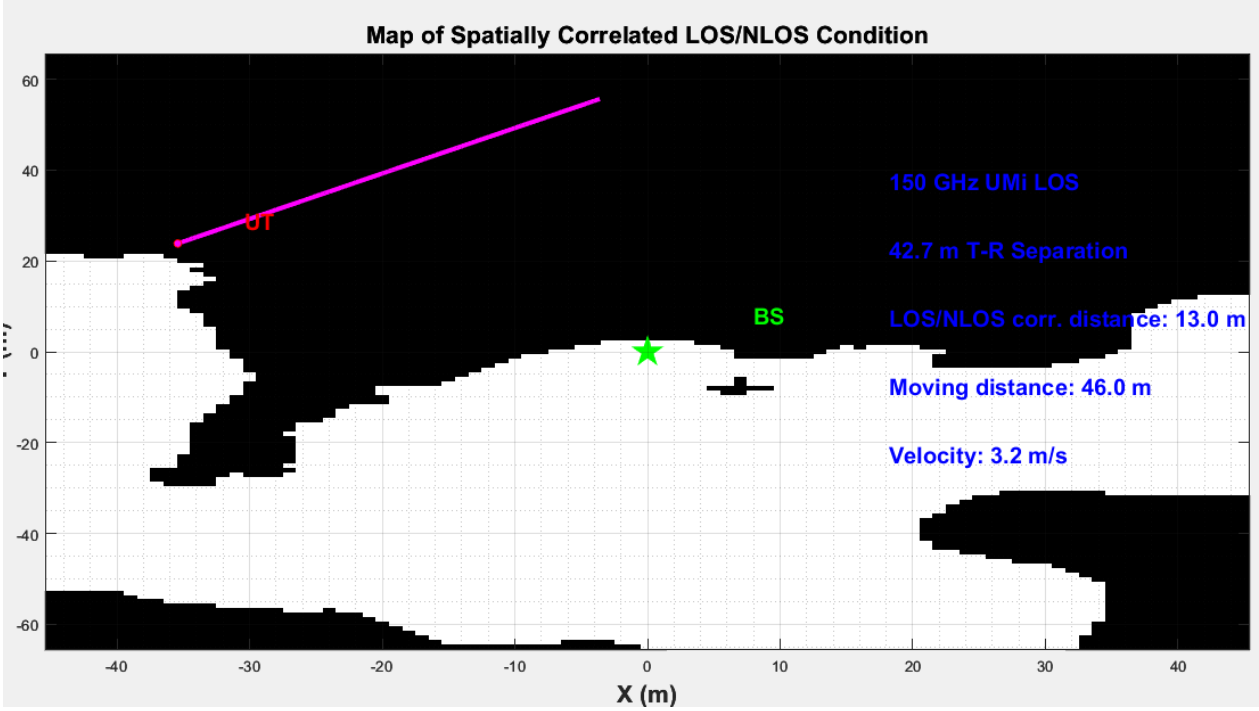

Figure IV.2: Sample map of spatially correlated LOS/NLOS condition (UMi scenario S1).

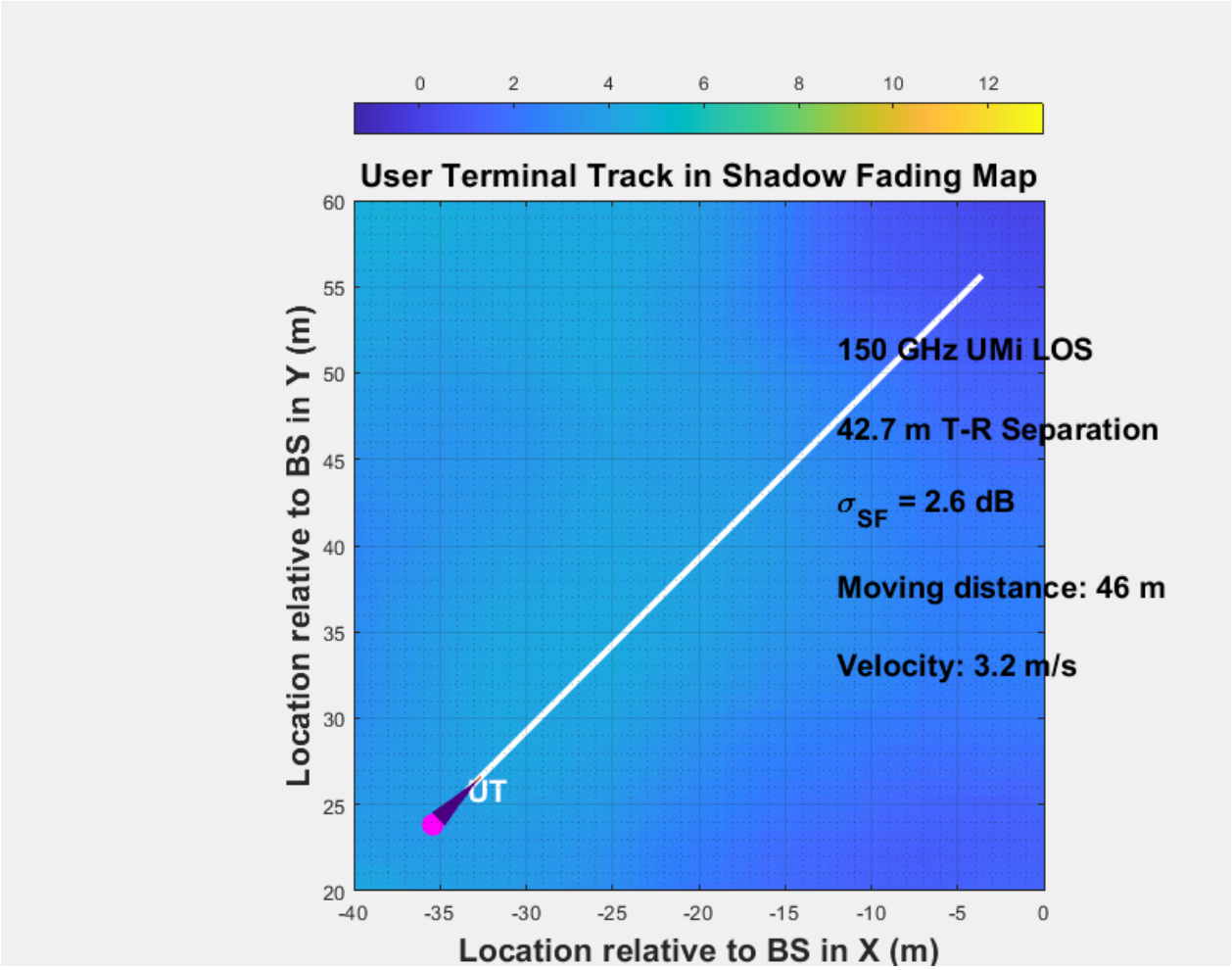

Figure IV.3: Sample user track (UMi scenario S1).

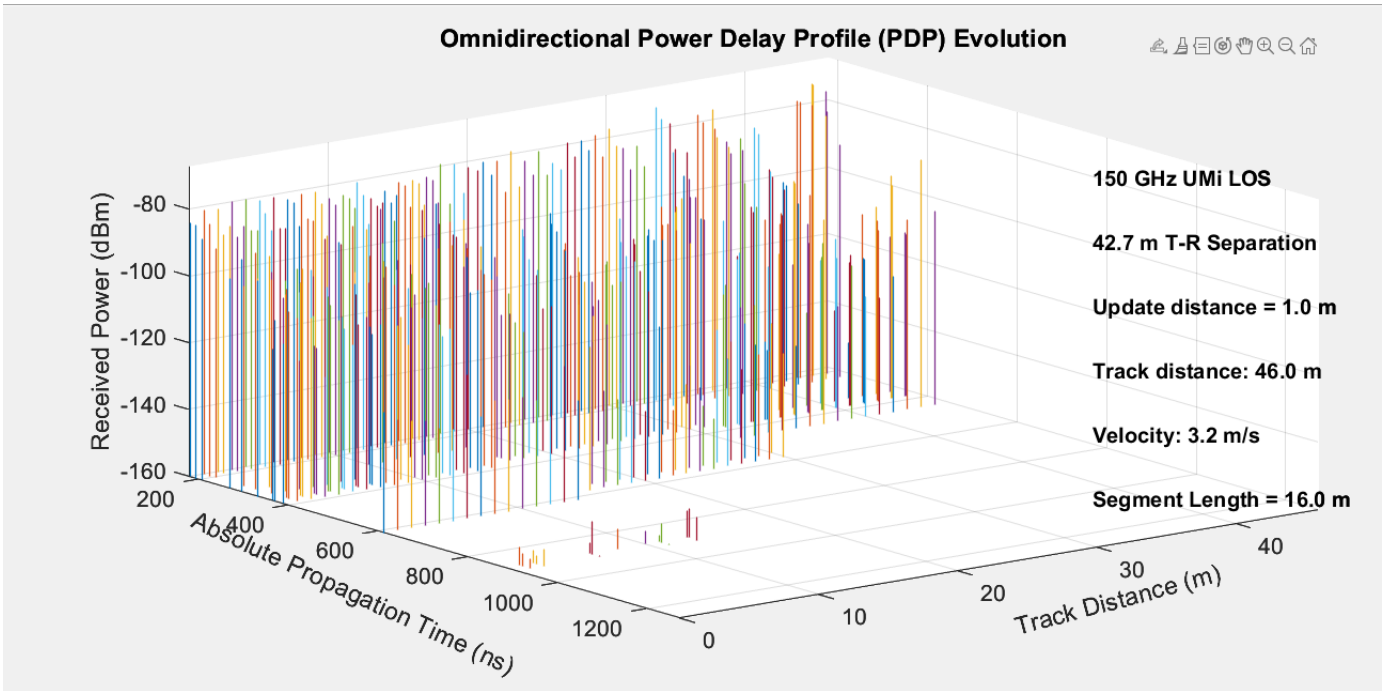

FigureIV.4: Sample consecutive omnidirectional PDPs (UMi scenario S1).

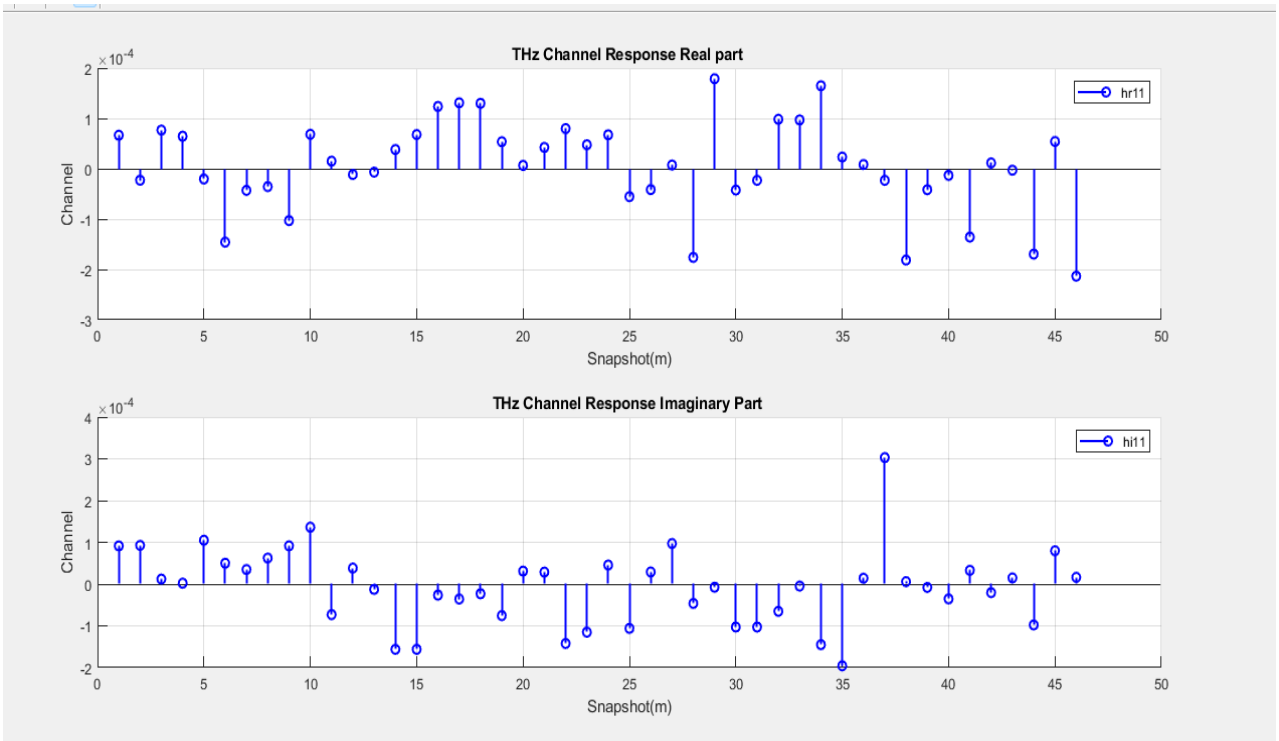

Figure IV.5: THz Channel response of real and imaginary part of $N_T = 1, N_R = 1$ for UMi scenario S1.

Parameter	Value	Parameter	Value
Frequency	150	RxAzHPBW	10
Bandwidth	800	RxElHPBW	10
TXPower	30	SCenable	On
Environment	LOS	CorrDistanceSF	16
Scenario	UMi	CorrDistanceLOS	13
TXHeight	35	TrackType	Linear
RXHeight	1.5	MovDistance	46
Pressure	1.0133e+03	MovDirection	45
Humidity	50	UpdateDist	1
Temperature	20	Velocity	3.2
RainRate	0	HBenable	On
Polarization	Co-Pol	HBdefault	No
Foliage	No	SEMean	15.8
DistFol	0	U2Drate	0.21
FoliageAttenuation	0.4	D2Srate	7.88
TxArrayType	ULA	S2Rrate	7.7
RxArrayType	ULA	R2Urate	7.67
NumberOfTxAntenna	2	distType	Standard (10-500 m)
NumberOfRxAntenna	2	dmin	10
NumberOfTxAntennaPerRow	2	dmax	50
NumberOfRxAntennaPerRow	2	Nsim	1
TxAntennaSpacing	0.5	o2iLoss	No
RxAntennaSpacing	0.5	o2iType	Low Loss

TxAzHPBW	10	side_length	12
TxElHPBW	10	orient	Clockwise
transExist	Yes		

Table IV.2: Parameters of channel (UMi scenario S2).

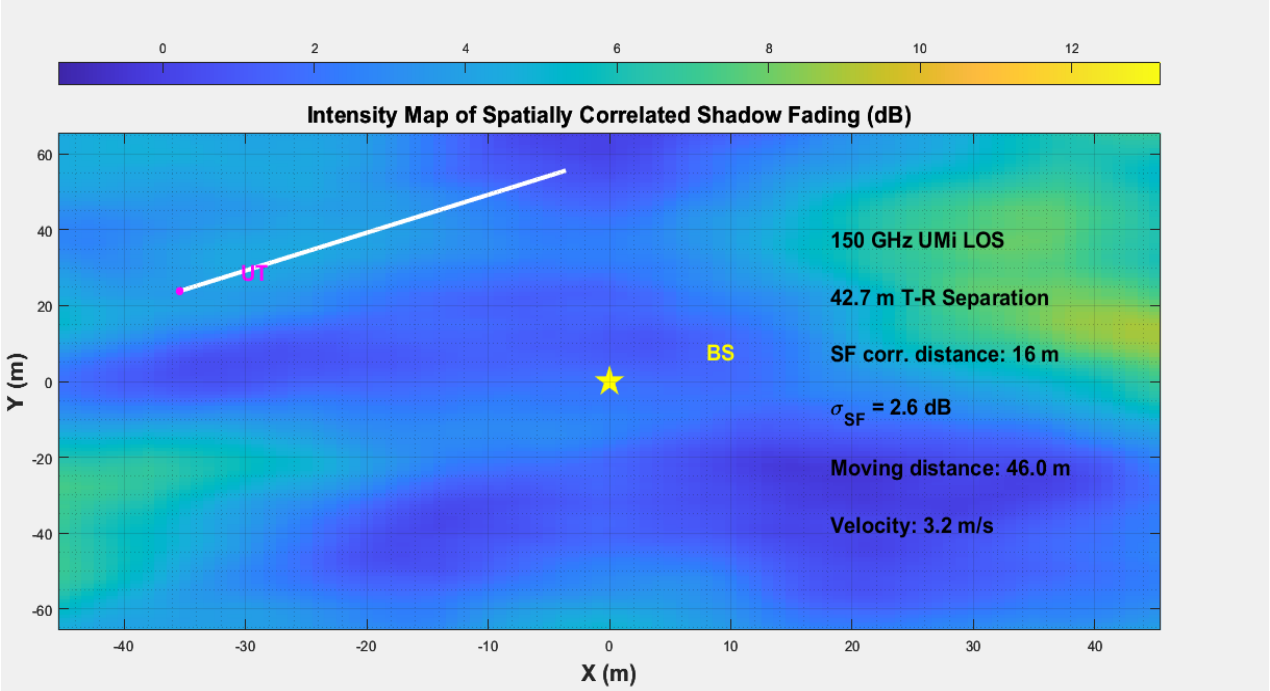

Figure IV.6: Map of spatially correlated shadow fading with the BS and UT locations (UMi scenario S2).

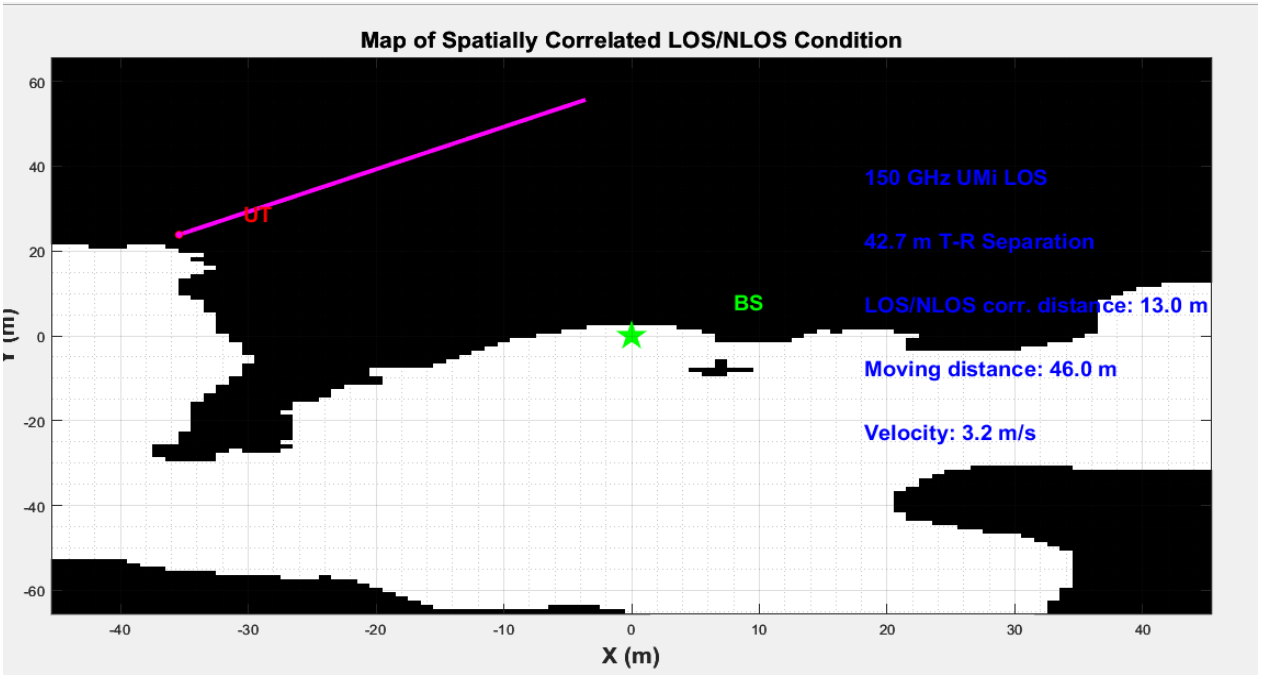

Figure IV.7: Sample map of spatially correlated LOS/NLOS condition (UMi scenario S2).

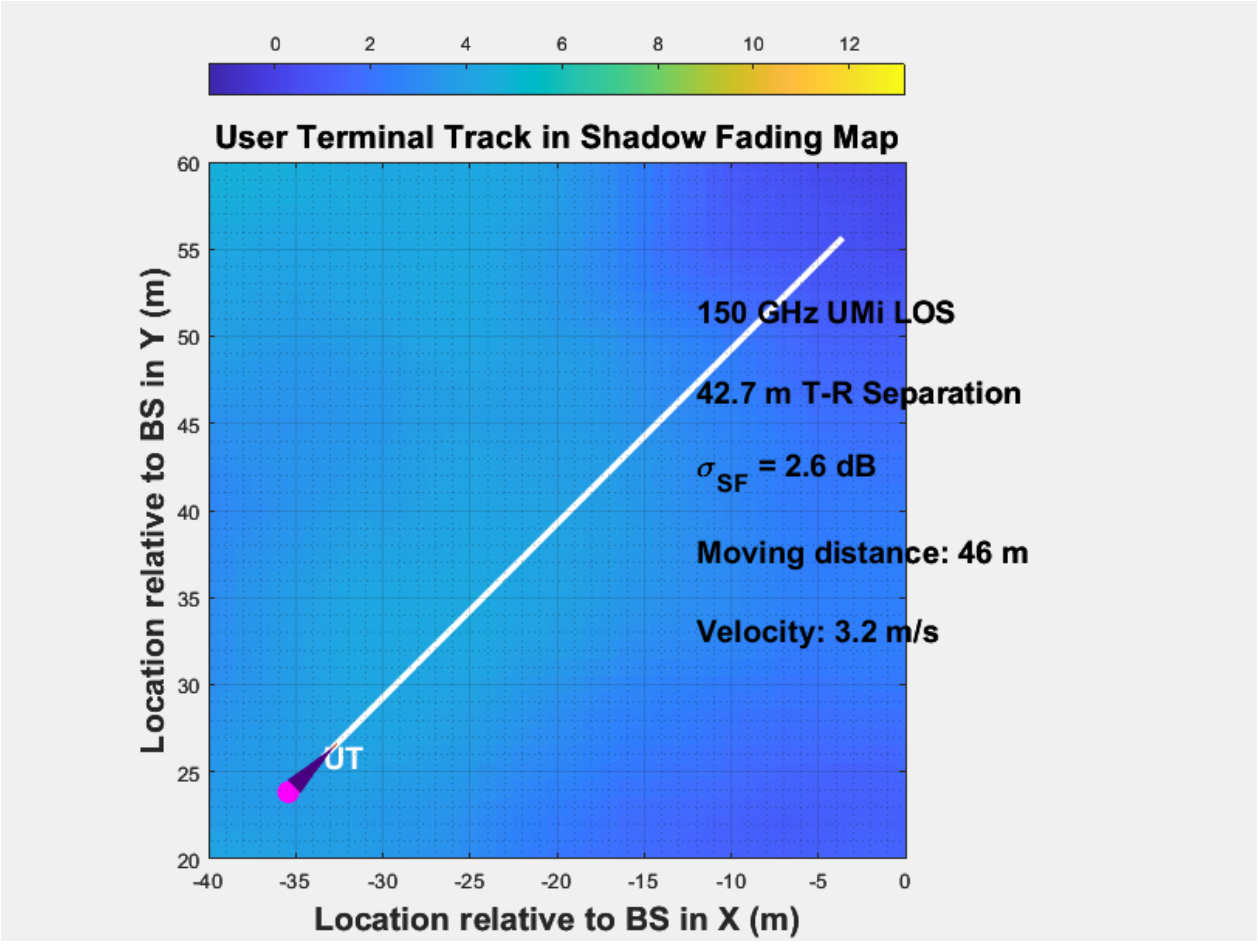

FigureIV.8: Sample user track (UMi scenario S2).

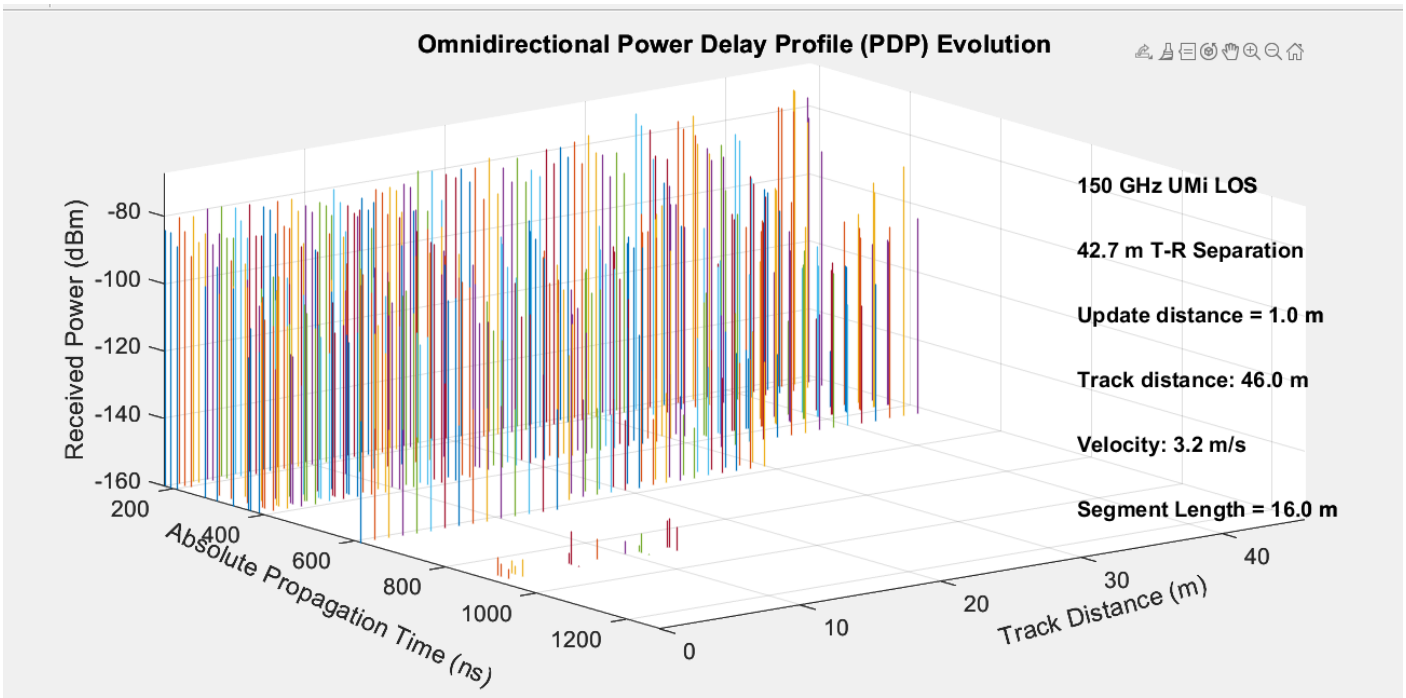

FigureIV.9: Sample consecutive omnidirectional PDPs (UMi scenario S2).

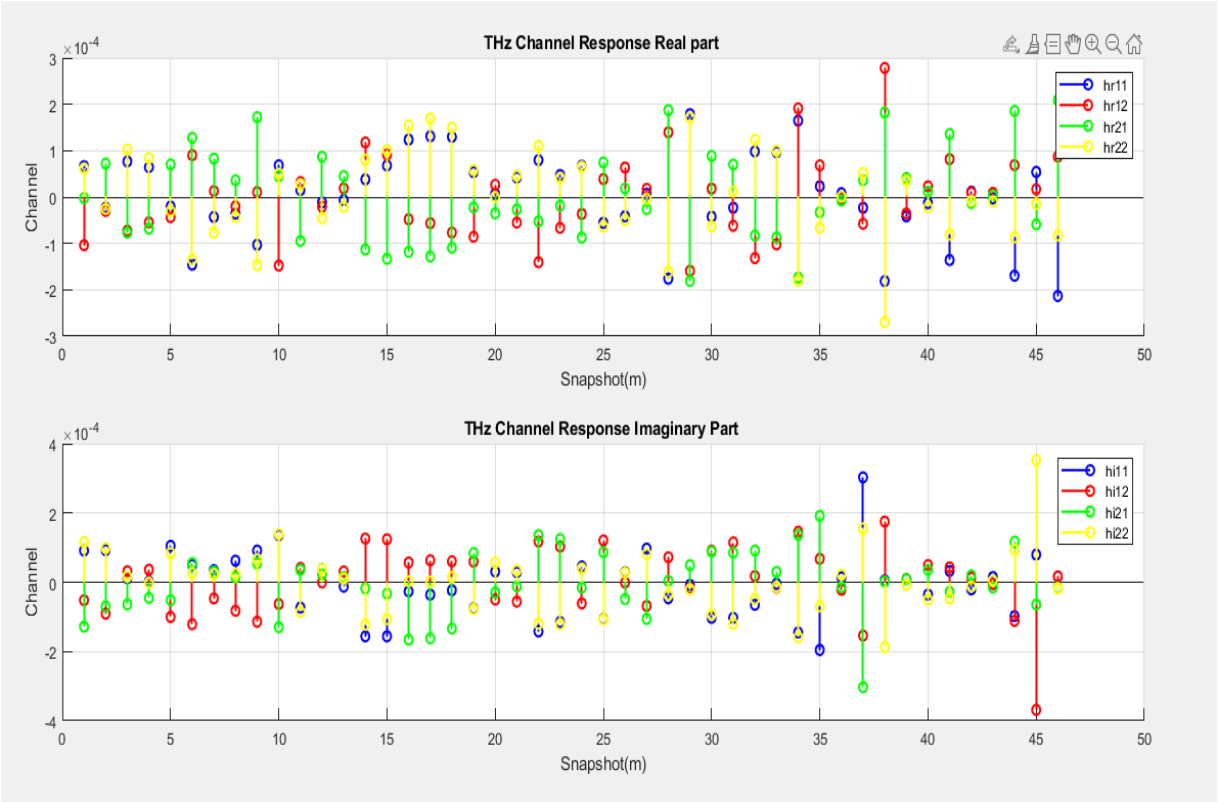

Figure IV.10: THz Channel response of real and imaginary part of $N_T = 2, N_R = 2$ for UMi scenario S2.

- For RMa scenarios:

Parameter	Value	Parameter	Value
Frequency	150	RxAzHPBW	10
Bandwidth	800	RxElHPBW	10
TXPower	30	SCenable	On
Environment	LOS	CorrDistanceSF	16
Scenario	RMa	CorrDistanceLOS	13
TXHeight	35	TrackType	Linear
RXHeight	1.5	MovDistance	46
Pressure	1.0133e+03	MovDirection	45
Humidity	50	UpdateDist	1
Temperature	20	Velocity	3.2
RainRate	0	HBenable	On
Polarization	Co-Pol	HBdefault	No
Foliage	No	SEMean	15.8
DistFol	0	U2Drate	0.21
FoliageAttenuation	0.4	D2Srate	7.88
TxArrayType	ULA	S2Rrate	7.7
RxArrayType	ULA	R2Urate	6.7
NumberOfTxAntenna	1	distType	Standard (10-500 m)
NumberOfRxAntenna	1	dmin	10
NumberOfTxAntennaPerRow	1	dmax	50
NumberOfRxAntennaPerRow	1	Nsim	1
TxAntennaSpacing	0.5	o2iLoss	No

RxAntennaSpacing	0.5	o2iType	Low Loss
TxAzHPBW	10	side_length	12
TxElHPBW	10	orient	Clockwise
transExist	Yes		

Table IV.3: Parameters of channel (RMa scenario S3).

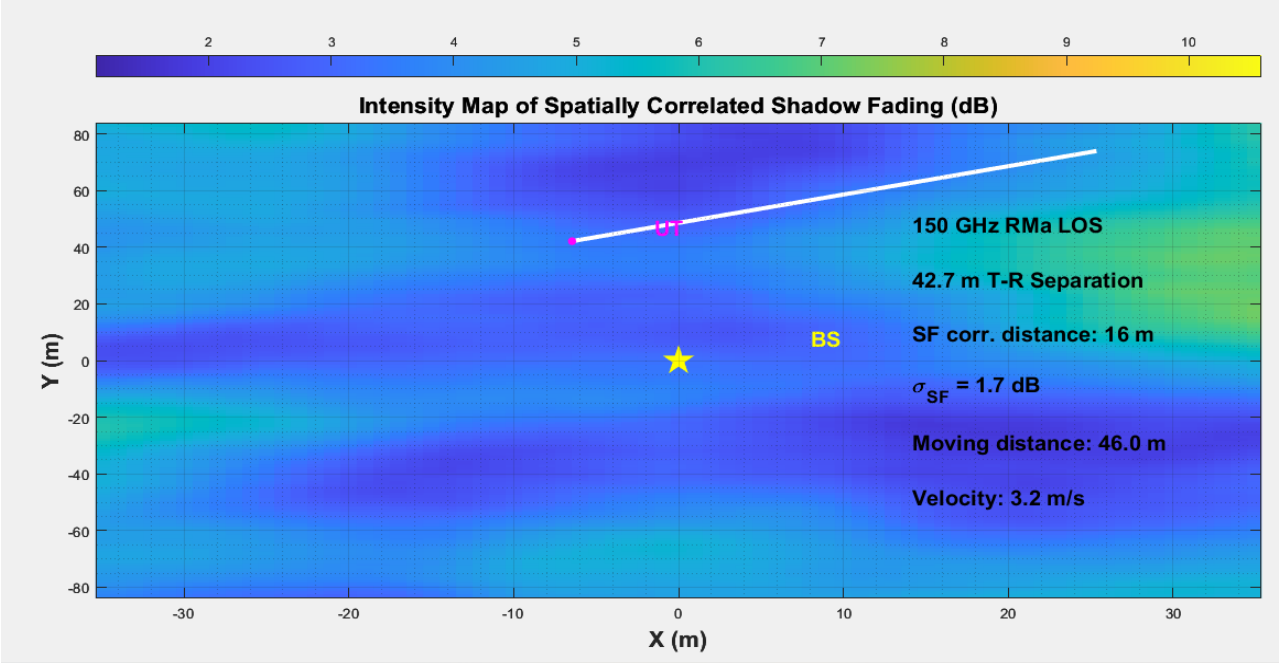

Figure IV.11: Map of spatially correlated shadow fading with the BS and UT locations (RMa scenario S3).

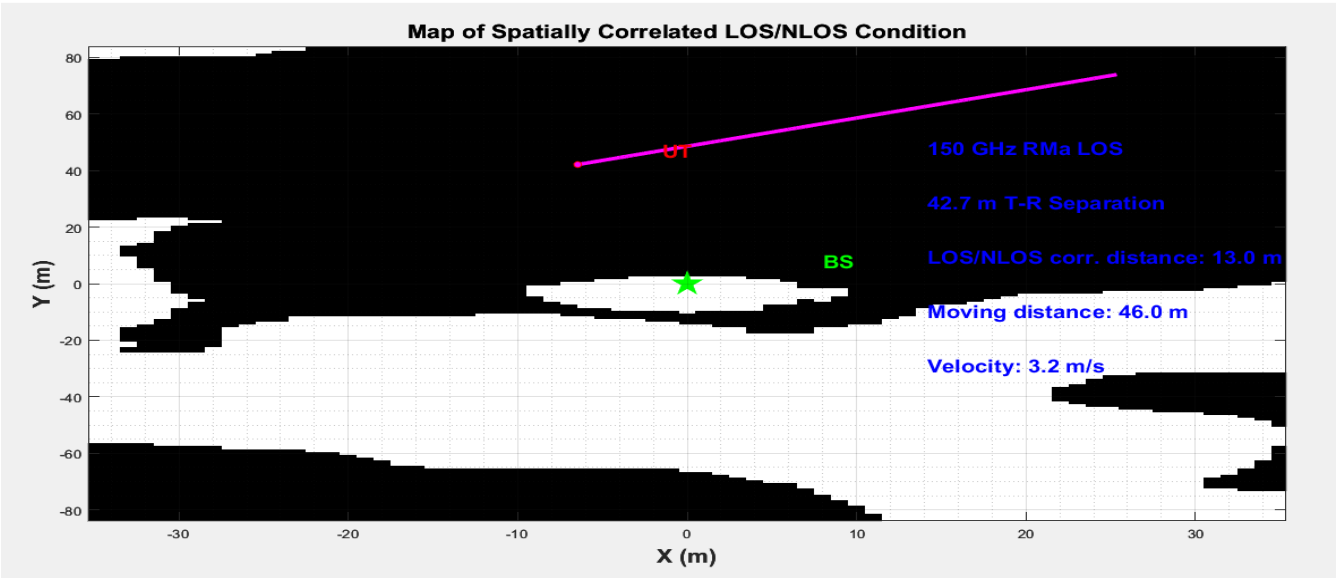

Figure IV.12: Sample map of spatially correlated LOS/NLOS condition (RMa scenario S3).

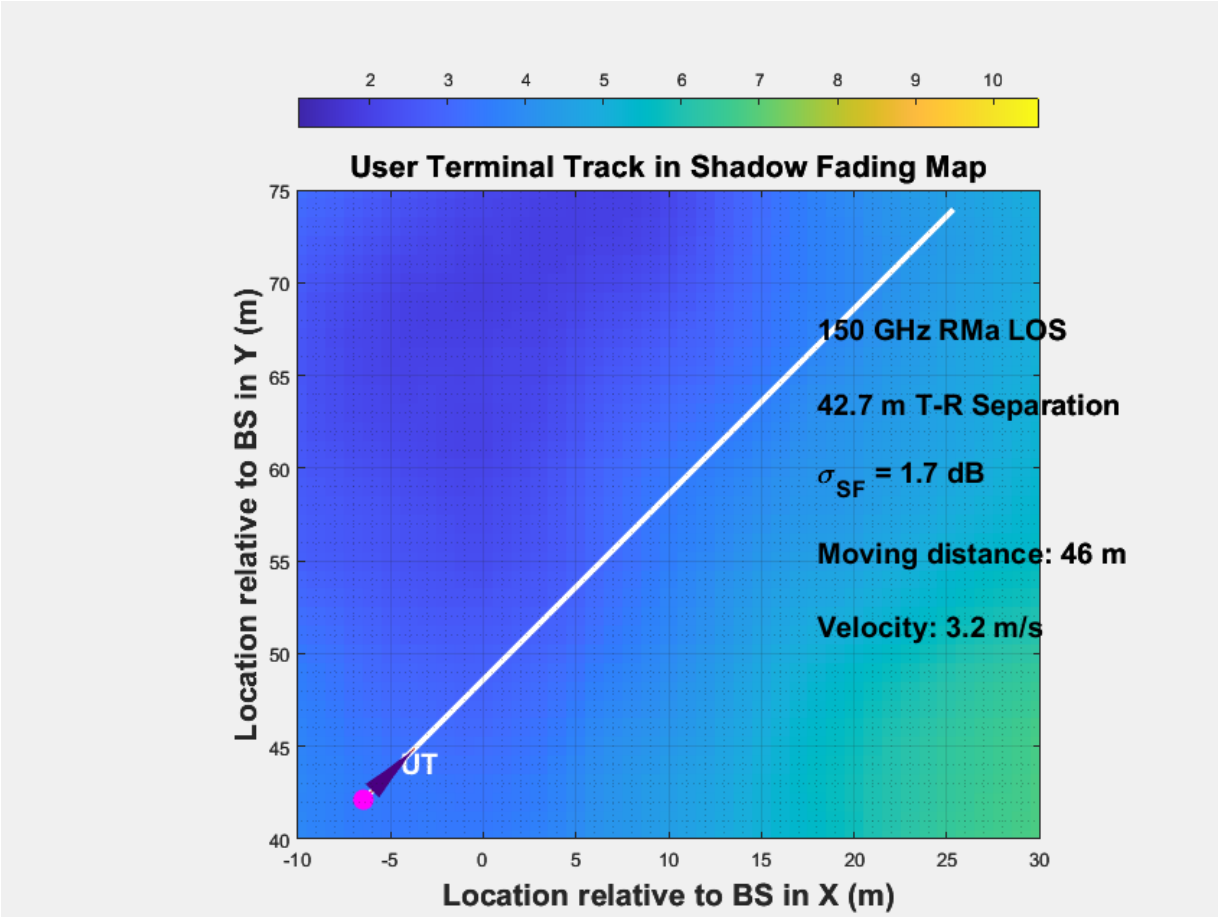

Figure IV.13: Sample user track (RMa scenario S3).

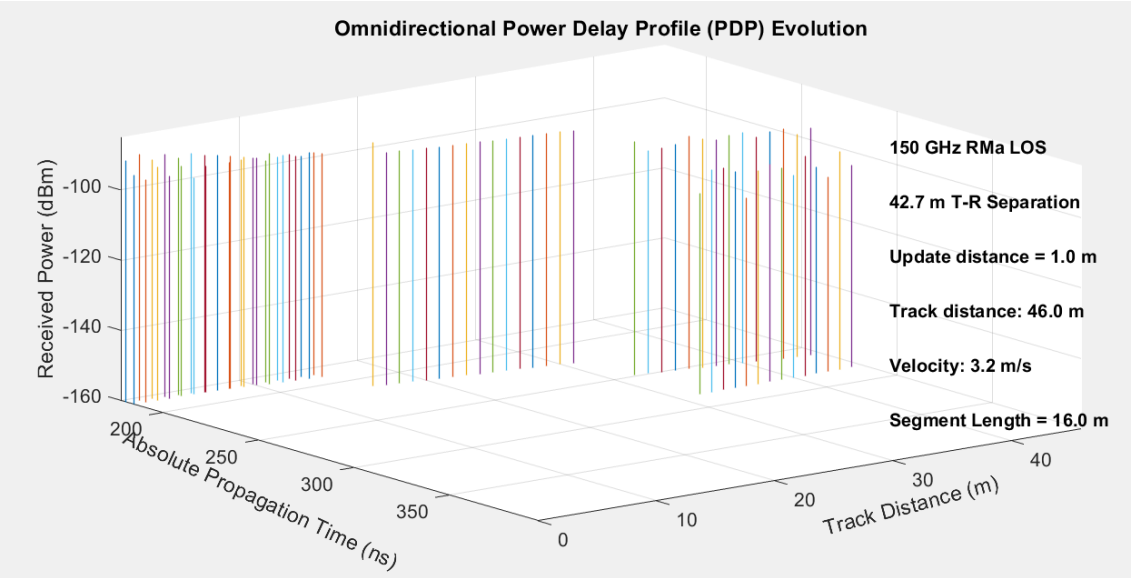

FigureIV.14: Sample consecutive omnidirectional PDPs (RMa scenario S3).

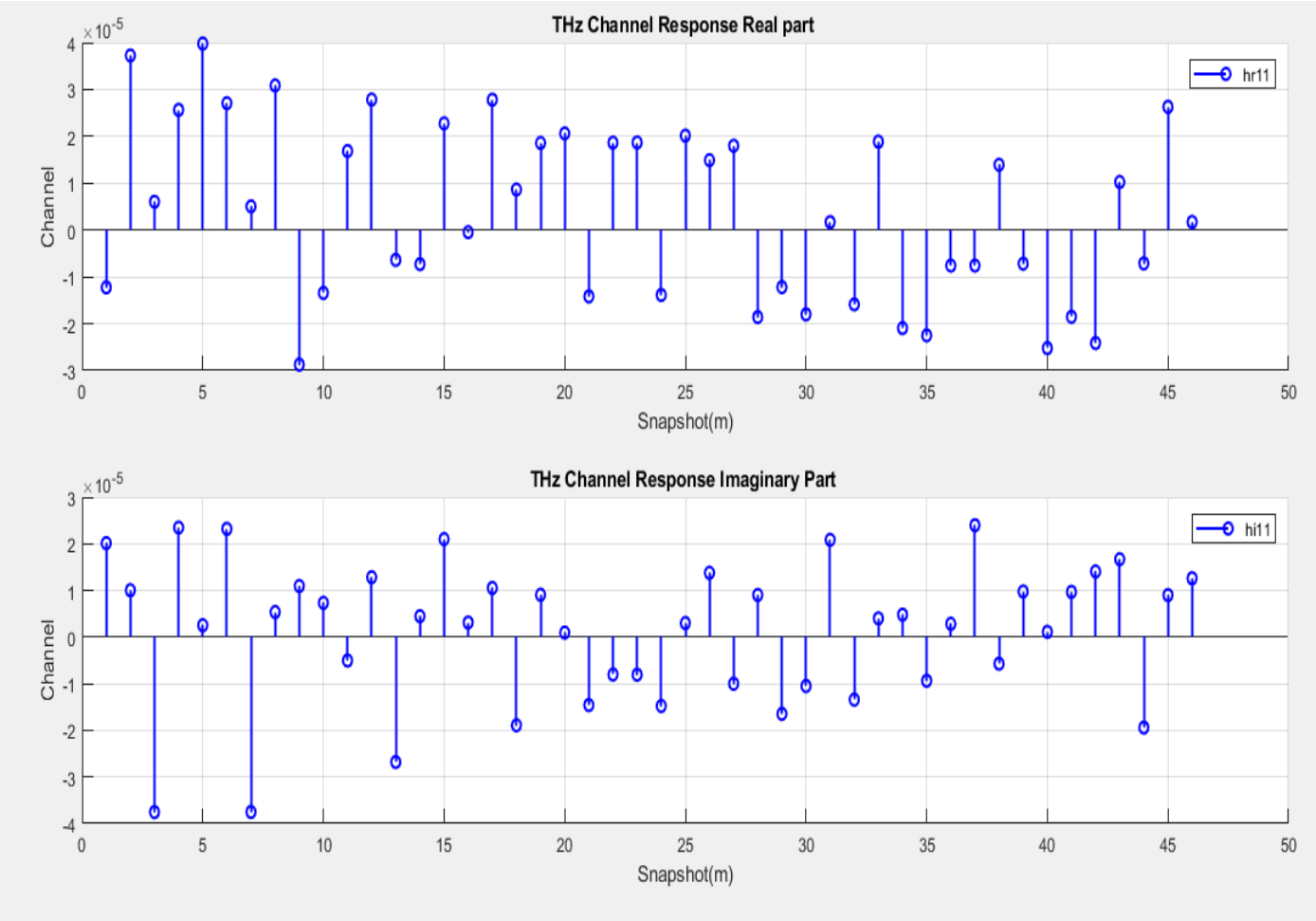

Figure IV.15: THz Channel response of real and imaginary part of $N_T = 1, N_R = 1$ for RMa scenario S3.

Parameter	Value	Parameter	Value
Frequency	150	RxAzHPBW	10
Bandwidth	800	RxElHPBW	10
TXPower	30	SCenable	On
Environment	LOS	CorrDistanceSF	16
Scenario	RMa	CorrDistanceLOS	13
TXHeight	35	TrackType	Linear
RXHeight	1.5	MovDistance	46
Pressure	1.0133e+03	MovDirection	45
Humidity	50	UpdateDist	1
Temperature	20	Velocity	3.2
RainRate	0	HBenable	On
Polarization	Co-Pol	HBdefault	No
Foliage	No	SEMean	15.8
DistFol	0	U2Drate	0.21
FoliageAttenuation	0.4	D2Srate	7.88
TxArrayType	ULA	S2Rrate	7.7
RxArrayType	ULA	R2Urate	6.7

NumberOfTxAntenna	2	distType	Standard (10-500 m)
NumberOfRxAntenna	2	dmin	10
NumberOfTxAntennaPerRow	2	dmax	50
NumberOfRxAntennaPerRow	2	Nsim	1
TxAntennaSpacing	0.5	o2iLoss	No
RxAntennaSpacing	0.5	o2iType	Low Loss
TxAzHPBW	10	side_length	12
TxElHPBW	10	orient	Clockwise
transExist	Yes		

Table IV.4: Parameters of channel (RMa scenario S4).

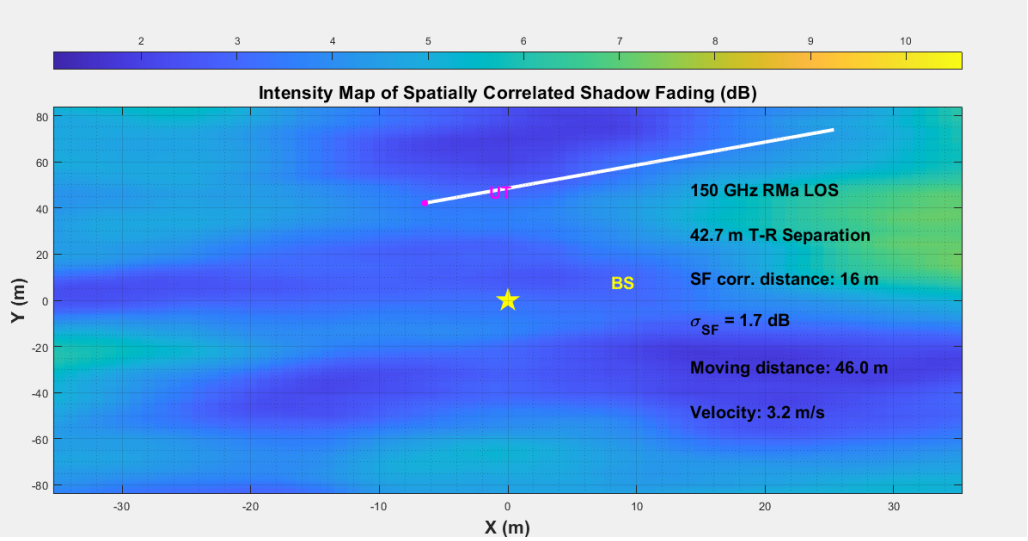

Figure IV.16: Map of spatially correlated shadow fading with the BS and UT locations (RMa scenario S4).

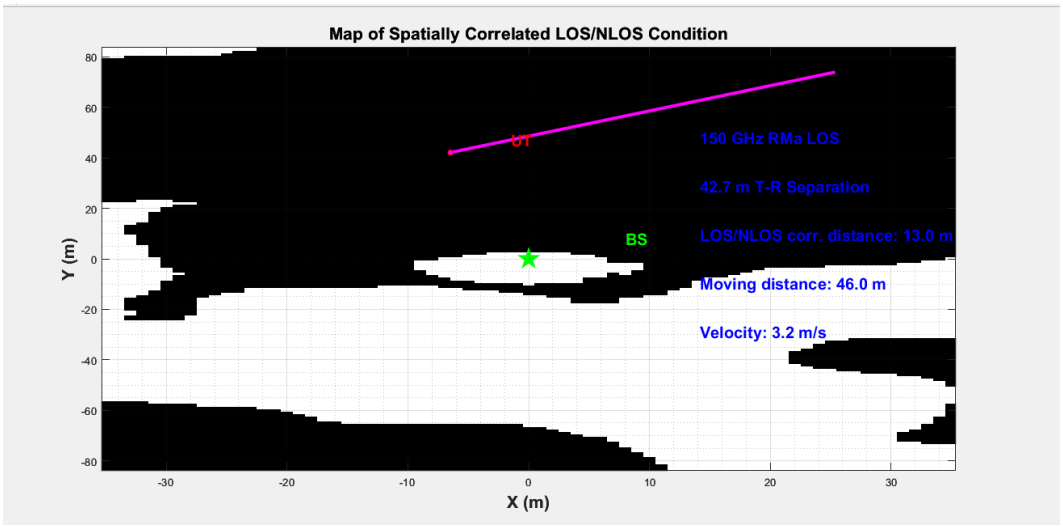

Figure IV.17: Sample map of spatially correlated LOS/NLOS condition (RMa scenario S4).

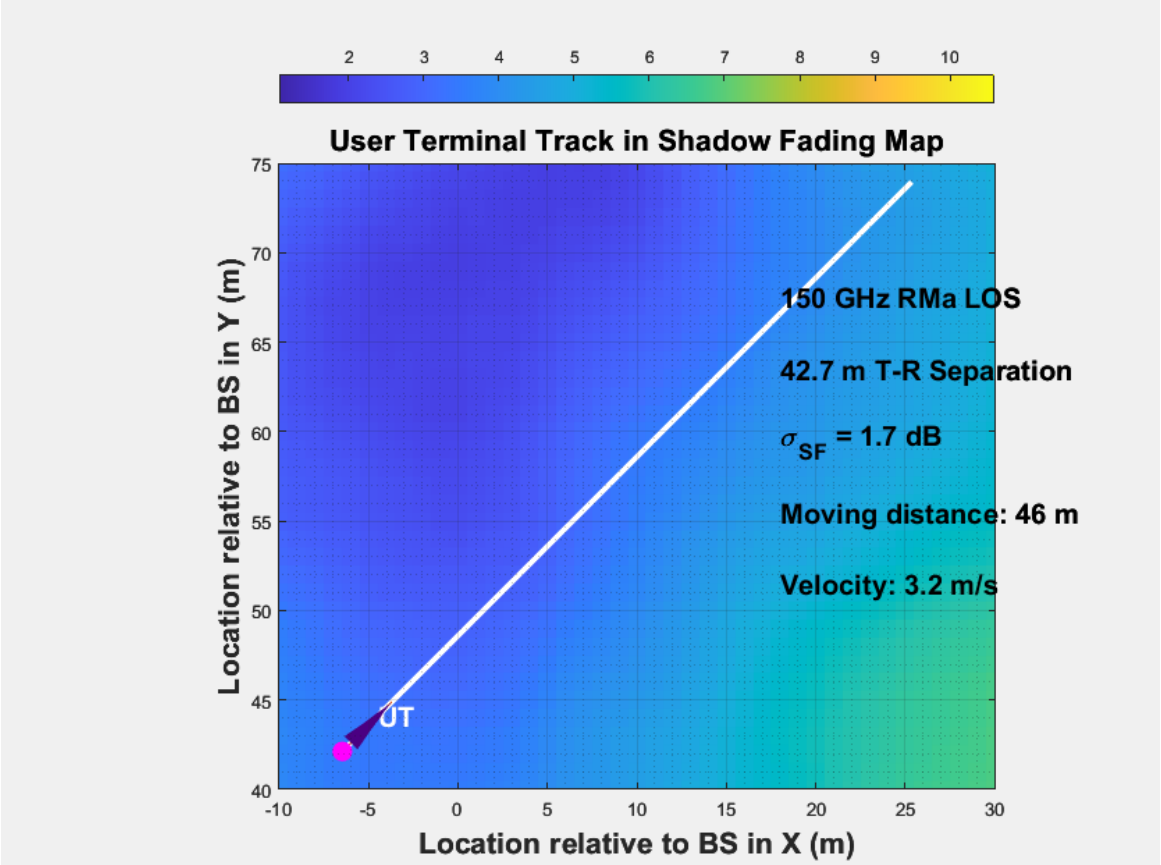

Figure IV.18: Sample user track (RMa scenario S4).

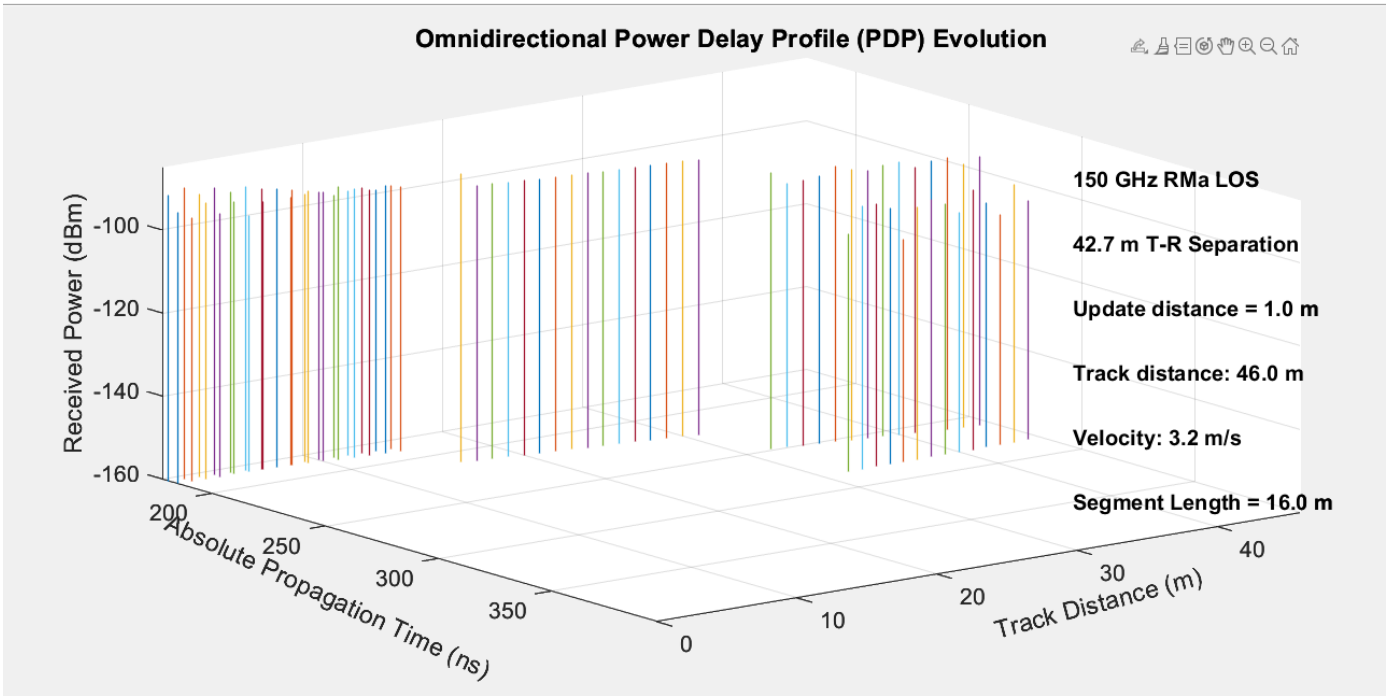

FigureIV.19: Sample consecutive omnidirectional PDPs (RMa scenario S4).

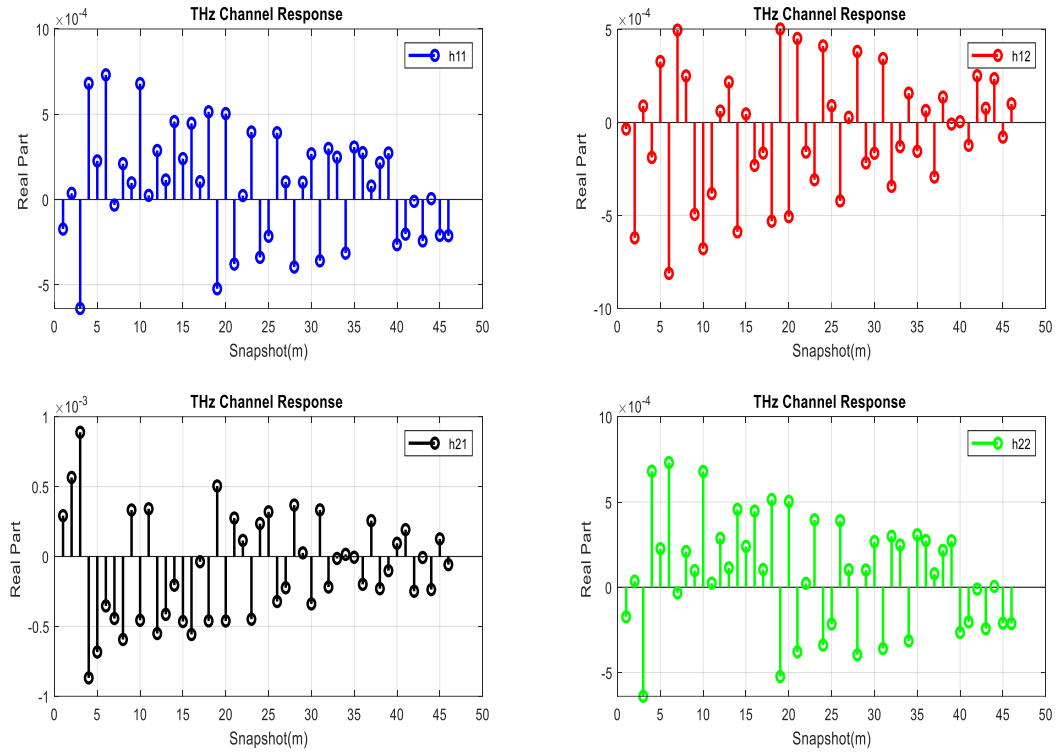

Figure IV.20: THz Channel response of real part of $N_T = 2, N_R = 2$ and RMa scenario S4.

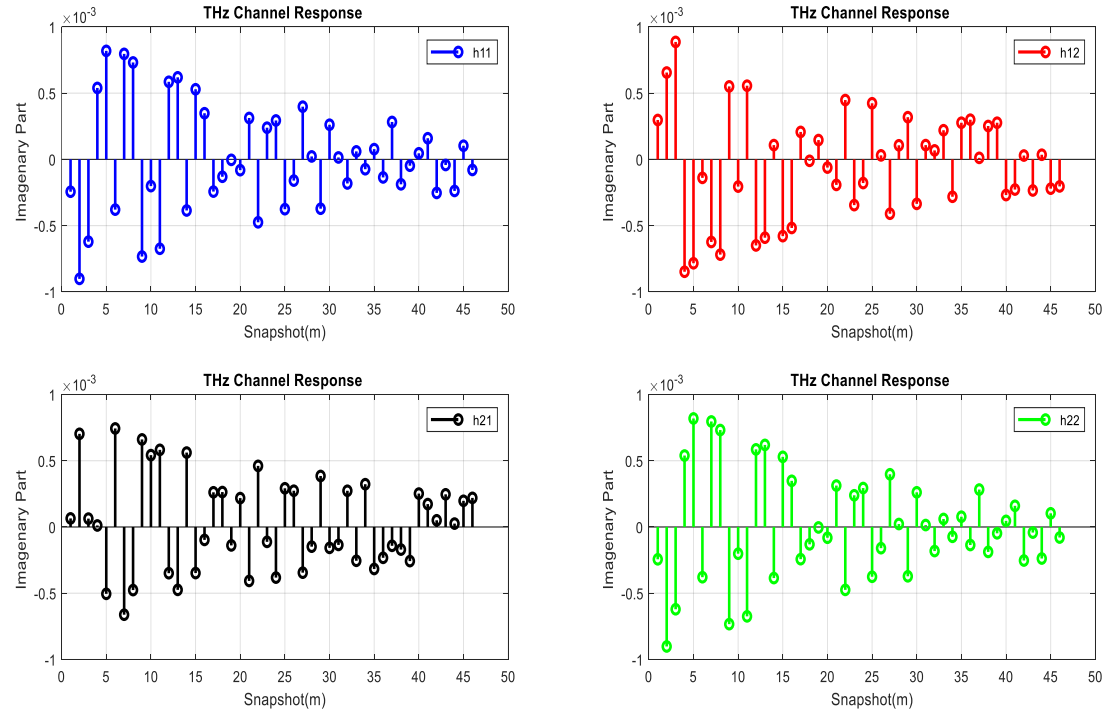

Figure IV.20: THz Channel response of imaginary part of $N_T = 2, N_R = 2$ and RMa scenario S4.

IV.5 DISCUSSION:

We presented in the results above the THz Channel response of real and imaginary part with dual-antenna systems for two different scenarios and it showed that In UMi environments, a high variability with multiple peaks. This indicates that there are several multipath components with different delays, characteristic of the dense urban environment with numerous reflecting and scattering objects.. On the other hand, RMa environments typically experience line-of-sight (LOS) propagation with fewer obstacles, leading to lower multipath interference. However it is more stable with fewer peaks. This suggests that the dominant path is the line-of-sight (LOS) path, with only a few multipath components.

For RMa there is only one path delay for each coefficient for channel h11, h12, h21, and h22, due to the dominance by the LOS path with a narrow delay spread and fewer multipath components.

The path delay profile (PDP) in RMa environments shows a dominant LOS path and fewer multipath components with smaller delays compared to UMi environments. While it might seem that there is only one significant path delay, in reality, there are multiple paths, but their impact is much less pronounced, leading to a simpler and more stable PDP.

For Path loss is generally more severe in UMi environments due to the dense urban landscape, which causes rapid attenuation of THz signals. Shadowing effects from buildings and other structures further exacerbate this issue. In contrast, while RMa environments benefit from lower pathloss over open fields, the greater distances involved necessitate higher transmission power or more sensitive receivers to maintain signal integrity. Shadowing in RMa environments is less frequent but can be more severe due to the large size of natural obstacles.

IV.6 CONCLUSION:

In this chapter we presented the simulations results of the THz Channel response of real and imaginary part with dual-antenna systems for two different scenarios (using (1x1) and (2x2) antennas on the emitter and the receiver).

In conclusion, the distinct characteristics of UMI and RMa environments necessitate specialized strategies for optimizing THz communication channels. UMi environments, with their dense infrastructure, exhibit a complex multipath profile with high variability and a wide delay spread, as reflected in the Power Delay Profile (PDP). This results in significant Inter-Symbol Interference (ISI) and severe fading, necessitating advanced equalization techniques and robust modulation schemes to maintain communication quality. In contrast, RMa environments are characterized by a dominant Line-of-Sight (LOS) path and fewer multipath components due to the sparse presence of

natural obstacles. The PDP for RMa shows a narrower delay spread, indicating reduced ISI and simpler receiver design requirements.. This comparative analysis not only highlights the challenges but also paves the way for innovative solutions tailored to the specific needs of urban and rural settings.

The use of dual-antenna systems in both UMi and RMa environments enhances the performance of THz communication channels by leveraging spatial diversity and beamforming techniques. In UMi environments, this setup helps manage the complex multipath and NLOS conditions, while in RMa environments, it improves LOS signal quality and extends coverage. Understanding these effects enables the design of robust and efficient THz communication systems tailored to the specific challenges of urban and rural settings.

GENERAL CONCLUSION

Terahertz (THz) channel models are essential for advancing 6G wireless communication, providing critical insights into the unique propagation characteristics of THz frequencies. These models account for factors such as high pathloss and atmospheric absorption, enabling accurate simulation and optimization of THz wireless links. As 6G development progresses, robust THz channel models will be indispensable for achieving reliable, high-speed connectivity and unlocking innovative applications in various fields, from ultra-fast data transmission to advanced sensing technologies.

In this study, a comparative analysis of Urban Micro (UMI) and Rural Macro (RMa) environments in the context of terahertz communication channels and a collection of characteristics was emulated through the utilization of MATLAB, while the NYUSIM Simulator was employed for the replication of the Terahertz channel in the study.

In the course of this study, we established, firstly a general Overview about 6G wireless communication system , Secondly, we proceeded to introduce Models of wireless THz channel , Next we presented a Description of the NYUSIM simulator , lastly we described a comparative examination is conducted on Urban Micro (UMI) and Rural Macro (RMa) environments within the framework of terahertz communication channels, focusing on a set of distinctive features.

Based on the results and discussions presented above, the channel response in UMI and RMa environments highlights the need for environment-specific strategies in THz communication systems. UMI environments require advanced techniques to handle multipath and shadowing, while RMa environments benefit from solutions that address long-range propagation and natural obstructions. By understanding these differences, network designers can develop tailored approaches to optimize the performance and reliability of THz communication systems in diverse settings.

By addressing these future work areas, researchers and engineers can continue to push the boundaries of THz communication, ensuring its successful deployment and operation in diverse environments. This will pave the way for next-generation wireless networks that offer unprecedented performance and reliability.

REFERENCES

[1] Cheng-Xiang Wang; Xiaohu You; XiqiGao; Xiuming Zhu; Zixin Li; Chuan Zhang; HaimingWang; Yongming Huang; Yunfei Chen; Harald Haas; John S. Thompson; Erik G. Larsson;Marco Di Renzo; Wen Tong; Peiying Zhu; H. Vincent Poor; LajosHanzo; 2023. "On TheRoad to 6G: Visions, Requirements, Key Technologies and Testbeds", ARXIV.

[2] Minoru Inomata; Wataru Yamada; Nobuaki Kuno; Motoharu Sasaki; KoshiroKitao; MitsukiNakamura; Hironori Ishikawa; Yasuhiro (2021). Terahertz Propagation Characteristics for 6GMobile Communication Systems.

[3] Sarthak Seth; Bikramjit Singh. (2022). Sensing Based Contention Access for 6G Low LatencyNetworks.

[4] GuangbinXu 2020 J. Phys.: Conf. Ser. 1693 012101.

[5] Terahertz Wireless Communications for 2030 andBeyond: A Cutting-Edge FrontierZhi Chen, Chong Han, Yongzhi Wu, Lingxiang Li, Chongwen Huang, Zhaoyang Zhang,Guangjian Wang, and Wen Tong.

[6] S. Dang, O. Amin, B. Shihada, and M.-S. Alouini, "What should 6G be?"Nature Electronics, vol. 3, no. 1, pp. 20–29, 2020.

[7] Y. Al-Eryani and E. Hossain, "The D-OMA method for massive multipleaccess in 6G: Performance, security, and challenges," IEEE VehicularTechnology Magazine, vol. 14, no. 3, pp. 92–99, 2019.

[8] S. Chen, Y.-C. Liang, S. Sun, S. Kang, W. Cheng, and M. Peng, "Vision,requirements, and technology trend of 6G: how to tackle the challengesof system coverage, capacity, user data-rate and movement speed," IEEEWireless Communications, vol. 27, no. 2, pp. 218–228, 2020.

[9] K. B. Letaief, W. Chen, Y. Shi, J. Zhang, and Y. A. Zhang, ''The roadmapto 6G: AI empowered wireless networks,'' IEEE Commun. Mag., vol. 57,no. 8, pp. 84–90, Aug. 2019, doi: 10.1109/MCOM.2019.1900271.

[10] T. Huang, W. Yang, J. Wu, J. Ma, X. Zhang, and D. Zhang, "A survey ongreen 6G network: Architecture and technologies," IEEE Access, vol. 7,pp. 175 758–175 768, 2019.

[11] I. F. Akyildiz, D. M. Gutierrez-Estevez, R. Balakrishnan, andE. Chavarria-Reyes, “LTE-advanced and the evolution to beyond 4G(B4G) systems,” Physical Communication, vol. 10, pp. 31–60, 2014.

[12] C.-X. Wang, F. Haider, X. Gao, X.-H. You, Y. Yang, D. Yuan, H. M.Aggoune, H. Haas, S. Fletcher, and E. Hepsaydir, “Cellular architectureand key technologies for 5G wireless communication networks,” IEEEcommunications magazine, vol. 52, no. 2, pp. 122–130, 2014.

[13] I. F. Akyildiz et al., “Combating the Distance Problem in the Millimeter Wave and TerahertzFrequency Bands,” IEEE Commun. Mag., vol. 56, no. 6, June 2018, pp. 102–08.

[14] Z.Zhang, Y. Xiao, Z. Ma, M. Xiao, Z. Ding, X. Lei, G. K. Karagiannidis, and P. Fan, “6G WirelessNetworks: Vision, Requirements, Architecture, and Key Technologies,” IEEE VehicularTechnology Magazine, vol. 14, no. 3, pp. 28–41, Sep. 2019.

[15] H. Guo, J. Li, J. Liu, N. Tian, and N. Kato, ‘‘A survey on space-air-ground-sea integrated network security in 6G,’’ IEEE Commun.Surveys Tuts., vol. 24, no. 1, pp. 53–87, 1st Quart., 2022, doi:10.1109/COMST.2021.3131332.

[16] A. Zappone, M. Di Renzo, M. Debbah, T. T. Lam, and X. Qian,“Model-aided wireless artificial intelligence: Embedding expert knowl-edge in deep neural networks for wireless system optimization,” IEEEVehicular Technology Magazine, vol. 14, no. 3, pp. 60–69, 2019.

[17] H. He, S. Jin, C.-K. Wen, F. Gao, G. Y. Li, and Z. Xu, “Model-drivendeep learning for physical layer communications,” IEEE WirelessCommunications, 2019.

[18] B. Zong, C. Fan, X. Wang, X. Duan, B. Wang, and J. Wang, “6Gtechnologies: Key drivers, core requirements, system architectures, andenabling technologies,” IEEE Vehicular Technology Magazine, vol. 14,no. 3, pp. 18–27, 2019.

[19] T. W. Crowe, W. R. Deal, M. Schroter, C.-K. C. Tzuang, and K. Wu, ‘“Terahertz RF Electronics and System Integration,” Proceedings of theIEEE, vol. 105, no. 6, pp. 985–989, 2017.

[20] V. Petrov, J. Kokkoniemi, D. Moltchanov, J. Lehtomaki, Y. Kouch-eryavy, and M. Juntti, “Last meter indoor terahertz wireless access: Per-formance insights and implementation roadmap,” IEEE CommunicationsMagazine, vol. 56, no. 6, pp. 158–165, June 2018.

[21] Z. Chen, X. Ma, B. Zhang, Y. Zhang, Z. Niu, N. Kuang, W. Chen,L. Li, and S. Li, “A Survey on Terahertz Communications,” ChinaCommunications, vol. 16, no. 2, pp. 1–35, Feb 2019.

[22] H. He et al., “Model-driven deep learning for physical layer communications,” IEEE Wireless Commun., vol. 26, no. 5, pp. 77–83, 2019.

[23] K. B. Letaief et al., “The roadmap to 6G: AI empowered wirelessnetworks,” IEEE Commun. Mag., vol. 57, no. 8, pp. 84–90, 2019.

[24] S. Mumtaz, J. M. Jornet, J. Aulin, W. H. Gerstacker, X. Dong, and B. Ai, “Terahertz Communication for Vehicular Networks,” IEEE Transactions on VehicularTechnology, vol. 66, no. 7, pp. 5617–5625, July 2017.

[25] T. W. Crowe, W. R. Deal, M. Schroter, C.-K. C. Tzuang, and K. Wu, ¨ “Terahertz RF Electronics and System Integration,” Proceedings of the IEEE, vol. 105, no. 6, pp. 985–989, 2017.

[26] C. Han and Y. Chen, “Propagation Modeling for Wireless Communications in the Terahertz Band,” IEEE Communications Magazine, vol. 56, no. 6, pp. 96–101, 2018.

[27] V. Petrov et al., “On unifiedvehicular communications and radar sensing in millimeter-wave and lowterahertz bands,” IEEE Wireless Commun., vol. 26, no. 3, pp. 146–153, 2019.

[28] S. Sun, T. S. Rappaport, M. Shafi, P. Tang, J. Zhang, and P. J. Smith, “Propagation Models and Performance Evaluation for 5G MillimeterWave Bands,” IEEE Transactions on VehicularTechnology, vol. 67, no. 9, pp. 8422–8439, Sep. 2018.

[29] S. A. Busari, K. M. S. Huq, S. Mumtaz, L. Dai, and J. Rodriguez, “Millimeter-Wave Massive MIMO Communication for Future Wireless Systems: A Survey,” IEEE Communications SurveysTutorials, vol. 20, no. 2, pp. 836–869, Secondquarter 2018

[30] R. M. Goody and Y. L. Yung, Atmospheric Radiation: Theoretical basis, 2nd ed. Oxford UniversityPress, 1989.

[31] N. J. Tro, Principles of Chemistry: amolecularapproach. Prentice- Hall, Inc., 2009.

[32] L. Rothman, I. Gordon, A. Barbe, D. C. Benner, P. Bernath, M.Birk, V. Boudon, L. Brown, and A.Campargue, “The hitran 2008 molecularspectroscopicdatabase,” Journal of Quantitative Spectroscopy and Radiative Transfer, vol. 110, no. 9-10, pp. 533–572, Jun 2009.

[33] J. H. Van Vleck and V. F. Weisskopf, “On the shape of collisionbroadenedlines,” Rev. Mod. Phys., vol. 17, no. 2-3, pp. 227–236, Apr1945.

[34] S. Clough, F. Kneizys, and R. Davies, “Line shape and the water vapor continuum,” Atmos. Res., vol. 23, no. 3-4, pp. 229 – 241, Oct 1989.

[35] Rappaport, T. S., Xing, Y., Kanhere, O., Ju, S., Murdock, J. N., & Fu, X. (2019). Wireless communications and applications above 100 GHz: Opportunities and challenges for 6G and beyond. *IEEE Access, 7*, 78729-78757.

[36] Han, C., OjaroudiParchin, N., &Alomainy, A. (2021). Statistical multi-pathchannelmodeling for terahertz band communications. *IEEE Access, 9*, 106287-106296.

[37] Kokkoniemi, J., &Haneda, K. (2020). Measurement-basedevaluation of THzwirelesssystems in a room environment. *IEEE Transactions on Terahertz Science and Technology, 10*(3), 225-233.

[38] Priebe, S., &Kurner, T. (2013). Stochasticmodeling of THz indoor radio channels. *IEEE Transactions on Wireless Communications, 12*(9), 4445-4455.

[39] T. Sarkar, Z. Ji, K. Kim, A. Medouri, and M. Palma, "A Survey of Various Propagation Models for Mobile Communication," IEEE Antennas and Propagation Magazine, vol. 45, no. 3, pp. 51–82, Jul. 2003

[40] A. Goldsmith, Wireless Communications. New York, USA: Cambridge UniversityPress, 2005.

[41] C. F. Yang, B. C. Wu, and C. J. Ko, "A ray-tracingmethod for modeling indoor wave propagation and penetration," in Proc. ofAntennas and Propagation Society (AP-S) International Symposium, pp. 907–919, Jul. 1998.

[42] H.-W. Son and N.-H. Myung, "A deterministic ray tube method for microcellularwave propagation prediction model," IEEE Transactions on Antennas and Propagation, vol. 47, no. 8, pp. 1344–1350, Aug. 1999

[43] S. Rachid and M. Wahbi, "UWB Indoor Radio Propagation Modelling in Presence of Human Body ShadowingUsing Ray Tracing Technique," International Journal of Communication Networks and Information Security, vol. 4, Aug. 2012.

[44] Y. Zhao, Y. Hao, and C. Parini, "FDTD Characterization of UWB Indoor Radio Channel IncludingFrequencyDependentAntenna Directivities," Antennas& Wireless Propagation Letters, vol. 6, no. 11, pp. 191–194, Apr. 2007.

[45] Y. Zhao, Y. Hao, and C. Parini, "FDTD Characterization of UWB Indoor Radio Channel IncludingFrequencyDependentAntenna Directivities," Antennas& Wireless Propagation Letters, vol. 6, no. 11, pp. 191–194, Apr. 2007.

[46] A. Fricke, C. Homann, and T. Kürner, "Time-domain propagation investigations for terahertz intra-device communications," in Proc. ofEuropeanConference on Antennas and Propagation (EuCAP), pp. 1760–1764, May 2014.

[47] N. I. of Standards and Technology. “nextgchannel model alliance,” accessedjune 6, 2021. [Online]. Available: ‘‘https://www.nist.gov/ctl/ nextg-channel-model-alliance’’

[48] J. J. Blanz and P. Jung, “A flexibly configurable spatial model for mobile radio channels,” IEEE Transactions on Communications, vol. 46, no. 3, pp. 367–371, Mar. 1998.

[49] A. F. Molisch, A. Kuchar, J. Laurila, K. Hugl, and R. Schmalenberger, “Geometry-baseddirectional model for mobile radio channels—principles and implementation,” European Transactions on Telecommunications, vol. 14, no. 4, pp. 351–359, Nov. 2003.

[50] D. Headland, Y. Monnai, D. Abbott, C. Fumeaux, and W. Withayachumnankul, “Tutorial: Terahertzbeamforming, from concepts to realizations,” AplPhotonics, vol. 3, no. 5, p. 051101, 2018.

[51] A. L. Imoize, A. E. Ibhaze, A. A. Atayero, and K. V. N. Kavitha, “Standard Propagation Channel Models for MIMO Communication Systems,” Wireless Communications and Mobile Computing, Feb. 2021.

[52] M. Lecci, M. Polese, C. Lai, J. Wang, C. Gentile, N. Golmie, and M. Zorzi, “Quasi-Deterministic Channel Model for mmWaves: MathematicalFormalization and Validation,” in Proc. of IEEE Global Communications Conference (GLOBECOM), pp. 1–6, Dec. 2020.

[53] Y. Wang, S. Safavi-Naeini, and S. Chaudhuri, “A hybrid technique based on combining ray tracing and FDTD methods for site-specificmodeling of indoor radio wave propagation,” IEEE Transactions on Antennas and Propagation, vol. 48, no. 5, pp. 743–754, May 2000

[54] A. Fricke, C. Homann, and T. Kürner, “Time-domain propagation investigations for terahertz intra-device communications,” in Proc. ofEuropeanConference on Antennas and Propagation (EuCAP), pp. 1760–1764, May 2014.

[55] G. R. MacCartney, Jr. and T. S. Rappaport, “A flexible millimeter-wave channel sounder with absolute timing,” IEEE Journal on Selected Areas in Communications, vol. 35, no. 6, pp. 1402–1418, Jun. 2017.

[56] G. R. MacCartney, Jr. et al., “A flexible wideband millimeter-wave channel sounder with local area and NLOS to LOS transition measurements,” in 2017 IEEE International Conference on Communications (ICC), May 2017, pp. 1–7.

[57] Y. Xing and T. S. Rappaport, “Propagation measurement system and approach at 140 ghz-moving to 6g and above 100 ghz,” in 2018 IEEE Global Communications Conference (GLOBECOM), Dec. 2018, pp. 1–6.

[58] T. S. Rappaport, S. Sun, R. Mayzus, et al., “Millimeter wave mobile communications for 5G cellular: It will work!” IEEE Access, vol. 1, pp. 335–349, 2013. [Online]. Available: http://ieeexplore.ieee.org/document/6515173/.

[59] T. S. Rappaport, S. Sun, and M. Shafi, “5G channel model with improved accuracy and efficiency in mmWave bands,” IEEE 5G Tech Focus, vol. 1, no. 1, Mar. 2017. [Online]. Available: https://5g.ieee.org/tech-focus/march-20 17/5g-channel-model.

[60] G. R. MacCartney and T. S. Rappaport, “Rural macrocell path loss models for millimeter wave wireless communications,” IEEE Journal on Selected Areas in Communications, vol. 35, no. 7, pp. 1663–1677, Jul. 2017. [Online]. Available: http://ieeexplore.ieee.org/stamp/stamp.jsp?tp=&arnumber=791 4696.

[61] S. Sun, G. R. MacCartney, and T. S. Rappaport, “A novel millimeter-wave channel simulator and applications for 5G wireless communications,” in 2017 IEEE International Conference on Communications (ICC), May 2017, pp. 1–7. [Online]. Available: https://arxiv.org/pdf/1703.08232.pdf.

[62] S. Ju and T. S. Rappaport, “Simulating motion - incorporating spatial consistency into the NYUSIM channel model,” 2018 IEEE 88th Vehicular Technology Conference Workshops, pp. 1–6, Aug. 2018.

[63] S. Ju and T. S. Rappaport, “Millimeter-wave extended nyusim channel model for spatial consistency,” 2018 IEEE Global Communications Conference (Globecom), pp. 1–6, Dec. 2018.

[64] S. Ju, Y. Xing, O. Kanhere, and T. S. Rappaport, “A Millimeter-Wave Channel Simulator NYUSIM with Spatial Consistency and Human Blockage,” IEEE 2019 Global Communications Conference, pp. 1–6, Dec. 2019.

[65] S. Ju, Y. Xing, O. Kanhere, and T. S. Rappaport, “3-D Statistical Indoor Channel

Model for Millimeter-Wave and Sub-Terahertz Bands,” IEEE 2020 Global Communications

Conference, pp. 1–7, Dec. 2020.

[66] S. Ju, Y. Xing, O. Kanhere, and T. S. Rappaport, “Millimeter wave and subterahertz spatial statistical channel model for an indoor office building,” IEEE Journal on Selected Areas in Communications, vol. 39, no. 6, pp. 1561–1575, 2021.

DOI: 10.1109/JSAC.2021.3071844.

[67] Y. Xing, T. S. Rappaport, and A. Ghosh, “Millimeter wave and sub-THz indoor radio propagation channel measurements, models, and comparisons in an office environment,” IEEE Communications Letters, vol. 25, no. 10, pp. 3151–3155, 2021.

DOI: 10.1109/LCOMM.2021.3088264.

[68] T. S. Rappaport, G. R. MacCartney, Jr., M. K. Samimi, and S. Sun, “Wideband millimeter-wave propagation measurements and channel models for future wireless communication system design (Invited Paper),” IEEE Transactions on Communications, vol. 63, no. 9, pp. 3029–3056, Sep. 2015. [Online]. Available:http://ieeexplore.ieee.org/document/7109864/.

[69] Y. Xing and T. S. Rappaport, “Millimeter wave and Terahertz urban microcell propagation measurements and models,” IEEE Communications Letters, vol. 25, no. 12, pp. 3755–3759, 2021. DOI: 10.1109/LCOMM.2021.3117900.

[70] S. Ju and T. S. Rappaport, “Sub-Terahertz spatial statistical MIMO channel model for urban microcells at 142 GHz,” in 2021 IEEE Global Communications Conference (GLOBECOM), 2021, pp. 1–6. DOI: 10.1109/GLOBECOM46510.202 1.9685929.

[71] S. Ju, Y. Xing, O. Kanhere, and T. S. Rappaport, “Sub-Terahertz channel measurements and characterization in a factory building,” in 2022 IEEE International Conference on Communications (ICC), May 2022, pp. 1–6.

[72] S. Ju, D. Shakya, Y. Xing, O. Kanhere, H. Poddar, and T. S. Rappaport, “140 GHz sub-THz propagation measurements and channel characterization in factory buildings,” Submitted to IEEE Transactions on antenna and propagation, Jan. 2023.

[73] S. Ju, D. Shakya, H. Poddar, O. Kanhere, Y. Xing, and T. S. Rappaport, “Indoor factory wideband sub-THz statistical channel model at 142 GHz for 6G industrial wireless networks,” Submitted IEEE Transactions onWireless Communications, Jan. 2023.

[74] M. K. Samimi and T. S. Rappaport, “3-D millimeter-wave statistical channel model for 5G wireless system design,” IEEE Transactions on Microwave Theory and Techniques, vol. 64, no. 7, pp. 2207–2225, Jul. 2016. [Online]. Available: http://ieeexplore.ieee.org/document/7501500/.

[75] M. K. Samimi and T. S. Rappaport, “Local multipath model parameters for generating 5G millimeter-wave 3GPP-like channel impulse response,” the 10th European Conference on Antennas and Propagation (EuCAP 2016), Apr. 2016. [Online]. Available: http://arxiv.org/abs/1511.06941.

[76] S. Sun et al., “Investigation of prediction accuracy, sensitivity, and parameter stability of large-scale propagation path loss models for 5G wireless communications,” IEEE Transactions on Vehicular Technology, vol. 65, no. 5, pp. 2843–2860, May 2016. [Online]. Available: http://ieeexplore.ieee.org/document/7434656/.

[77] S. Sun, G. R. MacCartney, M. K. Samimi, and T. S. Rappaport, “Synthesizing omnidirectional antenna patterns, received power and path loss from directional antennas

for 5G millimeter-wave communications," in 2015 IEEE Global Communications Conference (GLOBECOM), Dec. 2015, pp. 1–7. [Online]. Available: http://arxiv.org/abs/1511.07271.

[78] G. R. MacCartney, Jr., T. S. Rappaport, S. Sun, and S. Deng, "Indoor office wideband millimeter-wave propagation measurements and channel models at 28 and 73 GHz for ultra-dense 5G wireless networks," IEEE Access, vol. 3, pp. 2388– 2424, 2015. [Online]. Available: http://ieeexplore.ieee.org/document/7289335/.

[79] T. S. Rappaport, S. Sun, and M. Shafi, "Investigation and comparison of 3GPP and NYUSIM channel models for 5G wireless communications," in 2017 IEEE 86th Vehicular Technology Conference (VTC-Fall), Sep. 2017, pp. 1–5. [Online]. Available: https://arxiv.org/pdf/1707.00291.pdf.

[80] G. R. MacCartney, Jr., S. Sun, T. S. Rappaport, et al., "Millimeter wave wireless communications: New results for rural connectivity," in All Things Cellular'16, in conjunction with ACM MobiCom, Oct. 2016. [Online]. Available: https://arxiv.org/abs/1608.05384.

[81] S. Ju and T. S. Rappaport, "140 GHz urban microcell propagation measurements for spatial consistency modeling," in ICC 2021 - IEEE International Conference on Communications, 2021, pp. 1–6.

[82] S. Ju and T. S. Rappaport, "142 GHz Multipath Propagation Measurements and Path Loss Channel Modeling in Factory Buildings," Submitted ICC'23, May 2023.

[83] S. Deng, C. J. Slezak, G. R. MacCartney, Jr., and T. S. Rappaport, "Small wavelengths-big potential: Millimeter wave propagation measurements for 5G," Microwave Journal, vol. 57, no. 11, pp. 4–12, Sep. 2014.

[84] S. Sun et al., "Propagation path loss models for 5G urban micro- and macrocellular scenarios," in 2016 IEEE 83rd Vehicular Technology Conference (VTC2016-Spring), May 2016, pp. 1–6.

[85] S. Sun, G. R. MacCartney, Jr., and T. S. Rappaport, "Millimeter-wave distancedependent large-scale propagation measurements and path loss models for outdoor and indoor 5G systems," in 2016 10th European Conference on Antennas and Propagation (EuCAP), Apr. 2016, pp. 1–5.

[86] G. R. MacCartney, Jr., "73 ghz urban microcell base station diversity propagation measurements in brooklyn, new york: A guide to understanding the measurements and raw files for post-processing purposes," NYU WIRELESS Technical Report, TR 2017-001, Dec. 2017.

[87] S. Ju and T. S. Rappaport, “Millimeter-wave extended NYUSIM channel model for spatial consistency,” 2018 IEEE Globecom, pp. 1–6, Dec. 2018.

[88] S. Ju and T. S. Rappaport, “Simulating motion - incorporating spatial consistency into the NYUSIM channel model,” 2018 IEEE 88th Vehicular Technology Conference Workshops, pp. 1–6, Aug. 2018.

[89] G. R. MacCartney, Jr., M. K. Samimi, and T. S. Rappaport, “Omnidirectional path loss models in New York City at 28 GHz and 73 GHz,” in IEEE 25th International Symposium on Personal Indoor and Mobile Radio Communications (PIMRC), Sep. 2014, pp. 227–331.

[90] A. I. Sulyman, A. T. Nassar, M. K. Samimi, G. R. MacCartney, Jr., T. S. Rappaport, and A. Alsanie, “Radio propagation path loss models for 5G cellular networks in the 28 GHz and 38 GHz millimeter-wave bands,” IEEE Communications Magazine,vol. 52, no. 9, pp. 78–86, Sep. 2014.

[91] A. I. Sulyman, A. Alwarafy, G. R. MacCartney, Jr., T. S. Rappaport, and A.Alsanie, “Directional radio propagation path loss models for millimeter-wave wireless networks in the 28-, 60-, and 73-GHz bands,” IEEE Transactions onWireless Communications, vol. 15, no. 10, pp. 6939–6947, Oct. 2016.

[92] G. R. MacCartney, Jr. et al., “Millimeter wave wireless communications: New results for rural connectivity,” in Proceedings of the 5th Workshop on All Things Cellular: Operations, Applications and Challenges: in conjunction with MobiCom 2016, ser. ATC ’16, New York City, New York: ACM, Oct. 2016, pp. 31–36.

[93] G. R. MacCartney, Jr. and T. S. Rappaport, “Study on 3GPP rural macrocell path loss models for millimeter wave wireless communications,” in 2017 IEEE International Conference on Communications (ICC), May 2017, pp. 1–7.

[94] S. Nie et al., “72 GHz millimeter wave indoor measurements for wireless and backhaul communications,” in 2013 IEEE 24th International Symposium on Personal Indoor and Mobile Radio Communications (PIMRC), Sep. 2013, pp. 2429–2433.

[95] G. R. MacCartney, Jr., T. S. Rappaport, and S. Rangan, “Rapid fading due to human blockage in pedestrian crowds at 5g millimeter-wave frequencies,” in 2017 IEEE Global Communications Conference (GLOBECOM), Dec. 2017, pp. 1–7.

[96] G. R. MacCartney, Jr. et al., “Millimeter-wave human blockage at 73 GHz with a simple double knife-edge diffraction model and extension for directional antennas,” in 2016 IEEE 84th Vehicular Technology Conference (VTC2016-Fall), Sep. 2016, pp. 1–6.

[97] S. Ju, “Channel modeling and channel simulation for fifth-generation and beyond millimeter-wave wireless communications,” Ph.D. dissertation, NEW

YORK UNIVERSITY, TANDON SCHOOL OF ENGINEERING, May 2019.

[98] V. Fung, T. S. Rappaport, and B. Thoma, “Bit error simulation for pi/4 DQPSK mobile radio communications using two-ray and measurement-based impulse response models,” IEEE Journal on Selected Areas in Communications, vol. 11, no. 3, pp. 393–405, Apr. 1993. [Online]. Available: http://ieeexplore.ieee.org /document/219546/.

[99] J. Lota, S. Sun, T. S. Rappaport, and A. Demosthenous, “5G uniform linear arrays with beamforming and spatial multiplexing at 28, 37, 64, and 71 GHz for outdoor urban communication: A two-level approach,” IEEE Transactions on Vehicular Technology, vol. 66, no. 11, pp. 9972–9985, Nov. 2017. [Online]. Available: http://ieeexplore.ieee.org/document/8012543/.

[100] M. K. Samimi and T. S. Rappaport, “3-D millimeter-wave statistical channel model for 5G wireless system design,” IEEE Transactions on Microwave Theory and Techniques, vol. 64, no. 7, pp. 2207–2225, Jul. 2016.

[101] 3GPP, “Study on channel model for frequencies from 0.5 to 100 GHz,” 3rd Generation Partnership Project (3GPP), TR 38.901 V14.1.1, Jul. 2017. [Online]. Available:https://portal.3gpp.org/desktopmodules/Specifications /SpecificationDetails.aspx?specificationId=3173.

[102] S. Sun, T. S. Rappaport, M. Shafi, and H. Tataria, “Analytical framework of hybrid beamforming in multi-cell millimeter-wave systems,” IEEE Transactions on Wireless Communications, vol. 17, no. 11, pp. 7528–7543, Nov. 2018.

[103] G. R. MacCartney et al., “Millimeter-wave base station diversity for 5G coordinated multipoint (CoMP) applications,” IEEE Transactions on Wireless Communications, May 2019.

[104] K. Haneda et al., “5G 3GPP-like channel models for outdoor urban microcellular and macrocellular environments,” in 2016 IEEE 83rd Vehicular Technology Conference (VTC2016-Spring), May 2016, pp. 1–7.

[105] Aalto University,AT&T, BUPT, CMCC, Ericsson, Huawei, Intel, KT Corporation, Nokia, NTT DOCOMO, New York University, Qualcomm, Samsung, University of Bristol, and University of Southern California, “5G channel model for bands up to 100 GHz,” 2016, Oct. 21. [Online]. Available: http://www.5gworkshop s.com/5GCM.html.

[106] H. J. Liebe, G. A. Hufford, and M. G. Cotton, “Propagation modeling of moist air and suspended water/ice particles at frequencies below 1000 GHz,” AGARD Conference Proceedings 542, May 1993. [Online]. Available: http://www.its.b ldrdoc.gov/publications/2670.aspx.

[107] J. J. A. Lempianen, J. K. Laiho-Steffens, and A. F. Wacker, “Experimental results of cross polarization discrimination and signal correlation values for a polarization diversity scheme,” in IEEE 47th Vehicular Technology Conference, vol. 3, May 1997, pp. 1498–1502. [Online]. Available: http://ieeexplore.ieee.org/document/605617/.

[108] T. S. Rappaport and S. Deng, “73 GHz wideband millimeter-wave foliage and ground reflection measurements and models,” in 2015 IEEE International Conference on Communication Workshop (ICCW), Jun. 2015, pp. 1238–1243. [Online]. Available: https://arxiv.org/pdf/1509.00436.

[109] K. Haneda et al., “Indoor 5G 3GPP-like channel models for office and shopping mall environments,” in 2016 IEEE International Conference on Communications Workshops (ICCW), May 2016, pp. 694–699.